

EVALUATION OF LANDSLIDE OCCURRENCE USING  
HYDROLOGICAL MODEL IN HUAI NAM PHUNG  
SUBBASIN, THAILAND

Acting SubLt. Rugkiet Chansorn



A Thesis Submitted in Partial Fulfillment of the Requirements  
for the Degree of Master of Science in Earth Sciences  
Department of Geology  
FACULTY OF SCIENCE  
Chulalongkorn University  
Academic Year 2019  
Copyright of Chulalongkorn University

การประเมินการเกิดแผ่นดินถล่มโดยใช้แบบจำลองทางอุทกวิทยาในพื้นที่ลุ่มน้ำสาขาห้วยน้ำพุ  
ประเทศไทย



วิทยานิพนธ์นี้เป็นส่วนหนึ่งของการศึกษาตามหลักสูตรปริญญาวิทยาศาสตรมหาบัณฑิต  
สาขาวิชาโลกศาสตร์ ภาควิชาธรณีวิทยา  
คณะวิทยาศาสตร์ จุฬาลงกรณ์มหาวิทยาลัย  
ปีการศึกษา 2562  
ลิขสิทธิ์ของจุฬาลงกรณ์มหาวิทยาลัย

Thesis Title                                   EVALUATION OF LANDSLIDE OCCURRENCE USING  
HYDROLOGICAL MODEL IN HUAI NAM PHUNG  
SUBBASIN, THAILAND  
By   Acting SubLt. Rugkiet Chansorn  
Field of Study                                 Earth Sciences  
Thesis Advisor                               Associate Professor SRILERT CHOTPANTARAT, Ph.D.  
Thesis Co Advisor                         Pawee Klongvessa, Eng.D.

---

Accepted by the FACULTY OF SCIENCE, Chulalongkorn University in Partial  
Fulfillment of the Requirement for the Master of Science

-----  
Dean of the FACULTY OF SCIENCE  
(Professor POLKIT SANGVANICH, Ph.D.)

THESIS COMMITTEE

----- Chairman  
(Associate Professor SANTI PAILOPLEE, Ph.D.)  
----- Thesis Advisor  
(Associate Professor SRILERT CHOTPANTARAT, Ph.D.)  
----- Thesis Co-Advisor  
(Pawee Klongvessa, Eng.D.)  
----- Examiner  
(Assistant Professor SOMBAT YUMUANG, Ph.D.)  
----- External Examiner  
(Assistant Professor Sawettachat Srisurat, Ph.D.)

  
จุฬาลงกรณ์มหาวิทยาลัย  
CHULALONGKORN UNIVERSITY

รักเกียรติ จันทร์สอน : การประเมินการเกิดแผ่นดินถล่มโดยใช้แบบจำลองทางอุทกวิทยาในพื้นที่ลุ่มน้ำสาขาห้วย  
น้ำพุ่ง ประเทศไทย. ( EVALUATION OF LANDSLIDE OCCURRENCE  
USING HYDROLOGICAL MODEL IN HUAI NAM PHUNG  
SUBBASIN, THAILAND) อ.ที่ปรึกษาหลัก : รศ. ดร.ศรีเลิศ โชติพันธรัตน์, อ.ที่ปรึกษาร่วม :  
ดร.ปวีร์ คล่องเวสสะ

แผ่นดินถล่มเกิดขึ้นบ่อยครั้งในพื้นที่ลุ่มน้ำสาขาห้วยน้ำพุ่งซึ่งตั้งอยู่บริเวณรอยต่อระหว่างจังหวัดเลยและเพชรบูรณ์ การศึกษาครั้งนี้จึงมีวัตถุประสงค์เพื่อประเมินโอกาสเกิดแผ่นดินถล่มในพื้นที่ดังกล่าวโดยใช้ข้อมูลแบบจำลองความสูงเชิงเลข (Digital Elevation Model) ข้อมูลอุตุนิชมวิทยา ข้อมูลทางอุทกวิทยา และข้อมูลคุณสมบัติทางกายภาพของดินมาทำการวิเคราะห์ผ่านกระบวนการระบบสารสนเทศภูมิศาสตร์ในการวิเคราะห์ข้อมูลทางกายภาพของพื้นที่ศึกษา และใช้แบบจำลอง TOPography based hydrological MODEL (TOPMODEL) ร่วมกับทฤษฎีสถิตส่วนความปลอดภัยทางเสถียรภาพลาดดิน (Factor of Safety in Slope Stability) ในการจำลองเสถียรภาพลาดดิน ในระหว่างปี พ.ศ. 2559 และ 2560 ผลการสำรวจด้วยภาพถ่ายดาวเทียม การสำรวจภาคสนาม พบแผ่นดินถล่มระดับต้นจำนวน 63 จุดในพื้นที่ศึกษาในปี พ.ศ. 2560 และทุกจุดตั้งอยู่ในพื้นที่ที่มีความลาดชันมากกว่า 20 องศา ผลการจำลองน้ำท่าและระดับน้ำบาดาลพบว่าปี พ.ศ. 2560 มีปริมาณน้ำมากกว่าปี พ.ศ. 2559 เป็นอย่างมาก ซึ่งสอดคล้องกับข้อมูลอุตุนิชมวิทยาและอุทกวิทยาในปีดังกล่าว และจากการยังผลตัวแปรของแบบจำลอง TOPMODEL พบว่ามี 3 ตัวแปรที่มีความอ่อนไหวต่อผลการจำลองเป็นอย่างมาก ได้แก่ ลอการีทึมของค่าเฉลี่ยเชิงพื้นที่ของสัมประสิทธิ์การจ่าน้ำอิ่มตัว (InTe) ความนำชลศาสตร์พื้นที่ผิว (k0) และแรงขับเคลื่อนลาด (CD) จากการวิเคราะห์เสถียรภาพลาดดินพบว่าลาดดินจะเริ่มขาดเสถียรภาพในพื้นที่ที่มีความลาดชันสูงขยตัวไปยังพื้นที่ที่มีความลาดชันต่ำ ทั้งนี้ลาดดินของจุดที่เกิดแผ่นดินถล่มมีการเริ่มขาดเสถียรภาพมากที่สุดในเดือนกรกฎาคม พ.ศ. 2560 และวันที่ลาดดินในพื้นที่ศึกษาขาดเสถียรภาพมากที่สุดคือวันที่ 30 ตุลาคม พ.ศ. 2560 จากการวิเคราะห์เสถียรภาพลาดดินในพื้นที่ที่มีความลาดชันมากกว่า 20 องศาในวันดังกล่าวพบว่ามี 4 ลุ่มน้ำย่อยที่มีความลาดดินขาดเสถียรภาพเป็นอย่างมาก ได้แก่ ลุ่มน้ำย่อยห้วยน้ำก้อ (92.49%) ลุ่มน้ำย่อยห้วยน้ำพุ่งตอนบน (90.14%) ลุ่มน้ำย่อยห้วยน้ำเสี้ย (89.97%) และลุ่มน้ำย่อยห้วยน้ำครั่ง (87.38%) ซึ่งลุ่มน้ำย่อยทั้งหมดนี้ตั้งอยู่บริเวณแนวเทือกเขาทางตอนเหนือและด้านตะวันตกของพื้นที่ศึกษา นอกจากนี้ยังพบว่าฝนที่ตกหนักติดต่อกันเป็นเวลานานจะทำให้ลาดดินขาดเสถียรภาพอย่างต่อเนื่อง และช่วงเวลาที่ฝนตกหนักอย่างฉับพลันก็ส่งผลให้ลาดดินขาดเสถียรภาพอย่างฉับพลันจนอาจทำให้เกิดแผ่นดินถล่มขึ้นได้เช่นกัน นอกจากนี้ผู้ศึกษาได้จัดทำแผนที่ความอ่อนไหวต่อการเกิดแผ่นดินถล่มในพื้นที่ลุ่มน้ำสาขาห้วยน้ำพุ่งโดยอิงจากเสถียรภาพลาดดินในวันที่ 30 ตุลาคม พ.ศ. 2560 อีกด้วยเพื่อเป็นแนวทางในการรับมือการเกิดแผ่นดินถล่มในอนาคต

จุฬาลงกรณ์มหาวิทยาลัย  
CHULALONGKORN UNIVERSITY

สาขาวิชา            โลกศาสตร์  
ปีการศึกษา         2562

ลายมือชื่อนิสิต .....  
ลายมือชื่อ อ.ที่ปรึกษาหลัก .....  
ลายมือชื่อ อ.ที่ปรึกษาร่วม .....

## 5972048223 : MAJOR EARTH SCIENCES

KEYWORD: LANDSLIDE, HYDROLOGICAL MODEL, HUAI NAM PHUNG  
SUBBASIN, PASAK RIVER BASIN, PHETCHABUN PROVINCE,  
LOEI PROVINCE

Rugkiet Chansorn : EVALUATION OF LANDSLIDE OCCURRENCE USING  
HYDROLOGICAL MODEL IN HUAI NAM PHUNG SUBBASIN,  
THAILAND. Advisor: Assoc. Prof. SRILERT CHOTPANTARAT, Ph.D. Co-  
advisor: Pawee Klongvessa, Eng.D.

Huai Nam Phung subbasin, which is located at the boundary between Loei and Phetchabun provinces, is the area where landslides occur frequently. Therefore, this study aims to evaluate the occurrence of landslides in this area by using the Digital Elevation Model (DEM), Meteorological data hydrological data and physical properties of soils processed with the Geographic Information System (GIS) to analyze the physical data of the study area and use the TOPography based hydrological MODEL (TOPMODEL) combined with the theory of factor of safety in slope stability to simulate the slope stability between 2016 and 2017. According to the satellite imageries and field survey, there were 63 shallow landslide points. These points have the slope higher than 20 degrees and the landslides at these points occurred in 2017. The model simulation shows that the volume of accumulated water in 2017 was much higher than in 2016. The volume of water was in accordance with the meteorological and hydrological data. From the calibration of parameters in the TOPMODEL, there are 3 most sensitive parameters, the logarithm of areal average of saturated soil transmissivity (lnTe), surface hydraulic conductivity (k0) and capillary drive (CD). From the analysis of slope stability, the slope became unstable from high slope areas and the instability expanded to lower slope areas. Most of becoming unstable of landslide points occurred in July 2017 and the unstable areas were highest on 30 October 2017. From the analysis of slope stability in areas with a slope higher than 20 degrees on that day, there were 4 sub-catchments that most of the areas were unstable, Huai Nam Ko (92.49%), the upper part of Huai Nam Phung (90.14%), Huai Nam Hia (89.97%), and Huai Nam Krang (87.38%). These sub-catchments were located on the areas of the mountain ranges in the northern and western parts of the study area. Moreover, it is found that consecutive heavy rain over a long time can cause the slope to become unstable and immediate heavy rainfall events can also cause the slope to become unstable immediately. This instability can lead to landslide occurrence. In addition, the author created a landslide susceptibility map of the Huai Nam Phung subbasin from slope stability on 30 October 2017 to be a way to cope landslides in the future.

Field of Study: Earth Sciences  
Academic Year: 2019

Student's Signature .....  
Advisor's Signature .....  
Co-advisor's Signature .....

## ACKNOWLEDGEMENTS

This research was funded by the Ratchadapisek Sompoch Endowment Fund (2020), Chulalongkorn University, in Climate Change and Disaster Management Cluster (grant number 763014). I am thankful for this fund which made this study run smoothly.

I would like to thank Associate Professor Dr. Srilert Chotpantararat, my thesis advisor, for good advices. He always taught me to do my best and make this research be the honor of my life. He had taught me to gradually absorb the philosophy of academic work until I was able to complete this thesis. When there were good opportunities, such as research funds or seminars, he let me know. My thesis advisor is considered a benefactor who encouraged me to graduate with a master's degree.

Another indispensable person is Dr. Pawee Klongvessa, my thesis co-advisor. He is a passionate new lecturer at the Department of Environmental Technology and Management, Faculty of Environment, Kasetsart University. He explained everything I did not understand and gave me ideas to answer difficult questions. He is also an important person who helped me in composition and language in this thesis. My thesis co-advisor is both a teacher and my kind brother.

In addition, I would like to thank Mr. Apiwat Intiyakoset for his assistance in field study and thank his research for allowing me to get soil properties data for further analysis in my research.

Finally, I would also like to thank Miss Kanokporn Thammiya and my family for their love, their encouragement, and their supports. They always looked after me and helped me in all matters. This master's thesis would not be completed without them.

Rugkiet Chansorn

# TABLE OF CONTENTS

|  | <b>Page</b> |
|--|-------------|
| .....  | iii         |
| ABSTRACT (THAI) .....  | iii         |
| .....  | iv          |
| ABSTRACT (ENGLISH).....  | iv          |
| ACKNOWLEDGEMENTS .....   | v           |
| TABLE OF CONTENTS.....   | vi          |
| LIST OF TABLES .....   | x           |
| LIST OF FIGURES .....  | xi          |
| CHAPTER I INTRODUCTION.....  | 1           |
| 1.1 The origin and significance .....  | 1           |
| 1.2 Objective.....   | 3           |
| 1.3 Hypothesis .....   | 3           |
| 1.4 Conceptual framework.....  | 3           |
| 1.5 Scope of the study.....  | 3           |
| 1.6 Research procedure.....  | 4           |
| CHAPTER II LITERATURE REVIEWS .....  | 5           |
| 2.1 Landslides .....   | 5           |
| 2.1.1 Landslide classification by the United States Geological Survey (USGS) ..... | 5           |
| 2.1.2 Another landslide classification .....                                       | 6           |
| 2.2 Watershed .....  | 8           |
| 2.3 The factor of safety in slope stability .....                                  | 9           |
| 2.4 Topography based hydrological model .....                                      | 9           |
| 2.5 Topographic wetness index .....  | 10          |
| 2.6 Linear regression.....   | 11          |
| 2.7 Inverse distance weighting .....   | 11          |

|  |    |
|--|----|
| 2.8 Monte Carlo algorithm .....  | 12 |
| 2.9 Nash–Sutcliffe model efficiency coefficient .....  | 13 |
| 2.10 Related research.....   | 13 |
| CHAPTER III METHODOLOGY .....  | 16 |
| 3.1 Physical appearance of the Huai Nam Phung subbasin.....  | 16 |
| 3.1.1 Territory and location.....  | 16 |
| 3.1.2 Topography .....   | 21 |
| 3.1.3 Hydrological gauging stations.....   | 21 |
| 3.1.4 Climatology and meteorology.....   | 26 |
| 3.1.5 Hydrogeology.....  | 28 |
| 3.1.6 Geology .....  | 30 |
| 3.1.7 Land use and land cover.....   | 32 |
| 3.1.8 Watershed quality class.....   | 35 |
| 3.1.9 Reservoir .....  | 35 |
| 3.2 Landslide survey.....  | 38 |
| 3.2.1 Imagery survey.....  | 38 |
| 3.2.2 Field survey.....  | 38 |
| 3.3 Soil thickness mapping.....  | 38 |
| 3.4 Meteorological data interpolation.....   | 38 |
| 3.5 Observed streamflow data transferring.....   | 39 |
| 3.6 Streamflow simulation using the TOPMODEL .....   | 41 |
| 3.6.1 Data gathering .....   | 41 |
| 3.6.2 Model processing .....   | 41 |
| 3.6.3 Model calibration .....  | 41 |
| 3.6.4 Sensitivity analysis of the model’s parameters .....   | 45 |
| 3.7 Average height between soil surface and groundwater level simulation using<br>the TOPMODEL ..... | 46 |
| 3.8 Evaluation of landslide occurrence using factor of safety in slope stability .....               | 47 |
| 3.9 Results validation.....  | 47 |



|   |    |
|---|----|
| CHAPTER IV RESULTS .....  | 48 |
| 4.1 Landslide occurrences .....   | 48 |
| 4.1.1 Landslide occurrences by visible imagery analysis .....                 | 48 |
| 4.1.2 Landslide occurrences by a field survey .....                           | 48 |
| 4.1.3 Landslides occurred in the Huai Nam Phung subbasin .....                | 48 |
| 4.2 Physical data of the study area.....                                      | 51 |
| 4.2.1 Slope map .....   | 51 |
| 4.2.2 Flow accumulation .....   | 51 |
| 4.2.3 Topographic Wetness Index (TWI).....                                    | 51 |
| 4.2.4 Soil thickness.....   | 55 |
| 4.2.5 Flow length.....  | 55 |
| 4.3 Meteorological data .....   | 55 |
| 4.3.1 Interpolated rainfall .....   | 55 |
| 4.3.2 Evaporation rates .....   | 55 |
| 4.4 Streamflow calculation .....  | 62 |
| 4.5 Parameters of the topography based on hydrological model.....             | 62 |
| 4.6 Simulated streamflow .....  | 65 |
| 4.7 Simulated average height between soil surface and groundwater level ..... | 65 |
| 4.8 Height between soil surface and groundwater level .....                   | 65 |
| 4.9 Groundwater depth determination .....                                     | 70 |
| 4.10 Estimation of factor of safety in slope stability .....                  | 70 |
| 4.11 Validation of landslide occurrence .....                                 | 75 |
| CHAPTER V DISCUSSIONS.....  | 78 |
| 5.1 Landslides occurrence .....   | 78 |
| 5.2 Soil thickness .....  | 81 |
| 5.3 Model simulation .....  | 83 |
| 5.3.1 Streamflow .....  | 83 |
| 5.3.2 Height between soil surface and groundwater level.....                  | 86 |
| 5.4 Model parameters .....  | 88 |

|   |     |
|---|-----|
| 5.5 Slope stability .....   | 90  |
| CHAPTER VI CONCLUSIONS AND RECOMMENDATIONS.....   | 100 |
| 6.1 Conclusions.....  | 100 |
| 6.2 Recommendations.....  | 101 |
| REFERENCES .....  | 102 |
| APPENDICES .....  | 111 |
| APPENDIX A Factor of safety in slope stability of the Huai Nam Phung subbasin<br>from 1 July, 2017 to 1 November, 2017..... | 112 |
| APPENDIX B Scars of 63 landslide points in the Huai Nam Phung subbasin in<br>2017 .....                                     | 118 |
| VITA.....   | 128 |



## LIST OF TABLES

|   | <b>Page</b> |
|---|-------------|
| Table 3.1 Aquifers in the Huai Nam Phung subbasin.....  | 28          |
| Table 3.2 Geology of the Huai Nam Phung subbasin.....   | 30          |
| Table 3.3 Comparison of land use and land cover in the Huai Nam Phung subbasin<br>between 2002 and 2016 .....   | 32          |
| Table 3.4 Watershed quality class of the Huai Nam Phung subbasin .....  | 35          |
| Table 3.5 Parameters in the TOPMODEL.....   | 45          |
| Table 4.1 The relationship between soil thickness and TWI in the Huai Nam Phung<br>subbasin with the slope of higher than 6% .....                                | 57          |
| Table 4.2 The values and sensitivity index of parameters used in the TOPMODEL ..  | 62          |
| Table 4.3 Times of the beginnings of instabilities at the points of landslides in the<br>Huai Nam Phung subbasin.....   | 75          |
| Table 5.1 News on floodings in Phetchabun Province, the location of the Huai Nam<br>Phung subbasin .....  | 86          |
| Table 5.2 Hydraulic conductivities of unconsolidated sedimentary materials,<br>sedimentary rocks and crystalline rock materials (Domenico and Schwartz, 1998) ... | 89          |

## LIST OF FIGURES

|   | <b>Page</b> |
|---|-------------|
| Figure 2.1 Occurrence of landslides (Highland and Bobrowsky, 2008).....   | 5           |
| Figure 2.2 Landslide classification by soil mantle that covering bedrock (Dou et al., 2015) .....   | 7           |
| Figure 2.3 Loess landslide classification (Li and Mo, 2019).....  | 7           |
| Figure 2.4 Schematic diagram of the landslide classification system (Sharpe, 1938)...   | 8           |
| Figure 2.5 Example of watershed .....   | 8           |
| Figure 2.6 Example of linear regression.....  | 11          |
| Figure 2.7 Comparison between inverse distance weighting, kriging and spline.....   | 12          |
| Figure 3.1 Location and subbasins of the Pasak river basin.....   | 18          |
| Figure 3.2 Topographic map of the Pasak river basin .....   | 19          |
| Figure 3.3 Location of the Huai Nam Phung subbasin.....   | 20          |
| Figure 3.4 Topographic map of the Huai Nam Phung subbasin.....  | 23          |
| Figure 3.5 Locations of stream gauges nearby the Huai Nam Phung subbasin.....   | 24          |
| Figure 3.6 Stream gauges of the Royal Irrigation Department Thailand which are nearby the Huai Nam Phung subbasin and the cross sections at those stream gauges | 25          |
| Figure 3.7 Relationship between annual average streamflow and catchment area (Institute of Water Resources and Agriculture Information Thailand, 2012).....     | 26          |
| Figure 3.8 Raingauges around the Huai Nam Phung subbasin.....   | 27          |
| Figure 3.9 Hydrogeological map of the Huai Nam Phung subbasin .....   | 29          |
| Figure 3.10 Geological map of the Huai Nam Phung subbasin.....  | 31          |
| Figure 3.11 Land use and land cover map of the Huai Nam Phung subbasin in 2002  | 33          |
| Figure 3.12 Land use and land cover map of the Huai Nam Phung subbasin in 2016  | 34          |
| Figure 3.13 Watershed quality class map of the Huai Nam Phung subbasin .....  | 36          |
| Figure 3.14 Huai Nam Ko reservoir (Google, 2017) .....  | 37          |
| Figure 3.15 Project of the Huai Nam Hia reservoir (Royal Irrigation Department Thailand, 2011) .....  | 37          |

|   |    |
|---|----|
| Figure 3.16 Topographic map of the Huai Nam Phung subbasin and catchment area of the S.3 station.....   | 40 |
| Figure 3.17 Flowchart of research procedure (page 1 of 3).....  | 42 |
| Figure 3.18 Flowchart of research procedure (page 2 of 3).....  | 43 |
| Figure 3.19 Flowchart of research procedure (page 3 of 3).....  | 44 |
| Figure 3.20 Schematic diagrams showing the relationship between soil thickness and groundwater depth .....  | 47 |
| Figure 4.1 Slope of the Huai Nam Phung subbasin showing in 3 classes .....  | 49 |
| Figure 4.2 Landslides occurrence in the Huai Nam Phung subbasin in 2017 .....   | 50 |
| Figure 4.3 Slope of the Huai Nam Phung subbasin .....   | 52 |
| Figure 4.4 Streams in the Huai Nam Phung subbasin generated by flow a.....  | 53 |
| Figure 4.5 The topographic wetness index of the Huai Nam Phung subbasin .....   | 54 |
| Figure 4.6 Sampling points of soil thickness in the Huai Nam Phung subbasin .....   | 56 |
| Figure 4.7 Linear relationship between soil thickness and the topographic wetness index in the Huai Nam Phung subbasin with the slope of higher than 6% ..... | 57 |
| Figure 4.8 Soil thickness of the Huai Nam Phung subbasin.....   | 58 |
| Figure 4.9 Flow length of the Huai Nam Phung subbasin.....  | 59 |
| Figure 4.10 Daily rainfall in the Huai Nam Phung subbasin in 2016.....  | 60 |
| Figure 4.11 Daily rainfall in the Huai Nam Phung subbasin in 2017.....  | 60 |
| Figure 4.12 Daily evaporation in the Huai Nam Phung subbasin in 2016 .....  | 61 |
| Figure 4.13 Daily evaporation in the Huai Nam Phung subbasin in 2017 .....  | 61 |
| Figure 4.14 Relationship between annual average streamflow and catchment area in the Pasak river basin in 2016 .....  | 63 |
| Figure 4.15 Relationship between annual average streamflow and catchment area in the Pasak river basin in 2017 .....  | 63 |
| Figure 4.16 Comparison between the observed streamflow at the S.3 station and the calculated streamflow of the Huai Nam Phung subbasin in 2016 .....          | 64 |
| Figure 4.17 Comparison between the observed streamflow at the S.3 station and the calculated streamflow of the Huai Nam Phung subbasin in 2017 .....          | 64 |
| Figure 4.18 Comparison between the observed streamflow and the simulated streamflow in the Huai Nam Phung subbasin in 2016.....                               | 66 |

|   |    |
|---|----|
| Figure 4.19 Comparison between the observed streamflow and the simulated streamflow in the Huai Nam Phung subbasin in 2017.....   | 66 |
| Figure 4.20 The simulated average height ( $Z$ ) between soil surface and groundwater level in the Huai Nam Phung subbasin in 2016.....   | 67 |
| Figure 4.21 The simulated average height ( $Z$ ) between soil surface and groundwater level in the Huai Nam Phung subbasin in 2017.....   | 67 |
| Figure 4.22 Comparison of the height between soil surface and groundwater level of the Huai Nam Phung subbasin from 1 April to 1 November, 2016.....                                    | 68 |
| Figure 4.23 Comparison of the height between soil surface and groundwater level of the Huai Nam Phung subbasin from 1 April to 1 November, 2017.....                                    | 69 |
| Figure 4.24 Comparison of groundwater depths of the Huai Nam Phung subbasin from 1 April to 1 November, 2016.....   | 71 |
| Figure 4.25 Comparison of groundwater depths of the Huai Nam Phung subbasin from 1 April to 1 November, 2017.....   | 72 |
| Figure 4.26 Factor of safety in slope stability of the Huai Nam Phung subbasin from 1 April to 1 November, 2017.....  | 73 |
| Figure 4.27 Factor of safety in slope stability of the Huai Nam Phung subbasin on 30 October, 2017.....   | 74 |
| Figure 5.1 Landslides occurred in the Huai Nam Phung subbasin in 2017 in each sub-catchment.....  | 79 |
| Figure 5.2 Comparison of satellite imageries in the Huai Nam Phung subbasin between 2016 and 2017 in areas of the Phu Thap Boek.....  | 80 |
| Figure 5.3 Soil thickness in the Huai Nam Phung subbasin in each sub-catchment... ..  | 82 |
| Figure 5.4 Streamflow and rainfall in the Huai Nam Phung subbasin and storm events in 2016.....   | 84 |
| Figure 5.5 Streamflow and rainfall in the Huai Nam Phung subbasin and storm events in 2017.....   | 85 |
| Figure 5.6 Locations of 27 landslide points in the Huai Nam Phung subbasin that become unstable on 1 July to 15 August, 2017.....   | 91 |
| Figure 5.7 Factor of safety in slope stability of 27 unstable locations in the Huai Nam Phung subbasin from 1 July to 15 August, 2017 due to two tropical storms (Talas and Sonca)..... | 92 |
| Figure 5.8 Factor of safety in slope stability in the Huai Nam Phung subbasin on 30 October, 2017 in each sub-catchment.....  | 93 |

- Figure 5.9 Factor of safety in slope stability in the areas with slope higher than 6% in 9 sub-catchments of the Huai Nam Phung subbasin on 30 October, 2017 .....94
- Figure 5.10 Slope stability map on 30 October, 2017 and scar-scouring on 14 January, 2003 of Yumuang (2005) in the western hillside of the Huai Nam Ko sub-catchment .....96
- Figure 5.11 Slope stability map on 30 October 2017, debris flow and debris flood susceptibility map by Yumuang (2005), and landslide and flash flood susceptibility map by the Department of Mineral Resources Thailand (2016) in the Huai Nam Ko sub-catchment .....98
- Figure 5.12 Shallow landslide susceptibility map of the Huai Nam Phung subbasin .99



# CHAPTER I

## INTRODUCTION

### 1.1 The origin and significance

Landslide is a disaster that has a severe impact and can cause enormous damage to human life and property. This disaster usually occurs in areas with very steep slopes. Therefore, it is often found in mountainous areas and often occurs during a storm or heavy rain (Casagli et al., 2006; Guthrie and Evans, 2004; Keefer et al., 1987). It is because when soil holds a large amount of water, causing that it is unstable and collapses by the gravity force. In addition, large amounts of rainwater accumulating in soil may cause debris flow in upstream areas with steep mountainous terrain. The debris flow generally is characterized by quick runoff flowing from highlands to low-lying areas (Bobrowsky and Highland, 2013). Landslides can cause severe losses of life and destruction of buildings in the foothills and lowland areas. There have been many researches about the occurrence of landslides in many areas around the world (Bera et al., 2019; Chen et al., 2018; Fowze et al., 2012; Jiao et al., 2019; Komori et al., 2018; Pal et al., 2018; Pham et al., 2020; Pradhan and Kim, 2016). Many studies were conducted in Thailand because of a tropical climate and heavy rain due to the influence of monsoon and storms that form in both the Indian ocean and the South China sea (Limsakul et al., 2010; Singhrattna et al., 2005), especially in the rainy season. Therefore, there is a chance that heavy rainfalls can trigger landslides, which can negatively affect both the human life and other properties. Based on the record of debris flow occurrence in the past, it is found that Thailand has experienced such disasters in many areas, especially in the northern region, where has a topographical landscape consisting of steep and complex mountains (Turkelboom et al., 2008), and the southern region, which has more rain than other areas (Wangwongchai et al., 2005).

The hydrological models are the tools used to analyze landslides occurrence (Bordoni et al., 2020; Bui et al., 2020; Depina et al., 2020; Du et al., 2020; Liu et al., 2020; Wang et al., 2020; Xing et al., 2020). Especially, the topography based hydrological model known as TOPMODEL. It is a hydrological model that is mostly used to evaluate the occurrence of landslides. It can simulate the rainfall-runoff and groundwater situation by using the terrain data and meteorological data including rainfall, evaporation, and streamflow (Bai et al., 2020; Beven and Kirkby, 1979; Mouri et al., 2011). The results generated from the TOPMODEL are important data to evaluate the landslide occurrence (Beven et al., 1984; Nicu and Asăndulesei, 2018). One of the theories that used to evaluate the landslide occurrence is the factor of safety in slope stability. This theory would evaluate the landslide occurrence by analyzing the stability of the hillslope (Arai and Tagyo, 1985; Chen and Shao, 1988; Cheng et al., 2007; McCombie and Wilkinson, 2002; Skempton and DeLory, 1984; Zheng et al., 2006). It can be analyzed by using the physical properties in the study areas, including slope rates, soil properties, soil thickness, and groundwater situations (Kim et al., 2019; Meisina and Scarabelli, 2007; Montgomery and Dietrich, 1994;



Pirone et al., 2015; Rahardjo et al., 2010). From the analysis of the hydrological model and the related theory, it is able to efficiently assess the occurrence of landslides.

The TOPMODEL can simulate the streamflow and groundwater level in each different time. The status of groundwater levels is a variable to calculate the factor of safety in slope stability that is a process to evaluate the landslide occurrence. The streamflow simulated from the TOPMODEL can calibrate appropriate parameters by using observed streamflow (Beven et al., 1984). There are many studies using the TOPMODEL to simulate streamflow and groundwater status (Chen and Wu, 2012; Gumindoga et al., 2014; Gumindoga et al., 2011; Peng et al., 2008) and there are many studies using the factor of safety in slope stability to evaluate landslide occurrence (Li et al., 2019; Marin and Velásquez, 2020; Naidu et al., 2018; Wang et al., 2020). There are many stream gauges nearby the study area. Therefore, the TOPMODEL is an appropriate model to generate groundwater status that a variable to calculate the factor of safety in slope stability which is a process to evaluate landslide occurrence.

Huai Nam Phung subbasin is a branch of the Pasak River basin located in the area of Phetchabun Province and Loei Province. This basin is a narrow and long basin flanked by Phetchabun mountains in both sides. There is a chance of streamflow from rainfall accumulated in the area which causes a turbulent flow (Weigel and Rotach, 2004). Mountains in this area appear to be the same as those in northern areas of the country, especially Phetchabun mountains in the west, which is characterized by high steepness. The lower plain area at the foot of the western mountains of the catchment mainly is residential and building areas (Leblond, 2019). As a result, it is very vulnerable to debris flow and flash flooding. Government and local agencies have conducted studies to propose the measures to prevent and/or mitigate the impact of landslides, as well as to educate people to adapt themselves to the disaster. Moreover, they also suggested to use buildings and engineering tools to reduce the effects of disasters (Oktorie, 2017).

Even there have been many studies conducted in this area (Fowze et al., 2012; Komori et al., 2018; McNamara et al., 2006; Ono et al., 2014; Thammapala and Weng, 2015; Yumuang, 2005; Ziegler et al., 2014), most of them overlaid geographic information to assess the vulnerable areas of landslide occurrence and explain the mechanism of debris flow and debris flood (Yumuang, 2005). This study used geographic information systems and remote sensing to explain the factors of debris flow. The researcher found that debris flow mechanisms were triggered by heavy rain and other physical factors (Long et al., 2020; Peng et al., 2015). In addition, there are studies in the northern Thailand about geomorphologic thresholds (metro) and turbidity-based sediment monitoring (Ziegler et al., 2014). In Thailand, there are previous studies about rain-triggered landslide hazards (Fowze et al., 2012) and distributed probability of slope failure (Komori et al., 2018). However, the

explanation of the landslide occurrences related to hydrological model is very limited in Thailand.

As mentioned, thus, the hydrological model was applied with the geographic information system (GIS) to predict and explain the hydrological mechanism that affects the occurrence of landslides in Thailand. The selected area is located in the Huai Nam Phung subbasin. Later, applying hydrological factors together with theory of slope stability can systematically reveal the vulnerable areas in terms of temporal and spatial distributions, which can be used as a guideline for relevant government agencies and local people to mitigate such disaster in this area.

## **1.2 Objective**

To apply the hydrological model to explain the occurrence of landslides in the Huai Nam Phung subbasin.

## **1.3 Hypothesis**

It is expected that the hydrological model combined with the factor of safety in slope stability theory can assess the occurrence of landslides in different time periods in the study area.

## **1.4 Conceptual framework**

This research aims to assess the occurrence of landslides by using hydrological models in the Huai Nam Phung subbasin, which is a branch of the Pasak River basin. The instruments used in this study include the TOPMODEL, a hydrological model widely used in the study of landslides and can be used in the ArcGIS Program, and R, which is a statistical calculation program. This study used the factor of safety in slope stability theory to create a map, showing the sensitivity of the stability of the slopes at various times.

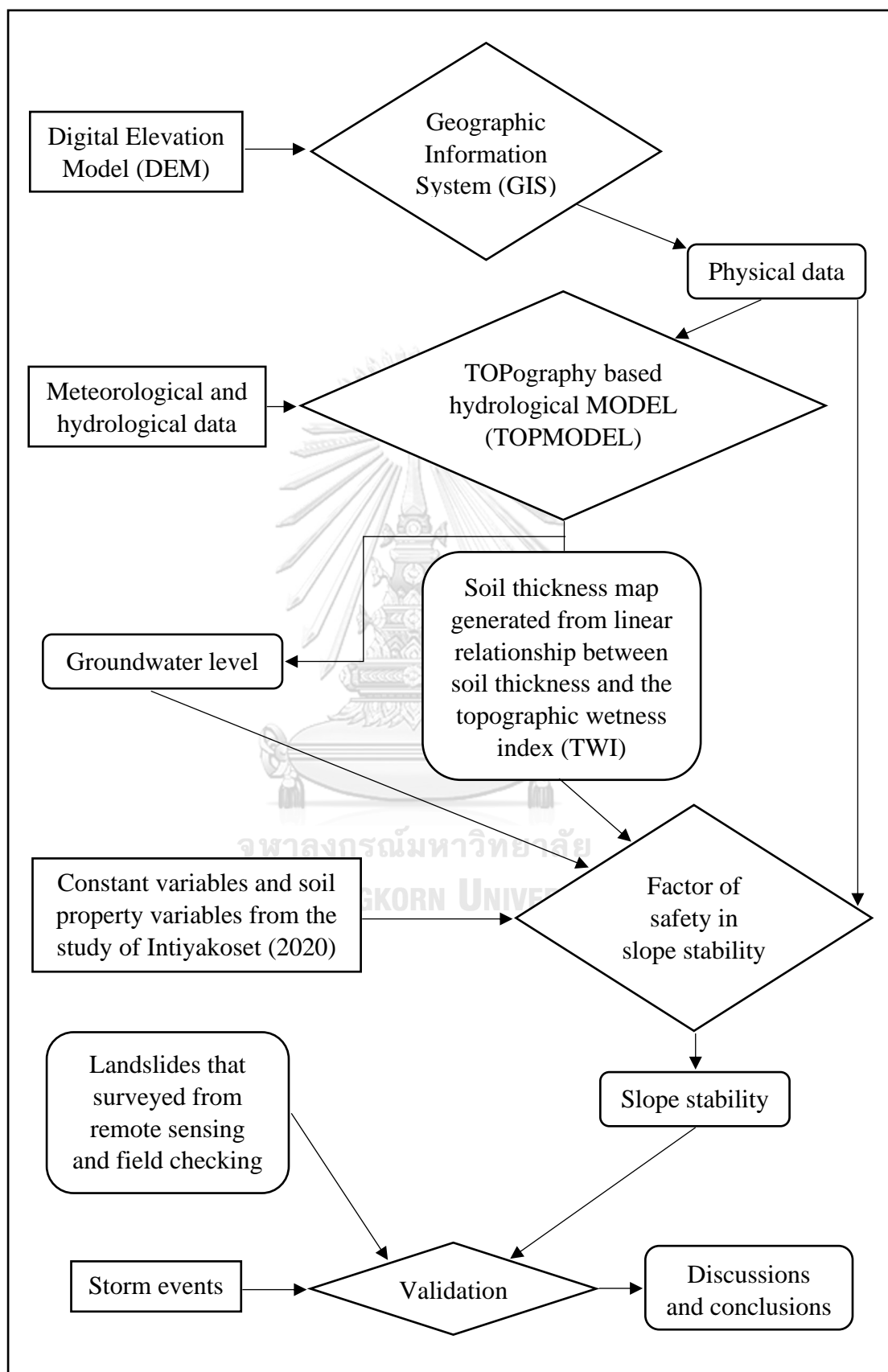
## **1.5 Scope of the study**

This study was conducted in the Huai Nam Phung subbasin, which covers some parts of Dan Sai district, Loei province, and Lom Kao and Lom Sak districts, Phetchabun province.

Analytical study to assess the occurrence of landslides in the Huai Nam Phung subbasin was based on the slope stability theory using hydrological models. The main hydrological model used in the study is the topography based hydrological model (TOPMODEL) and the theory used to evaluate the occurrence of landslides is the factor of safety in slope stability.

This study was focused the landslides occurred in 2016 that is a year with drought weather and 2017 that is heavy rainfall season. The resolution of the Digital Elevation Model (DEM) that used in this study is  $12.5 \times 12.5$  meters, it was provided by the National Aeronautics and Space Administration (NASA).

### 1.6 Research procedure



## CHAPTER II LITERATURE REVIEWS

This study assesses the occurrence of landslides in the Huai Nam Phung subbasin. There are related theories and researches as the following:

### 2.1 Landslides

Landslides are a disaster that is caused by the movement of soil masses from high elevation to low elevation on the steep slope area. It causes extensive damage, both in the area where the mass of the soil collapsed and the area where the mass of the soil moved down to cover. It occurs in areas with slopes because the slopes cause the mass of the accumulated soil to move down by the gravity of the earth. The occurrence of landslides results in soil mass covering the area at the bottom of the slope which collapses when the soil mass is unstable (**Figure 2.1**).

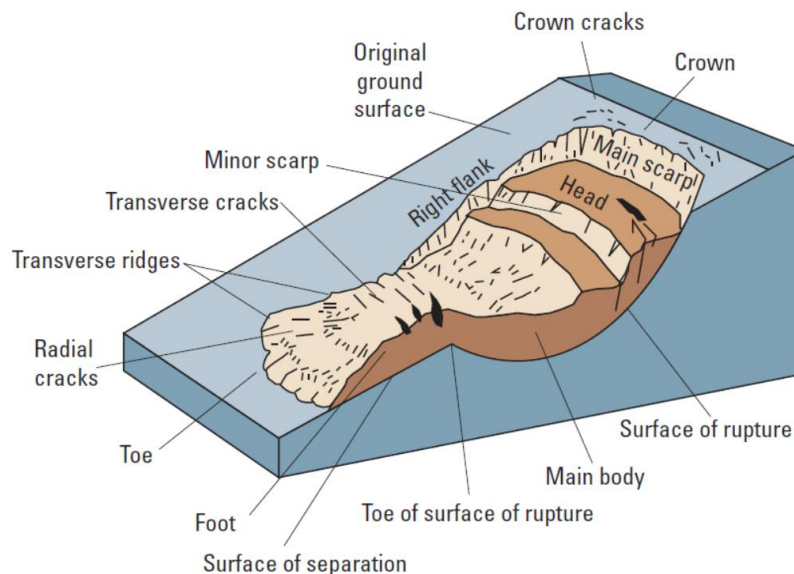


**Figure 2.1** Occurrence of landslides (Highland and Bobrowsky, 2008)

#### 2.1.1 Landslide classification by the United States Geological Survey (USGS)

From the landslide handbook prepared by the USGS, there are 4 major types of landslides: fall, shift, spread, and flow.

**Fall** is the movement of soil and rocks from high elevation to low elevation in areas with very steep slopes, such as cliffs, where land and rocks can rapidly fall down.

**Rockfall** is the rock movement at a steep slope or cliff, caused by the erosion of the rock in that area which causes the rock to fall down.

**Topple** is the breaking down of soil mass or rock mass which causes the broken rock to topple over the slope.

**Slides** are shifts of soil or rock mass in areas with a certain slope. Due to the instability of the slope area, soil and rock mass moves from high elevation to low elevation in accordance with the gravity.

**Rotational Landslide** is the soil mass in the slope area that collapses from the higher area and accumulates in the lower area. It is raised according to the deposition of the soil mass in the higher area.

**Translational Landslide** is the soil mass in the area where the slope moves from high elevation to low elevation as a whole panel.

**Spread** is the movement of soil or rock in a relatively low slope area. It is a widely spread which usually occurs in areas where the soil texture is characterized by peat soil. For the spread of landslides, lateral spreads occur in areas with low slopes or flat areas where the soil is quite soft, in the form of peat soil. Therefore, it collapses from a higher area to a lower area according to the gravity of the earth.

**Flows** are the movement of soil mass with high liquidity which washes away sediment and rock mass, including objects from high elevation to low elevation.

**Debris Flows** is the flowing of various sizes sediments mixed with sediments, rocks and tree remains. It often occurs along the existing waterway or on a small rut on the slope with water, which receive a large amount of rainwater during the rainy season. It is an intermediary to remove sediments and rocks, including tree remains and grasses. They flow down together to the foothill and form a sediment-shaped fan in front of the valley.

**Lahars** are magma flows caused by volcanic eruptions. Lava that flows from the crater washes sediments as well as soils and rocks away and causes them flowing down the hill. The word “Lahar” is from Indonesian language which means a volcanic area that often explodes.

**Debris Avalanche** is a movement of a mass consisted of multiple sized sediments down the slope which causes a landslide in a large area.

**Earthflow** is a movement of soil mass consisted of fine sediment such as clay and silty soil in areas with gentle slope.

**Creep** is a slow movement of the soil mass due to a loss of resistance to the flow resulting in a motivation for the soil to move slowly which is not enough to cause a soil erosion. The evidence of the creep which can be observed is the fence, wall and the trees that grow in that area are tilted or distorted from the origin.

### 2.1.2 Another landslide classification

The landslides which occur in cliff or high slope areas can be classified into 2 types, shallow landslide and deep-seated failure (Dou et al., 2015). If the thickness of surface soil mantle that covers bedrock is lower than 10 meters, it is classified as the shallow landslide. On the other hand, if the thickness of surface soil mantle that

covers bedrock is higher than 10 meters, it is classified as the deep-seated failure (Figure 2.2).

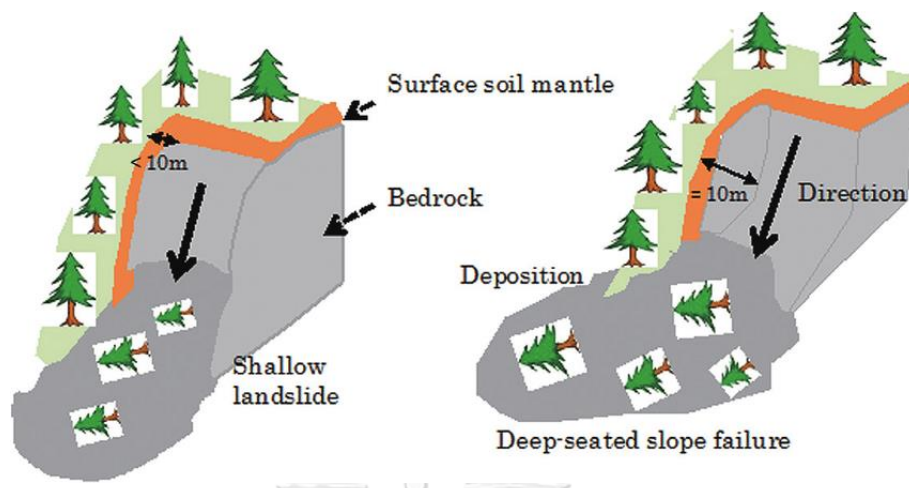


**Figure 2.2** Landslide classification by soil mantle that covering bedrock (Dou et al., 2015)

The landslides occur in the loess slope area can be classified into 11 types, rotational slide, planar slide, crack slide, fall, topple, deep-seated flow, surficial mudflow, spall, interface slide, bedding slide, and intersection slide (Li and Mo, 2019) (Figure 2.3). In addition, landslides can also be classified according to the amount of water and sediments (Sharpe, 1938) (Figure 2.4).

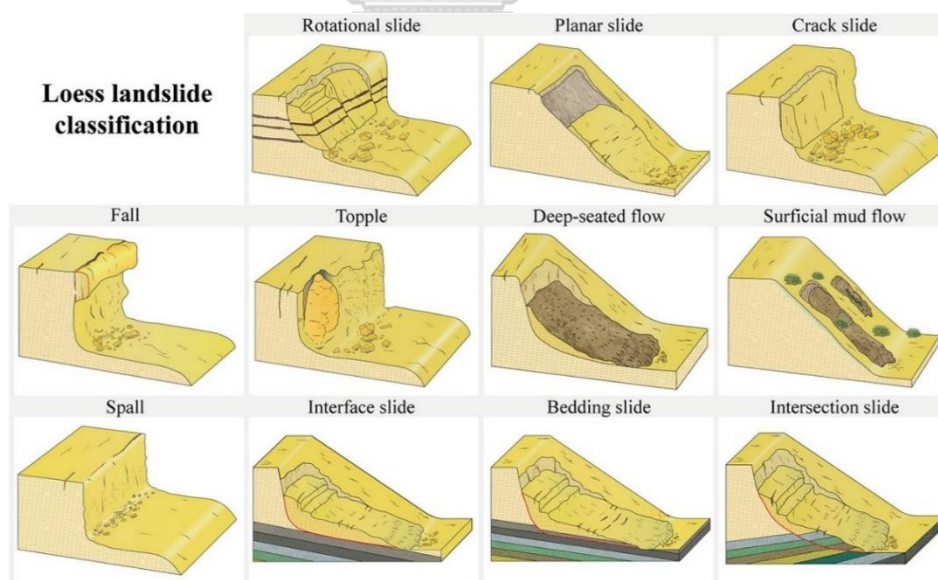


**Figure 2.3** Loess landslide classification (Li and Mo, 2019)

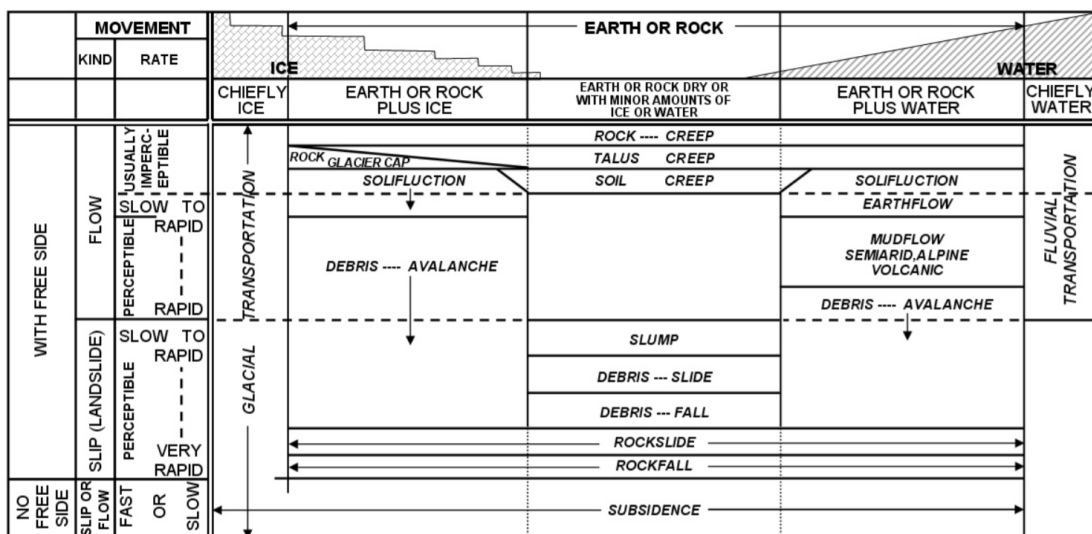


Figure 2.4 Schematic diagram of the landslide classification system (Sharpe, 1938)

## 2.2 Watershed

Ruangpanit and Songprai (1984) quoted the meaning of watershed based on the United States department of agriculture that the basin is the area that supports all the rainwater that is above the specified point. The rainwater that falls in that area flows to the same outlet (Figure 2.5).

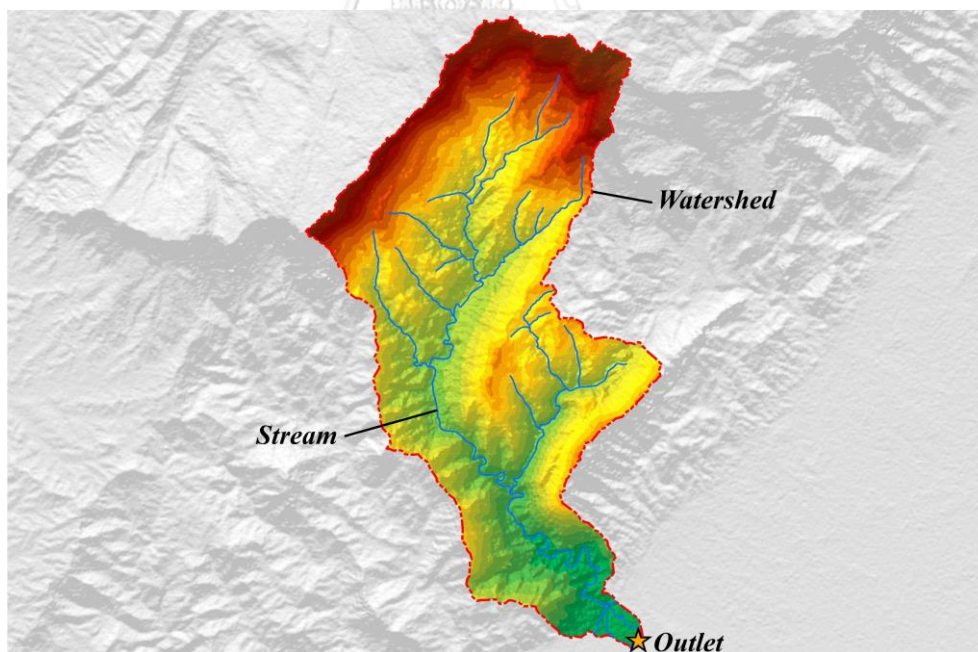


Figure 2.5 Example of watershed

Estimation of watershed areas can be done by measuring the area surrounded by the watershed line on the topographic map. The size of the basin can be large or small depending on the position of the designated outlet in that river. The size of the river basin will be larger if the designated exit points in that river is in the more

downstream side. In contrast, the basin will be smaller if the designated outlet point is in the more upstream side. The term "river source" means a high area that is the origin of a small stream. Most of the origins are steep mountainous areas covered by forests and have high rainfall amount. It is suitable for supporting rainwater and is able to absorb and store a large amount of water in the form of groundwater. The source of the stream is like a natural reservoir that slowly discharges water to nourish the stream so that the water flows consistently throughout the year.

### 2.3 The factor of safety in slope stability

The safety ratio of the stability of the soil slope is the proportion of 1.2 to  $\infty$ . This proportion is used to calculate the likelihood of landslides occurrence. The proportions are calculated from various physical parameters such as the slope of the area, the thickness of the soil, the density of the soil, adhesion rate of soil texture, groundwater level. For the Factor of Safety (FS), if it is greater than 1.2, the area at that time is stable. On the other hand, if FS is less than 1.2, the area at that time is unstable and landslides may occur. In addition, if FS less than 1, the area at that time is highly unstable (Aversa et al., 2018; Naidu et al., 2018). The FS values in the same area can be different for each time period. The FS can be calculated from equation 2.1.

$$FS = \frac{C + (D\rho_s - h_w\rho_w)g \cos^2 \beta \tan \phi}{\rho_s g D \sin \beta \cos \beta} \quad 2.1$$

where  $FS$  is the factor of safety in slope stability

$C$  is effective cohesion (kPa)

$D$  is soil thickness (meters)

$\rho_s$  is soil bulk density ( $\text{kg/m}^3$ )

$h_w$  is groundwater depth (meters)

$\rho_w$  is water density ( $997 \text{ kg/m}^3$ )

$g$  is gravitational acceleration ( $9.80665 \text{ m/s}^2$ )

$\phi$  is soil effective friction angle (degree)

$\beta$  is slope (radians)

The FS values can be calculated in different areas and different times. For the same area, the FS values may change over time. At the same time, the FS may have different values for different areas.

### 2.4 Topography based hydrological model

The topography based hydrological model is also known as TOPMODEL. It is a mathematical model used to show statistical results in hydrology. The model is a physical model that simulates physical characteristics of a river basin (Beven and Kirkby, 1979). It can simulate water flow, including changes in groundwater levels,



by using topographic and other hydrological factors such as topographic wetness index, rainfall, evaporation rate and delay in water flow within the basin.

The TOPMODEL can be used in the Windows operating system via software such as the R Program and Grass GIS. The simulation results are statistical data such as streamflow and groundwater levels at various times.

This study uses the average height between soil surface and groundwater level ( $\bar{Z}$ ) to calculate the factor of safety in slope stability. TOPMODEL generate the  $\bar{Z}$  at every time interval  $\Delta t$  by using equation 2.2.1.

$$\bar{Z}^t = \bar{Z}^{t-\Delta t} - \frac{(Q_V^t - Q_B^t)}{A} \Delta t \quad 2.2.1$$

where  $Q_V^t$  is recharge of the saturated zone from the unsaturated zone over the interval  $(t - \Delta t, t)$  ( $\text{m}^3\text{s}^{-1}$ )

$Q_B^t$  is the subsurface flow contribution over the same interval ( $\text{m}^3\text{s}^{-1}$ ), to calculate it using equation 2.2.2

$A$  is the basin area ( $\text{m}^2$ )

$$Q_B^t = A \cdot \frac{K_0}{f} \exp[-\lambda] \exp[-f\bar{Z}^t] \quad 2.2.2$$

where  $K_0$  is the watershed average value of the surface saturated hydraulic conductivity

$\lambda$  is inversely related to the potential rate of subsurface flow

## 2.5 Topographic wetness index

The topographic wetness index, also known as TWI, is an index that indicates the humidity rate according to the topography. It is one of the important variables for the simulation of the TOPMODEL. The index is calculated from the topographic characteristics by the slope of the area as equation 2.3.

$$TWI = \ln \frac{\alpha}{\tan \beta} \quad 2.3$$

where  $TWI$  is the topographic wetness index

$\alpha$  is the flow accumulation

$\beta$  is the slope (radians)

Because it is an index that is the result from the slope of the terrain, it quite high in the area near the rut or the trench and low in the area near the ridge. At the highest point of the ridge, the wet-dry index maybe 0 or nearly 0 since the ridge area has a lower moisture than hills or valleys (Romeo et al., 2015).

## 2.6 Linear regression

Linear regression is a linear approach to model the relationship between a scalar response and one or more explanatory variables. The multiple variables give more accuracy than a single variable (Rencher and Christensen, 2012). In a graph plotted by x and y values, the group of points would show a trend as a single trend line (**Figure 2.5**). From this process, the linear equation is generated by the relationship between x and y values.

This study used linear regression to generate a streamflow in the study area and find the relationship between soil thickness and the topographic wetness index (TWI) for soil thickness mapping.

The slope equation of linear regression is showing in equation 2.4.

$$y = \alpha + \beta x \quad 2.4$$

where  $x$  is the explanatory variable

$y$  is is the dependent variable

The slope of the line is  $\beta$ , and  $\alpha$  is the intercept (the value of  $y$  when  $x = 0$ )

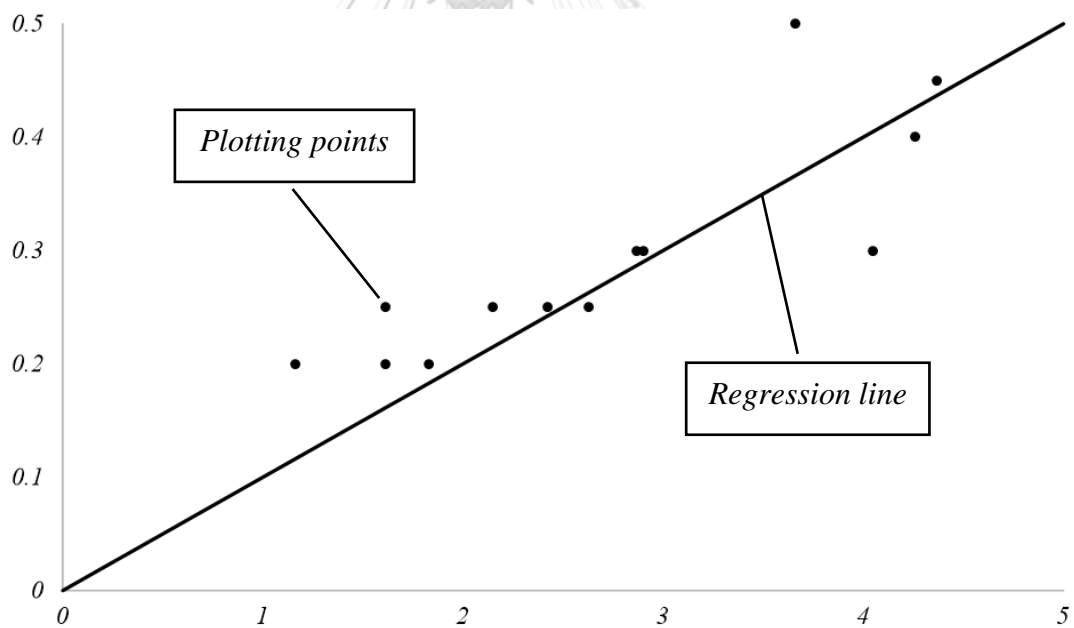


**Figure 2.6** Example of linear regression

## 2.7 Inverse distance weighting

For the geospatial process, there are 3 processes to interpolate the data including inverse distance weighting, kriging, and spline (**Figure 2.7**).

This study used the process of inverse distance weighting to interpolate the distributed data because the study area is wide and most of the terrains are plain. The

IDW is more suitable than the kriging that is used for the short distance (Ikechukwu et al., 2017). Meanwhile, in the geospatial interpolation, the IDW and kriging are better than spline (Wu and Hung, 2016).

Inverse distance weighting (IDW) is a type of deterministic method for multivariate interpolation from a scattered set of points with known values. Interpolated values are calculated from the average value among points of known values weighted by inverse distance.

The IDW can calculate with equation 2.5.

$$\hat{v} = \frac{\sum_{i=1}^n \frac{1}{d_i} v_i}{\sum_{i=1}^n \frac{1}{d_i}} \quad 2.5$$

where  $\hat{v}$  is value to be estimated

$v_i$  is known value

$d_i, \dots, d_n$  are distances from the  $n$  data points to the point estimated  $n$

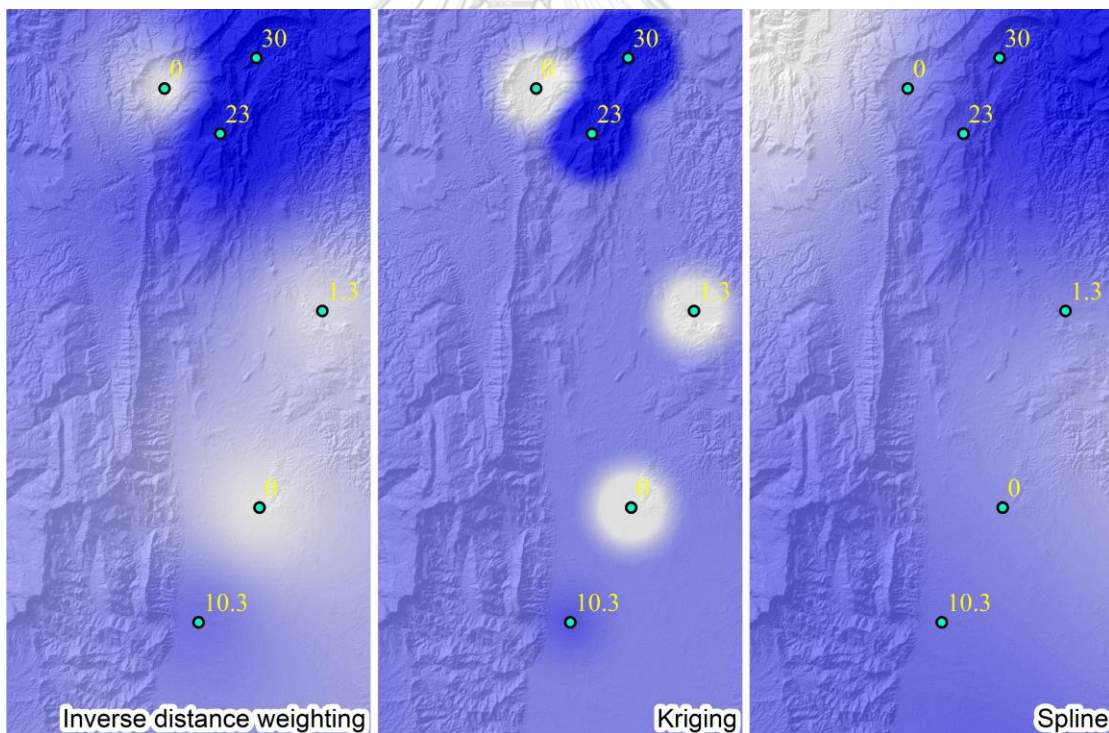


**Figure 2.7** Comparison between inverse distance weighting, kriging and spline

## 2.8 Monte Carlo algorithm

Monte Carlo algorithm is a process of calibrating by random sampling to make numerical estimations of the unknown parameters (Metropolis, 1987). The calibration of the TOPMODEL can be done by the Monte Carlo method to estimate the unknown parameters to reliably simulated the streamflow. In the process of randomization, the

maximum and minimum values must be set for each parameter and the number of randomized times should be specified. All of these processes can be done by the TOPMODEL package in the R program.

## 2.9 Nash–Sutcliffe model efficiency coefficient

Nash–Sutcliffe model efficiency coefficient is used to assess the predictive power of hydrological models. It indicates the compatibility of the observed streamflow and simulated streamflow (Nash and Sutcliffe, 1970). The values of the NSE is between  $-\infty$  and 1. The value of 1 means the observed data and simulated data are equal. Meanwhile, the  $NSE > 0.5$  means the simulated value is considered acceptable for research (Ritter and Muñoz-Carpena, 2013). The NSE is defined as equation 2.6.

$$NSE = 1 - \frac{\sum_{t=1}^T (Q_m^t - Q_o^t)^2}{\sum_{t=1}^T (Q_o^t - \bar{Q}_o)^2} \quad 2.6$$

where  $NSE$  is the Nash–Sutcliffe model efficiency coefficient

$\bar{Q}_o$  is the mean of observed streamflow

$Q_m$  is the simulated streamflow

$Q_o^t$  is the observed streamflow at time  $t$

This study uses this coefficient to calibrate the unknown parameters of the TOPMODEL by comparing the observed and simulated streamflow to find the values of the parameters which make NSE highest. All of these processes can be done by the TOPMODEL package in the R program.

## 2.10 Related research

Throughout the years, researchers and related agencies have conducted researches on various sediment disasters in many areas around the world. For the Huai Nam Phung subbasin, there is an interesting research on the evaluation of the potential of sludge and shoulder sediment (Yumuang, 2005), which has used geographic information systems to analyze and explain the occurrence of sediment flow. Landslides and mixed sediment flooded the Ban Nam Ko community in 2001 and caused large damage to lives and properties of people. From that research, it was found that, in addition to the factor of the amount of rainfall that accumulates from continuous heavy rain in this area, there are also other physical factors. They cause this disaster being especially violent. For example, the collapsed trees blocked the waterway and when the amount of water is enough, there was a pressure to let the debris flow down and the damping force of the water causes the sediment to flow more heavily than usual. In addition, there is a research that compared the occurrence of shallow landslide in Phetchabun province and Krabi province (Ono et al., 2014). The factor of safety in slope stability was used to evaluate the shallow landslide occurrence. Their results showed that the shallow landslide in Phetchabun province

occurred in the western mountain range which is the same area as that mentioned in Yumuang (2005) and the shallow landslide in Krabi province occurred in the areas of Phanom Bencha mountain in Khao Phanom district. Landslides can occur in every type of high slope mountain due to soil mantle saturate with water.

There are several researches that used the factor of safety (FS) in slope stability in the evaluation of landslide occurrence (Aversa et al., 2018; Naidu et al., 2018). Previous studies of Aversa et al. (2018) and Naidu et al. (2018) have explained that value of FS can be classified into 3 classes. If the FS value is more than 1.2, the slope is stable. If the FS value is between 1.0 and 1.2, the slope is unstable. If the FS value is less than 1, the slope is highly unstable. In our study, the author used this classification to evaluate the slope stability in the Huai Nam Phung subbasin.

In modelling, researchers have used the TOPMODEL (TOPography based hydrological MODEL) (Beven and Kirkby, 1979) to study landslides in Taiwan, such as predictions of landslides caused by instability of the area by using the model, Hydrology (Lee and Ho, 2009) Influence of soil thickness distribution on small landslides (Ho et al., 2012) and evaluation of the efficiency of physical models for predicting occurrences. land Small Wind (Ho and Lee, 2017). Research conducted by Lee et al. (2009) is a research using the TOPMODEL to predict the occurrence of landslides in the basin in northern Taiwan. By taking the thickness of the soil covering the rock in that area together with the Wetness index, the Factor of Safety can be determined. The result is a map showing potential for landslides which highly varies upon the locations. Later, Ho and the team (2012) used the same model to study the influence of the distribution of thickness of the soil layer that causes a small landslide. This study was conducted in the southern region of Taiwan. By using the data of spatial distribution of the thickness of the soil layer together with the soil moisture index, it can be seen that the unstable area has a high level of predicted vulnerability. For stable areas with low predicted vulnerability, Ho and the group (2017) conducted a research to compare the potential of physical models used to predict small landslides. The study was conducted in 2 areas in Taiwan by using the TOPMODEL model to analyze 3 processes which are 1. Probability of detection (POD) 2. False alarm ratio (FAR) and 3. Threat score (TS). For all 3 processes, TOPMODEL was used to analyze landslide occurrence in various cases. It is found that the use of POD analysis process provides the most accurate forecasting results when comparing the landslide record data with the real area. According to the analysis of landslide disasters in each area, it is necessary to apply the appropriate principles and theories to do an effective analysis. Therefore, the TOPMODEL model, which is used in the above researches, is one of the models that are very useful for landslides prediction.

There are also researches that used other models to create a disaster map. For example, the research on flood risk areas in the Chi Basin and climate change management (Arunyanart et al., 2017), which used combination of models such as the General Circulation Model (GCM), Statistical Down Scaling Model (SDSM), Soil

and Water Assessment Tool (SWAT), Hydrological Engineering Center - River Analysis System (HEC-RAS) and Geographic Information System (GIS) to create a map of flood risk areas in Chi River Basin, and the research for disaster predictions, landslides and floods using the iCRESTRIGRS (Zhang et al., 2016) model, which is an integration model between Coupled Routing and Excess Storage landslide models (CREST) and the Transient Rainfall Infiltration and Grid-Based Regional Slope-Stability (TRIGRS) hydrographic model for mapping the disaster risk areas. Theories in the above researches can be used to conduct a concrete study on the assessment of landslides in the Huai Nam Phung subbasin. The results of this study will be able to be used as basic information for the development of knowledge about landslide disasters in the future.



## CHAPTER III METHODOLOGY

The methods of consisted of data gathering in Huai Nam Phung subbasin, data preparation for the TOPMODEL and simulation of the factors of safety. The simulation included calibration to adjust the variables in the model, evaluation of the model accuracy, and simulation of factors of safety in Huai Nam Phung subbasin.

### **3.1 Physical appearance of the Huai Nam Phung subbasin**

#### **3.1.1 Territory and location**

The Pasak river basin has an area of approximately 15,625.98 square kilometers and consists of 8 subbasins (**Figure 3.1**), including the upper part of Pasak River subbasin, Huai Nam Phung subbasin, the second part of Pasak River subbasin, the third part of Pasak River subbasin, Huai Ko Kaew subbasin, Lam Sonthi subbasin, the lower part of Pasak River subbasin and Huai Muak Lek subbasin. The shape of the Pasak river basin is long and the parallel to mountain ranges in north-south direction along the eastern and western boundaries. It has a narrow-long plain area lying in the north-south direction between those mountain ranges (**Figure 3.2**).

**The upper part of Pasak River subbasin** has a water storage area of approximately 1,531.97 square kilometers accounting for about 9.76% of the total area in the Pasak river basin. This subbasin covers areas of Dan Sai district in Loei province and Lom Kao district, Lom Sak district and Nam Nao district in Phetchabun province.

**Huai Nam Phung subbasin** has a water storage area of approximately 686.43 square kilometers accounting for about 4.39% of the total area in the Pasak river basin. The subbasin covers areas of the Dan Sai district in Loei province and Lom Kao district and Lom Sak district in Phetchabun province.

**The second part of Pasak River subbasin** has a water storage area of approximately 2,556.59 square kilometers accounting for about 16.36% of the total area in the Pasak river basin. This subbasin cover areas of Khao Ko district, Lom Sak district, and Mueang Phetchabun district in Phetchabun province.

**The third part of Pasak River subbasin** has a water storage area of approximately 4,207.316 square kilometers accounting for about 26.93% of the total area in the Pasak river basin. This subbasin covers areas of Mueang Phetchabun district, Nong Phai district, Bueng Sam Phan district, Wichian Buri district, Si Thep district in Phetchabun province and Chai Badan district in Lopburi province.

**Huai Ko Kaew subbasin** has a water storage area of approximately 496.93 square kilometers accounting for about 3.18% of the total area in the Pasak river basin. This subbasin covers areas of Si Thep district in Phetchabun province and Chai Badan district in Lopburi province.

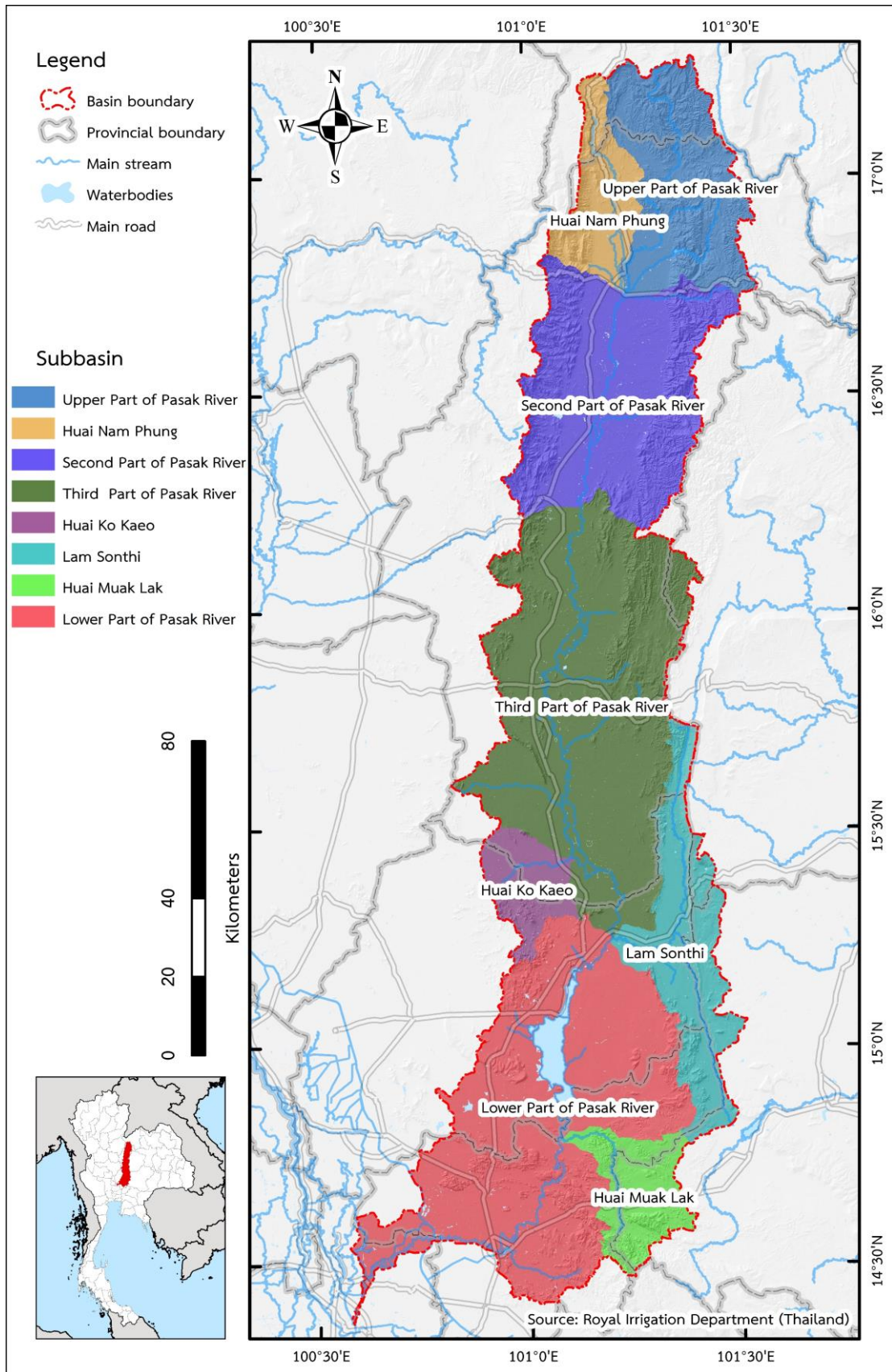
**Lam Sonthi subbasin** has a water storage area of approximately 1,336.96 square kilometers accounting for about 8.56% of the total area in the Pasak river basin. This subbasin covers areas of Thep Sathit district in Chaiyaphum province, Thepharak district, Dan Khun Thot district, Sikhio district, Pak Chong district in Nakhon Ratchasima province, Muak Lek district in Saraburi province and Chai Badan district and Lam Sonthi district in Lopburi province.

**The lower part of Pasak River subbasin** has a water storage area of approximately 4,149.70 square kilometers accounting for about 26.56% of the total area in the Pasak river basin. This subbasin covers areas of Chai Badan district, Phatthana Nikhom district, Tha Luang district, Sa Bot district, Mueang Lopburi district in Lopburi province, Phra Phutthabat district, Sao Hai district, Chaloem Phra Kiat district, Wang Muang district, Muak Lek district, Kaeng Khoi district, Ban Mo district, Nong Don district, Mueang Saraburi in Saraburi province and Tha Ruea district, Nakhon Luang district and Phra Nakhon Si Ayutthaya district in Phra Nakhon Si Ayutthaya province.

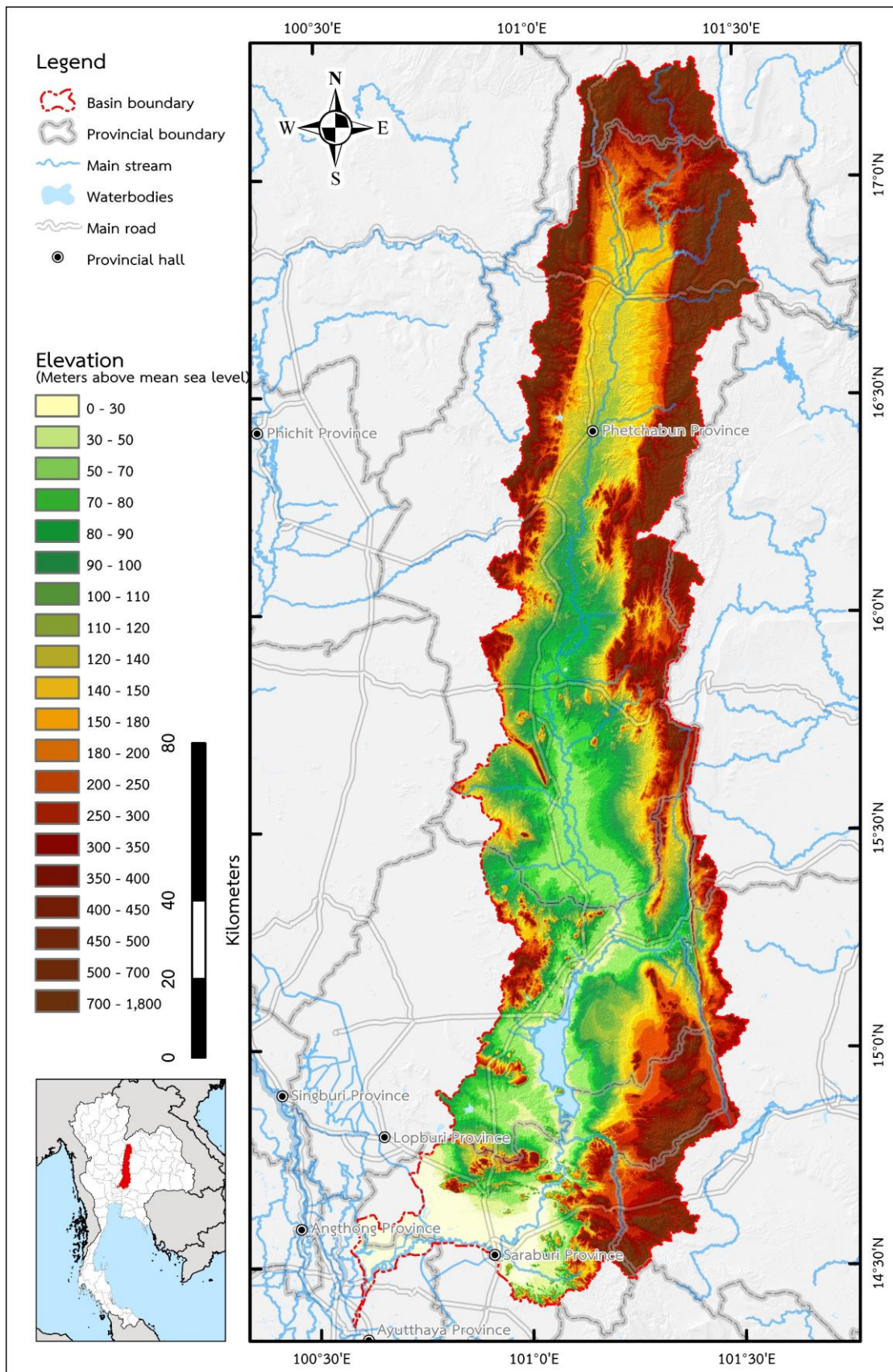
**Huai Muak Lek subbasin** has a water storage area of approximately 665.09 square kilometers accounting for about 4.26% of the total area in the Pasak river basin. This subbasin covers areas of Pak Chong district in Nakhon Ratchasima province and Muak Lek district and Wang Muang district in Saraburi province.

Huai Nam Phung subbasin is a subbasin of the Pasak river basin. It has Nam Phung creek as the mainstream located in the Northwest of the Pasak river basin. This subbasin is small with the total area of 686.43 square kilometers covering the parts of 2 provinces, Loei province and Phetchabun province. It is located between the longitude of 101° 03' 41" E and 101° 17' 17" E and the latitude of 16° 43' 49" N and 17° 14' 22" N (**Figure 3.3**). The upper part of the Huai Nam Phung subbasin covers an area of the Dan Sai district in Loei province while the central and the lower parts cover areas of Lom Kao district and Lom Sak district in Phetchabun province. Huai Nam Phung subbasin has a water storage area of approximately 686.43 square kilometers accounting for about 4.39% of the total area in the Pasak river basin (Royal Irrigation Department Thailand, 2009; Tangtham and Yuwananont, 1996).





**Figure 3.1** Location and subbasins of the Pasak river basin



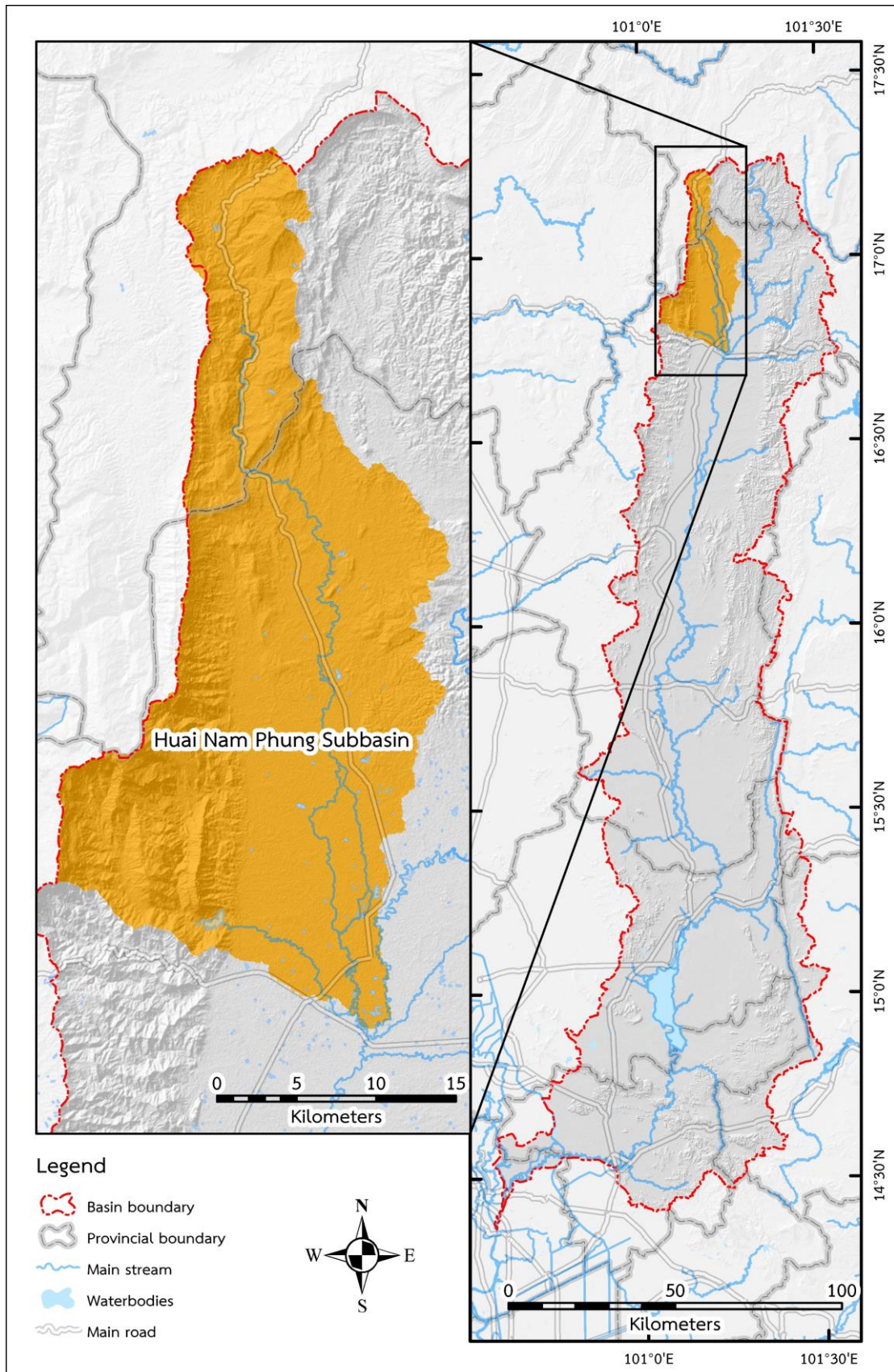


**Figure 3.3** Location of the Huai Nam Phung subbasin

### 3.1.2 Topography

Huai Nam Phung subbasin is a catchment which drain the water from the north to the south. The upper part of catchment is in the area of the Pong subdistrict, Dan Sai district, Loei province. There are many mountains in the northern part of the subbasin, mountains in the east and west lie parallel. The mountain in the northern border is Khao Thong Thaen. The eastern border are Khao Khrok Ma Hon, Phu Pae Nong Klai, Khao Hin Koi, and Khao Sam Si Mon Kaeo in order. The western border are Phu Noi, Khao Sam Muen, and Phu Phaeng Ma in order. Between the parallel mountain ranges, there is a narrow rolling plain along the area of Na Sam subdistrict, Lom Kao district, Phetchabun province. The central and the lower parts of the catchment, there is a mountain range along the west consisted of Phu Thap Boek and Khao Khat that are connected to the Phu Hin Rong Kla national park, and a big plain in the east which is in the areas of Lom Kao district and Lom Sak district, Phetchabun province. The mainstream of the Huai Nam Phung subbasin is Huai Nam Phung, a creek that drains the water from the north to the Pasak river at the outlet in the south in the area of Nong Khwai subdistrict, Lom Sak district, Phetchabun province (**Figure 3.4**).

### 3.1.3 Hydrological gauging stations

This study used the gauging station of the Royal Irrigation Department Thailand (RID Thailand) as a base for the hydrological model. There are 5 gauging stations nearby Huai Nam Phung subbasin (**Figure 3.5**) including S.10, S.41, S.3, S.33, and S.36 (**Figure 3.6**). The details of each station are as the followings,

**S.10 station** is located under the bridge of the road number 21 at the longitude of  $101^{\circ} 12' 54''$  E and the latitude of  $16^{\circ} 56' 53''$  N in the area of Hin Hao subdistrict, Lom Kao district, Phetchabun province. The drainage area covers the area of the upper part of the Huai Nam Phung subbasin, about 269.14 square kilometers or 39.21% of the Huai Nam Phung subbasin. According to the data in 2019, the elevation of the river bed at this station was 162.23 meters above mean sea level and the elevations of both banks were about 171.51 – 172.63 meters above mean sea level.

**S.41 station** is located under the bridge of the road number 2372 at the longitude of  $101^{\circ} 10' 35''$  E and the latitude of  $16^{\circ} 47' 34''$  N in the area of Nam Ko subdistrict, Lom Sak district, Phetchabun province. The drainage area covers the area of the southwestern part of the Huai Nam Phung subbasin, about 70.68 square kilometers or 10.3% of the Huai Nam Phung subbasin. According to the data in 2019, the elevation of the river bed at this station was 164.95 meters above mean sea level and the elevations of both banks were about 171.35 – 171.45 meters above mean sea level.

**S.3 station** is located under the bridge of the road number 2010 at the longitude of  $101^{\circ} 14' 45''$  E and the latitude of  $16^{\circ} 47' 03''$  N in the area of Tan Diao subdistrict, Lom Sak district, Phetchabun province. The drainage area covers the area of the upper part of the Pasak River subbasin, about 1,064.21square kilometers, the

mainstream is the Pasak river. According to the data in 2019, the elevation of the river bed at this station was 139.32 meters above mean sea level and the elevations of both banks were about 146.21 – 146.38 meters above mean sea level.

**S.33 station** is located under the bridge of the road number 2216 at the longitude of 101° 21' 09" E and the latitude of 17° 00' 16" N in the area of Sila subdistrict, Lom Kao district, Phetchabun province. The drainage area covers the area of the upper part of the upper part of Pasak river subbasin, about 516 square kilometers or 48.49% of the upper part of Pasak river subbasin. In 2019, the elevation of the river bed at this station was 190.93 meters above mean sea level and the elevations of both banks were about 198.76 – 198.82 meters above mean sea level.

**S.36 station** is located under the bridge of the road number 12 at the longitude of 101° 14' 21" E and the latitude of 16° 43' 47" N in the area of Pak Duk subdistrict, Lom Sak district, Phetchabun province. The drainage area covers the area of the upper part of Pasak river subbasin, Huai Nam Phung subbasin, and Huai Khon Kaen catchment, about 2,220.6 square kilometers or 14.21% of Pasak river basin. According to the data in 2019, the elevation of the river bed at this station was 138.15 meters above mean sea level and the elevations of both banks were about 139.46 – 141.15 meters above mean sea level.

The streamflow of the Huai Nam Phung subbasin is directly varies with the rainfall. the streamflow is high in the rainy season and low in the winter and summer. In the winter and summer, drought occurs in some areas because there is no streamflow.

The annual average streamflow of the Huai Nam Phung subbasin is about 153.36 million cubic meters. The information of Pasak River basin from the Hydro Informatics Institute suggests that the relationship between the catchment area and the streamflow in Pasak River basin is as the equation 3.1 with the  $a$  and  $b$  equal to 0.5785 and 0.8545, respectively. This equation yields the coefficient of determination ( $R^2$ ) of 0.9761 (**Figure 3.7**).

$$Q_F = aA^b \quad 3.1$$

where  $Q_F$  is annual average streamflow (million cubic meter)  
 $A$  is the catchment area (square kilometers)  
 $a$  and  $b$  are the regression coefficients



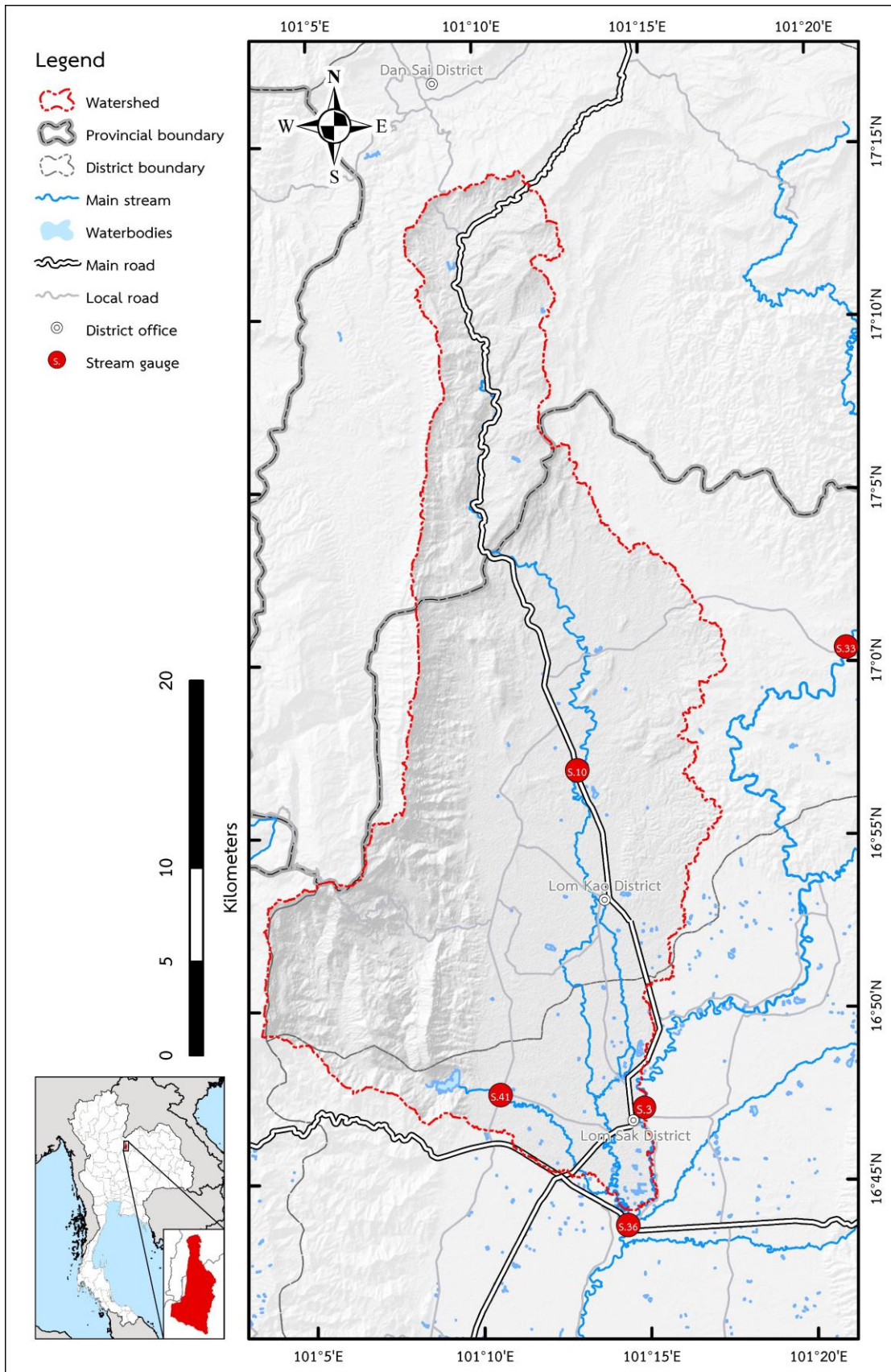
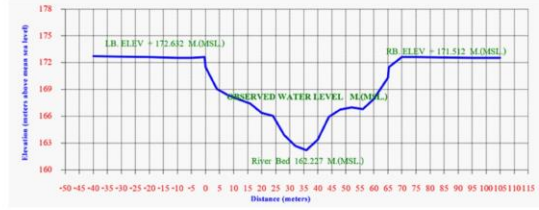


**Figure 3.5** Locations of stream gauges nearby the Huai Nam Phung subbasin



**S.10**  
Huai Nam Phung, rd.no. 21, Hin Hao, Lom Kao, Phetchabun



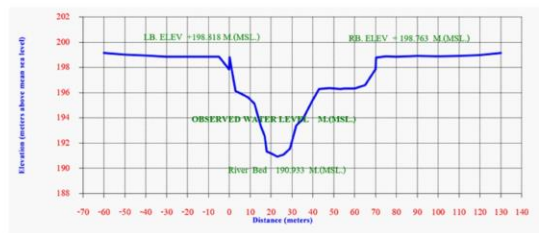
**S.41**  
Huai Nam Ko, rd.no. 2372, Nam Ko, Lom Sak, Phetchabun



**S.3**  
Pasak river, rd.no. 2010, Tan Diao, Lom Sak, Phetchabun



**S.33**  
Pasak river, rd.no. 2216, Sila, Lom Sak, Phetchabun



**S.36**  
Pasak river, rd.no. 12, Pak Duk, Lom Sak, Phetchabun

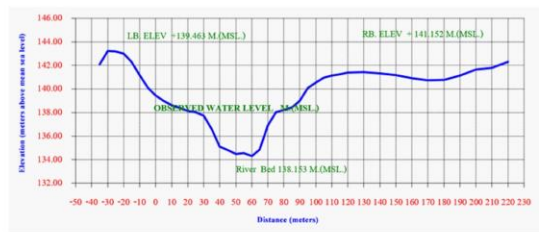


**Figure 3.6** Stream gauges of the Royal Irrigation Department Thailand which are nearby the Huai Nam Phung subbasin and the cross sections at those stream gauges



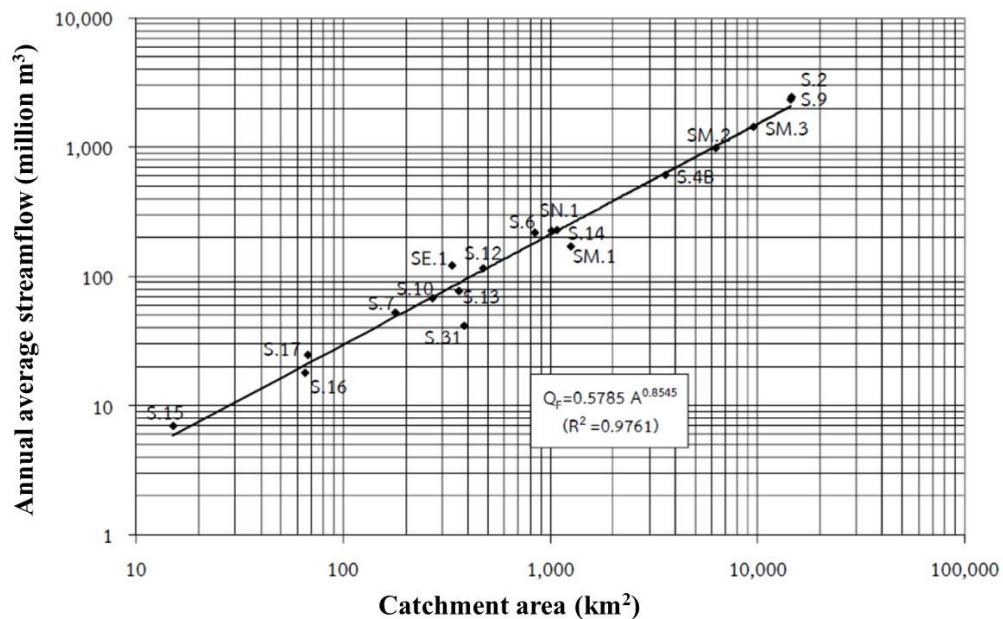


**Figure 3.7** Relationship between annual average streamflow and catchment area (Institute of Water Resources and Agriculture Information Thailand, 2012)

### 3.1.4 Climatology and meteorology

Huai Nam Phung subbasin is located in the upper central part of Thailand. There are 2 monsoons that influence the area in each year which includes the southwest monsoon and the northeast monsoon. The southwest monsoon blows from the southwest to the northeast from May to October. It causes the rainy season. The northeast monsoon blows from the northeast to the southwest from November to January. It causes the winter. In addition, there is summer from February to April. In the summer, the weather is dry and there is little rainfall.

The annual average rainfall in the Huai Nam Phung subbasin is about 100 millimeters per year. Most of the rainfalls occur in the rainy season, from May to October (170 millimeters). The highest amount of rainfall is in about September. In the winter and summer, from November to April, the rainfall amount is little (20 millimeters). There are 11 raingauges around the Huai Nam Phung subbasin (**Figure 3.8**). They are operated by the Thai Meteorological Department.

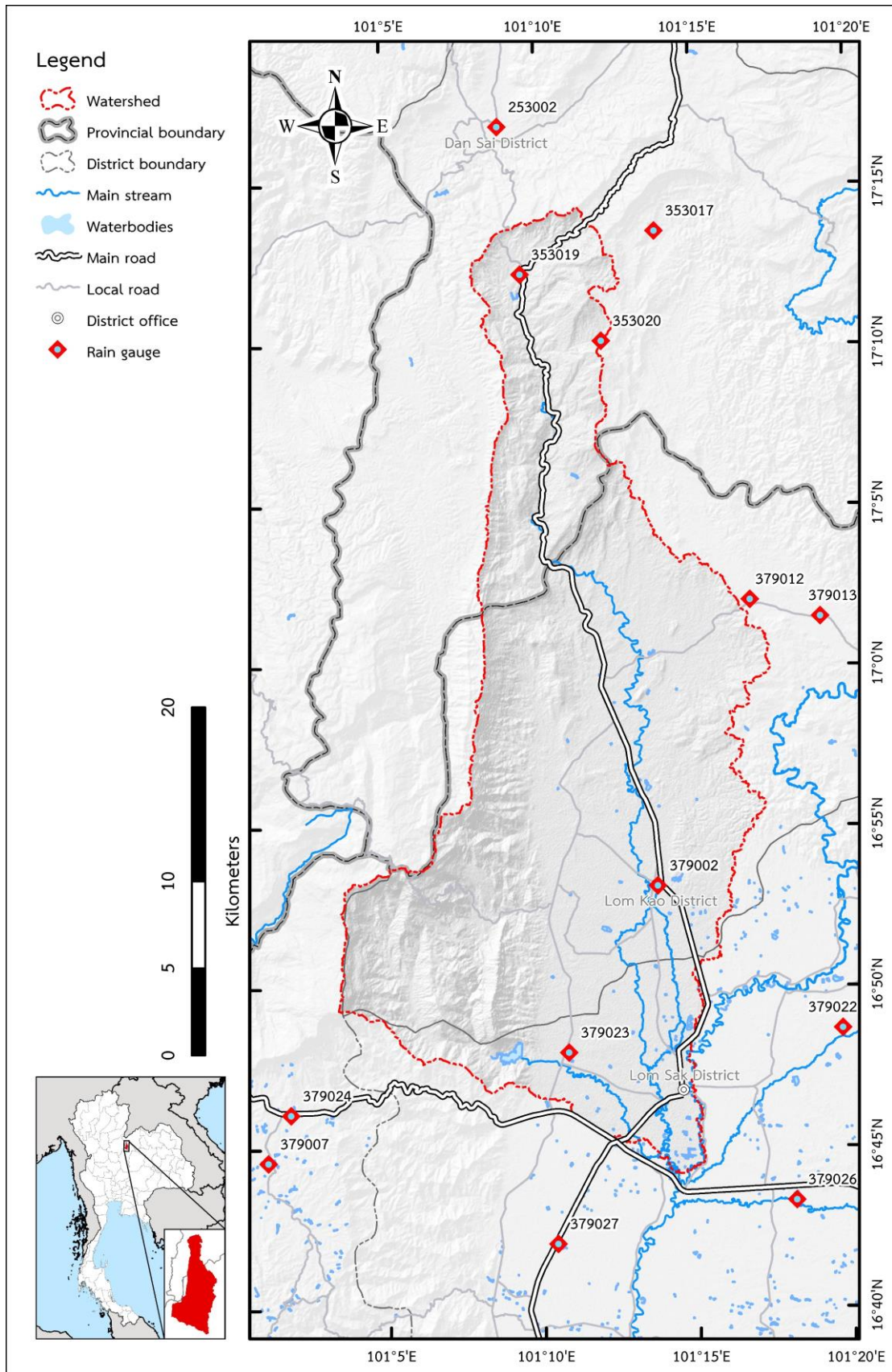


**Figure 3.8** Raingauges around the Huai Nam Phung subbasin

### 3.1.5 Hydrogeology

The hydrogeological map with a scale of 1:100,000 has been provided by the Department of Mineral Resources of Thailand. It shows that the Huai Nam Phung subbasin have 10 types of the hydrogeological structure. The largest proportion is the Lower Khorat aquifer (TRJlk), which accounts for 47.12% of the total catchment area, followed by the Semiconsolidated aquifer (Tsc), which accounts for 18.09% of the total catchment area (**Figure 3.9**).

**Table 3.1** Aquifers in the Huai Nam Phung subbasin

| Symbol  | Aquifer                                    | The depth of the groundwater layer (m) | Watering ability (m <sup>3</sup> /h) | Area (km <sup>2</sup> ) | %     |
|---------|--|--|--------------------------------------|-------------------------|-------|
| TRJlk   | Lower Khorat aquifer                       | 30 – 60                                | 2 – 10                               | 323.03                  | 47.12 |
| Tsc     | Semiconsolidated aquifer                   | 30 – 50 / 200                          | 1 – 20                               | 124.05                  | 18.10 |
| Np      | Namphong aquifers                          | –                                      | –                                    | 88.23                   | 12.87 |
| PCms    | Permian Carboniferous Metasedments aquifer | 10 – 60                                | 1 – 20                               | 47.01                   | 6.86  |
| Pp      | Phuphan aquifers                           | –                                      | –                                    | 34.16                   | 4.98  |
| Jmk     | Middle Khorat aquifer                      | 30 – 60                                | 2 – 10                               | 33.30                   | 4.86  |
| Pc      | Permian Carbonate aquifer                  | 20 – 40                                | 1 – 40                               | 15.08                   | 2.20  |
| Pk      | Phu Kradung aquifers                       | –                                      | –                                    | 3.31                    | 0.48  |
| Qfd     | Floodplain Deposits aquifer                | 15 – 50                                | 5 – 30                               | 1.72                    | 0.25  |
| Kk      | Khok Kruat aquifers                        | –                                      | –                                    | 1.61                    | 0.23  |
| No data | No data                                    | –                                      | –                                    | 14.07                   | 2.05  |

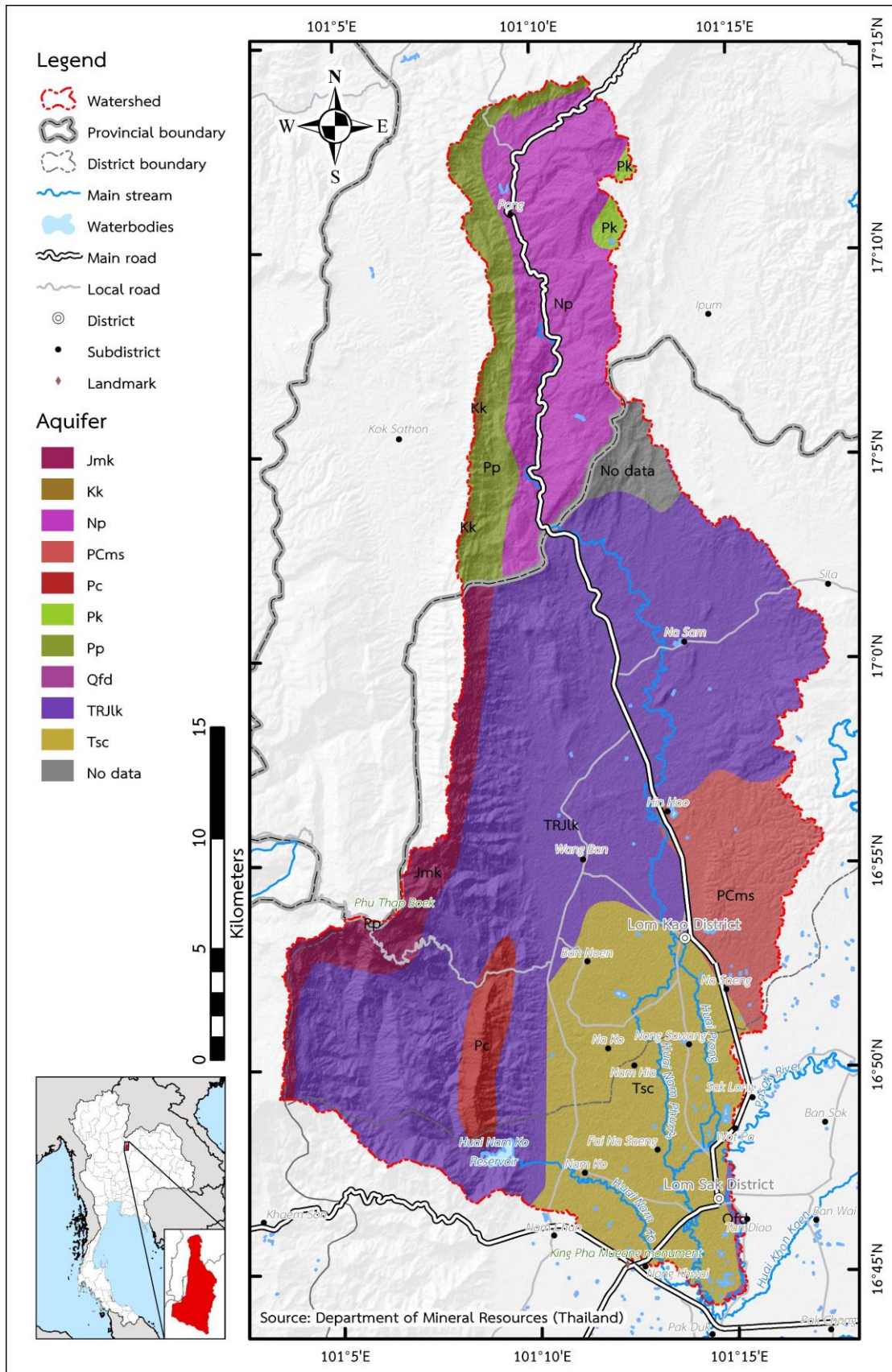


**Figure 3.9** Hydrogeological map of the Huai Nam Phung subbasin

### 3.1.6 Geology

The geological map in 2007 with the scale of 1:250,000 has been provided by the Department of Mineral Resources of Thailand. It shows that the Huai Nam Phung subbasin has 8 types of geological structure. The largest proportion is consisted of conglomerate, gray and reddish-brown sandstone and siltstone, gray, grayish-yellow, and reddish-brown, shale and gray calcareous mudstone, limestone and gray argillaceous (Trhl), which accounts for 32.31% of the total catchment area, followed by siltstone, purplish-red, reddish-brown to brown micaceous sandstone, brown to gray sandstone and some lime nodule conglomerate (Jpk), which accounts for 13.44% of the total catchment area (**Table 3.2 and Figure 3.10**).

**Table 3.2** Geology of the Huai Nam Phung subbasin

| Symbol | Description  | Formation    | Group  | Age                   | Area (km <sup>2</sup> ) | %     |
|--------|--|--------------|--------|-----------------------|-------------------------|-------|
| Qa     | Alluvial deposits: river gravel, sand, silt and clay   | Q2-NE47-16   |        | Quaternary            | 52.38                   | 7.64  |
| Qt     | Terrace, talus and colluvial deposits: gravel, sand, silt and clay   | Q1-NE47-16   |        | Quaternary            | 87.80                   | 12.81 |
| Kpp    | Sandstone and conglomerate, greenish-gray, white, commonly cross-bedded, intercalated with reddish-brown siltstone and limestone conglomerate                          | Phu Phan     | Khorat | Cretaceous            | 31.20                   | 4.55  |
| Ksk    | Sandstone, reddish-brown, micaceous; sandstone, grayish-brown, reddish-brown; shale, purplish-brown, brick red, micaceous; and lime-nodule conglomerate                | Sao Khua     | Khorat | Cretaceous            | 74.24                   | 10.83 |
| JKpw   | Sandstone, white to pale brown, cross-bedded, massive; siltstone, reddish-brown to gray sandstone, micaceous   | Phra Wihan   | Khorat | Lower-Middle Jurassic | 87.91                   | 12.82 |
| Jpk    | Siltstone, purplish-red, reddish-brown to brown, micaceous; sandstone, brown to gray sandstone; and some lime nodule conglomerate                                      | Phu Kradung  | Khorat | Lower Jurassic        | 92.16                   | 13.44 |
| Trhl   | Conglomerate, gray and reddish-brown sandstone and siltstone, gray, grayish-yellow, and reddish-brown; shale, gray, calcareous; mudstone; limestone, gray argillaceous | Huai Hin Lat | Khorat | Upper Triassic        | 221.49                  | 32.31 |
| Ps     | Thin-bedded, gray, and chert, intercalated with gray limestone; locally phyllite and schist  | Sap Bon      |        | Middle-Upper Permian  | 38.38                   | 5.60  |

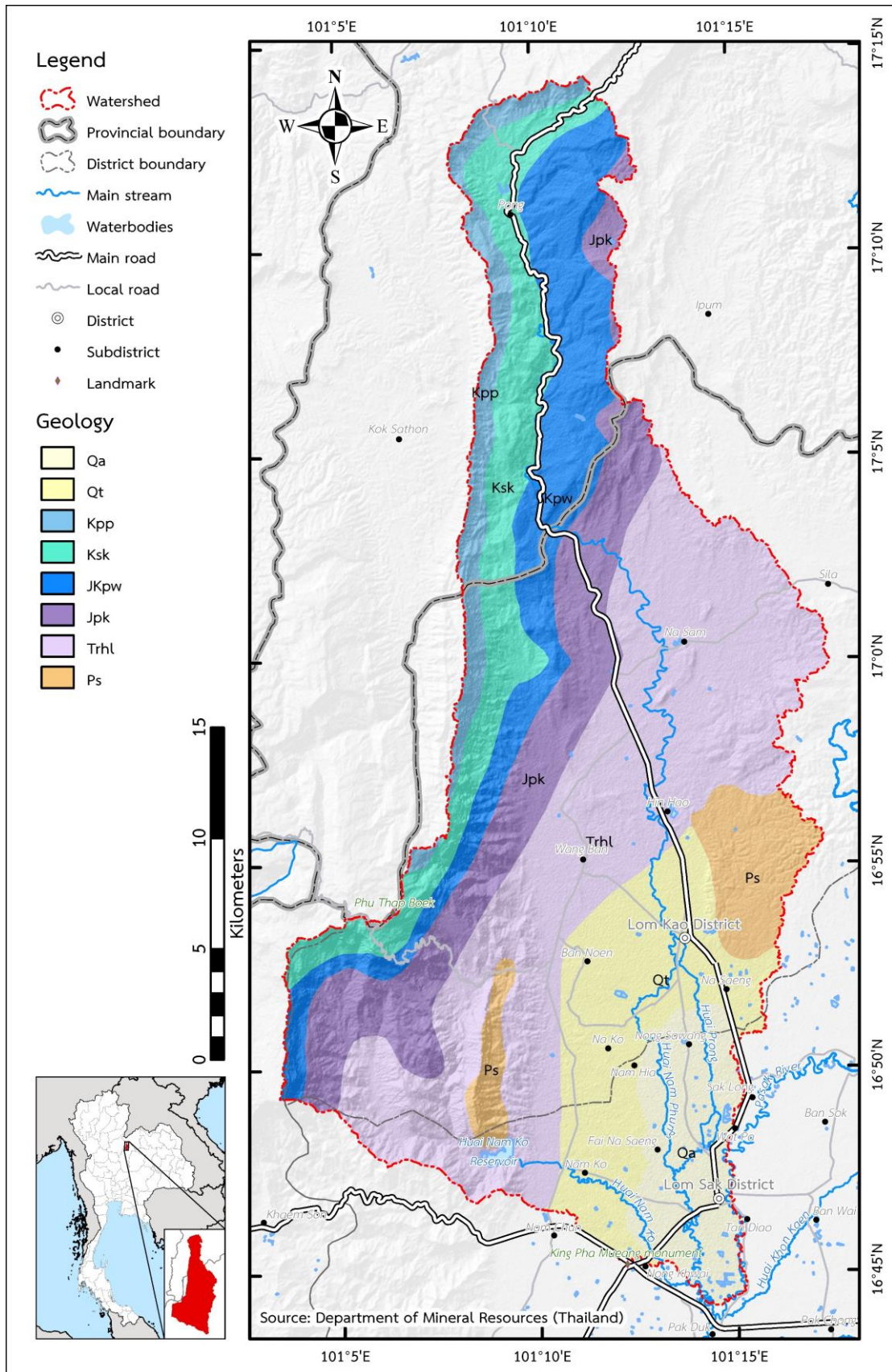


**Figure 3.10** Geological map of the Huai Nam Phung subbasin

### 3.1.7 Land use and land cover

The Huai Nam Phung subbasin is located in the Loei and Phetchabun provinces. The majority of land use type is agricultural area, such as corn fields and cassava fields. From a field survey and an imagery survey in 2018, most communities are located on plains, especially in the western part of the catchment. There are a lot of populated communities. The eastern part is mainly agricultural area with some sparse city area. In the watershed area of the Huai Nam Phung subbasin, there are 2 cities, namely Lom Kao district and Lom Sak district of Phetchabun province. In addition, there is a forest area in Phu Thap Boek which is connected with Phu Hin Rong Kla National Park. This national park also covers some part of the Huai Nam Ko catchment. The upper part of the Huai Nam Phung subbasin in Dan Sai district, Loei province, is characterized by its corrugated plains alternating with mountains. The western edge of the catchment has a mountainous landscape stretching in a long line. The area is mainly covered by forested area interspersed with hilltop agricultural area. Because these agricultural areas have relatively high slopes, these areas are more vulnerable to landslides than on the plains.

From the study of land use and land cover maps provided by the Land Development Department Thailand (**Table 3.3**) in 2002, most of the land was agricultural areas which are account for 52.16%, followed by forested areas which are accounted for 41.83% (**Figure 3.11**). In 2016, agricultural areas remained the majority of the basin with the coverage of 58.95%, increasing from 2002 by 6.79%, followed by the forest area with the coverage of 32.19%, decreasing from 2002 by 9.64% (**Figure 3.12**).

**Table 3.3** Comparison of land use and land cover in the Huai Nam Phung subbasin between 2002 and 2016

| Code | Land use and land cover | 2002                    |       | 2016                    |       |
|------|-------------------------|-------------------------|-------|-------------------------|-------|
|      |                         | Area (km <sup>2</sup> ) | %     | Area (km <sup>2</sup> ) | %     |
| A    | Agriculture             | 357.41                  | 52.16 | 404.13                  | 58.95 |
| F    | Forest                  | 286.64                  | 41.83 | 220.69                  | 32.19 |
| U    | Urban                   | 9.66                    | 1.41  | 42.18                   | 6.15  |
| W    | Water                   | 0.86                    | 0.13  | 4.74                    | 0.69  |
| M    | Miscellaneous           | 30.64                   | 4.47  | 13.82                   | 2.02  |

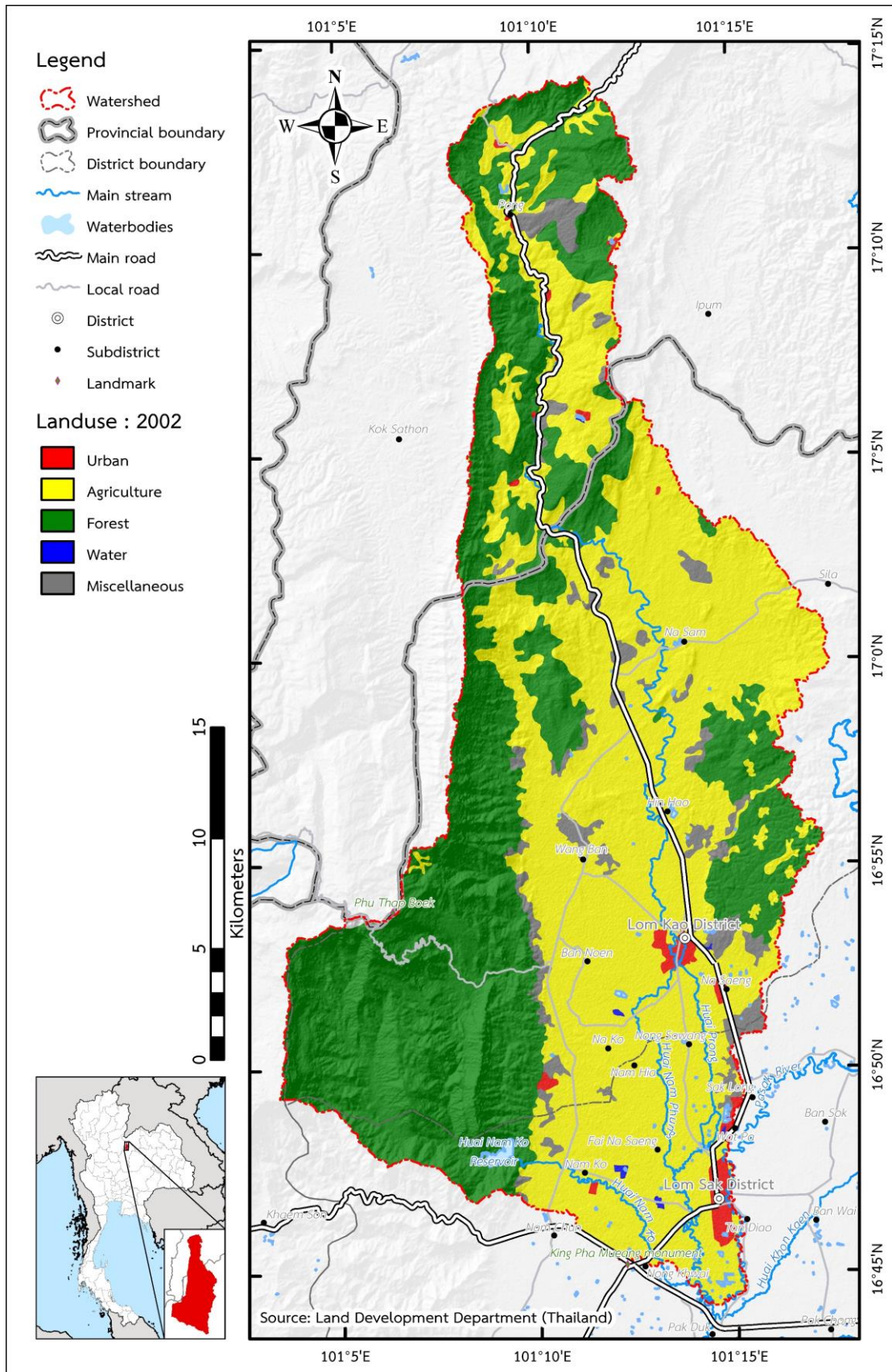


**Figure 3.11** Land use and land cover map of the Huai Nam Phung subbasin in 2002



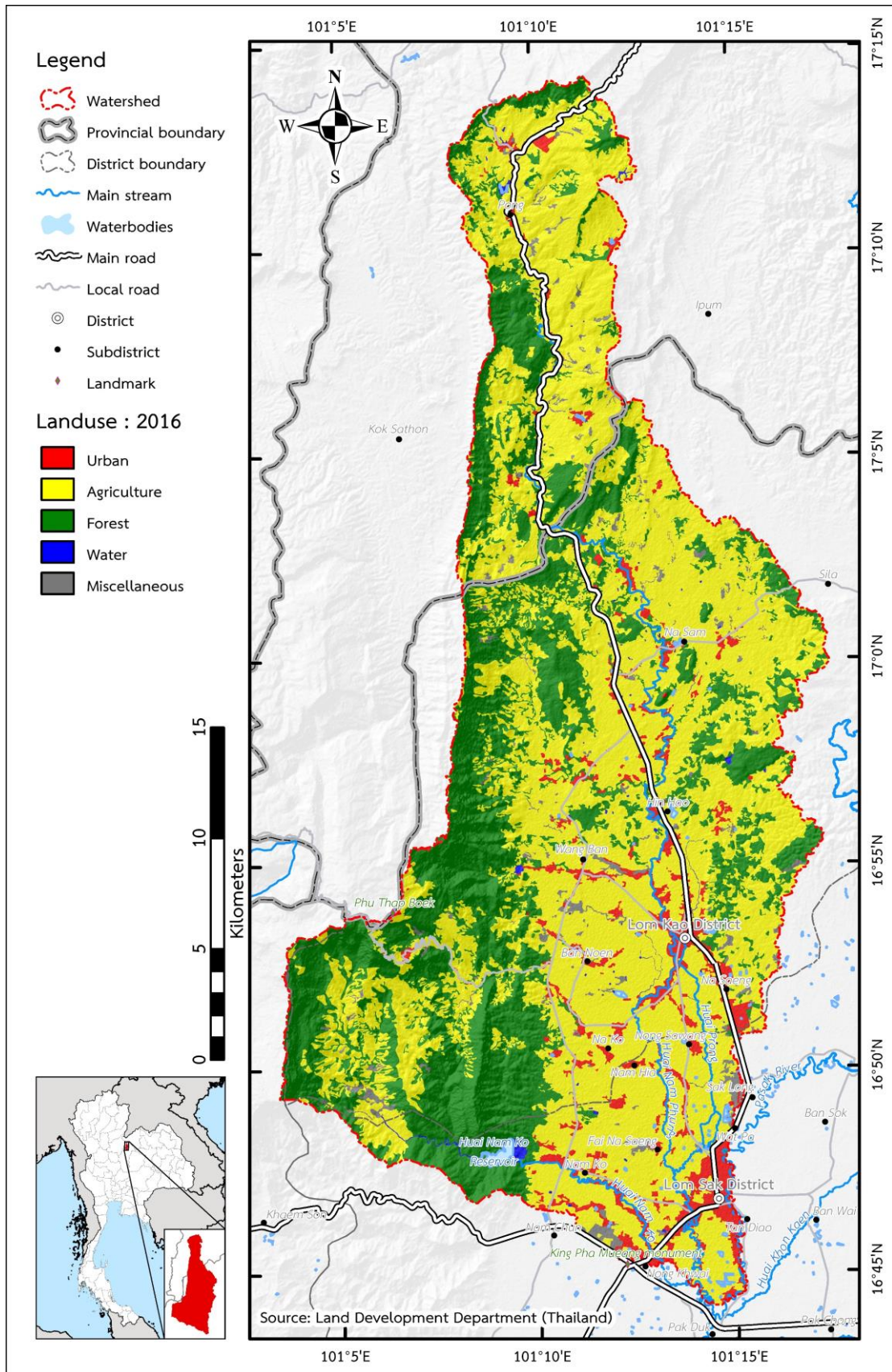


**Figure 3.12** Land use and land cover map of the Huai Nam Phung subbasin in 2016

### 3.1.8 Watershed quality class

According to the watershed class map provided by the Office of Natural Resources and Environmental Policy and Planning of Thailand, most areas of the Huai Nam Phung subbasin fall into 5<sup>th</sup> quality class which is accounted for 29.01% of the total area. The area with 5<sup>th</sup> quality class are mainly found in the plains of the east and south of the catchment. The second largest class is the 1<sup>st</sup> A quality class which is accounted for 27.64% of the total area. The area with 1<sup>st</sup> A quality class are found in the upstream areas of the north and west of the catchment (**Table 3.4 and Figure 3.13**).

The 1<sup>st</sup> A and 1<sup>st</sup> B classes are the upstream areas while 1<sup>st</sup> A is upper than 1<sup>st</sup> B, most of these areas are forest. The 2<sup>nd</sup> class is the lower upstream areas, most of this area is forest and agriculture. The 3<sup>rd</sup> class is the middle class of basin, the area that is forest or agriculture. The 4<sup>th</sup> and 5<sup>th</sup> classes are the lowland within the basin while 5<sup>th</sup> class is lower than 4<sup>th</sup> class, most of these areas are agriculture.

**Table 3.4** Watershed quality class of the Huai Nam Phung subbasin

| Watershed quality class | Area (km <sup>2</sup> ) | %     |
|-------------------------|-------------------------|-------|
| 1 <sup>st</sup> A       | 189.46                  | 27.64 |
| 1 <sup>st</sup> B       | 54.18                   | 7.90  |
| 2 <sup>nd</sup>         | 63.02                   | 9.19  |
| 3 <sup>rd</sup>         | 73.96                   | 10.79 |
| 4 <sup>th</sup>         | 106.09                  | 15.47 |
| 5 <sup>th</sup>         | 198.85                  | 29.01 |

### 3.1.9 Reservoir

There are 2 large water reservoirs in the Huai Nam Phung subbasin, the Huai Nam Ko reservoir and the Huai Nam Hia reservoir. Both reservoirs are located in the southwestern valley of the subbasin, near the entry of Phu Thap Boek. The details of the reservoirs are as follows:

**Huai Nam Ko reservoir** is a soil dam. The ridge of the dam is located at the longitude of 101° 09' 19" E and the latitude of 16° 48' 00" N, in the area of Nam Ko subdistrict, Lom Sak district, Phetchabun province. This reservoir covers an area of approximately 70 square kilometers (**Figure 3.14**).

**Huai Nam Hia reservoir** has been under construction since 2018. The project area is located at the longitude of 101° 08' 37" E and the latitude of 16° 51' 52" N, in Ban Noen subdistrict, Lom Kao district, Phetchabun province. It has an area of approximately 21 square kilometers (**Figure 3.15**).

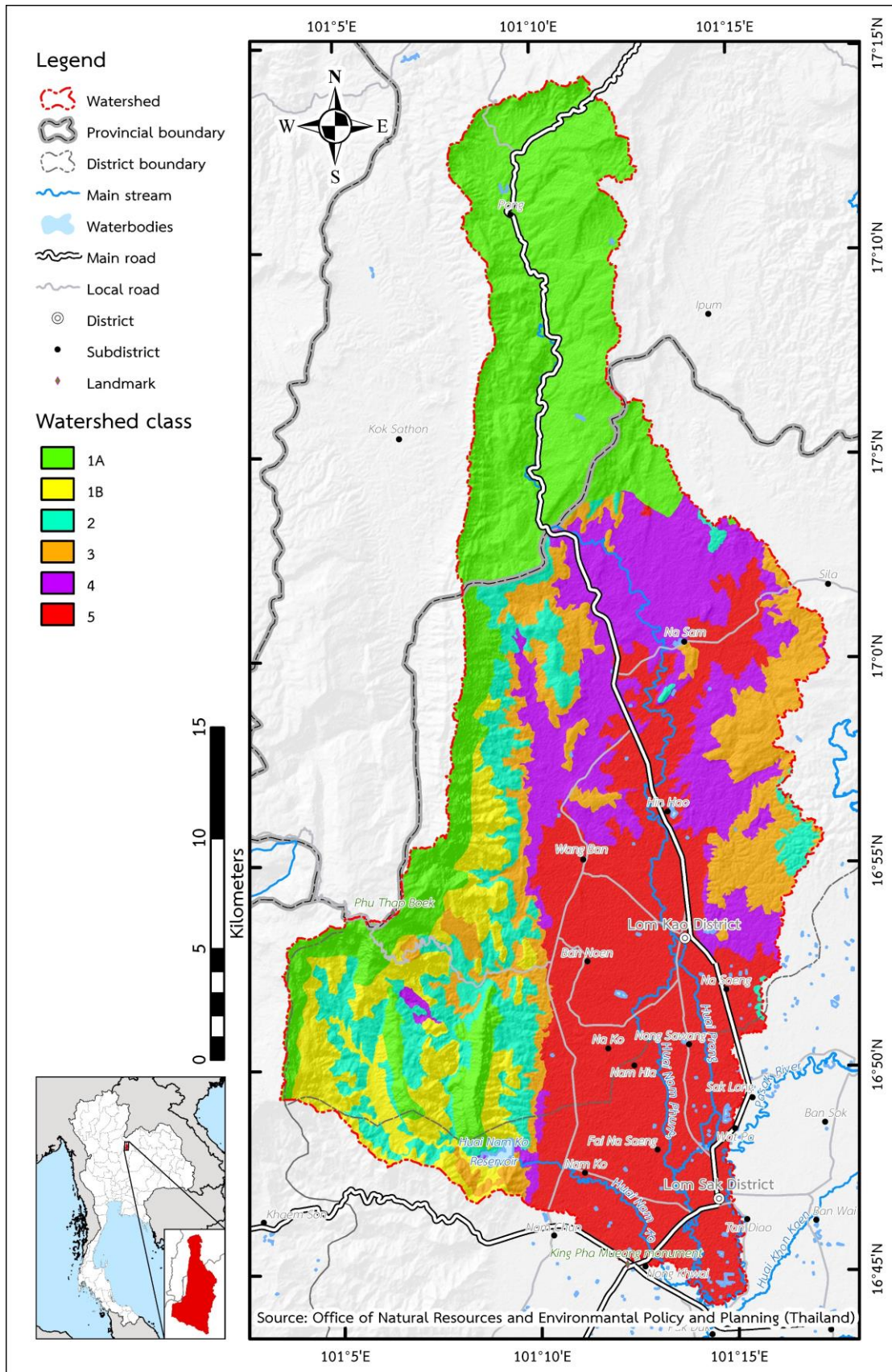


**Figure 3.13** Watershed quality class map of the Huai Nam Phung subbasin



**Figure 3.14** Huai Nam Ko reservoir (Google, 2017)

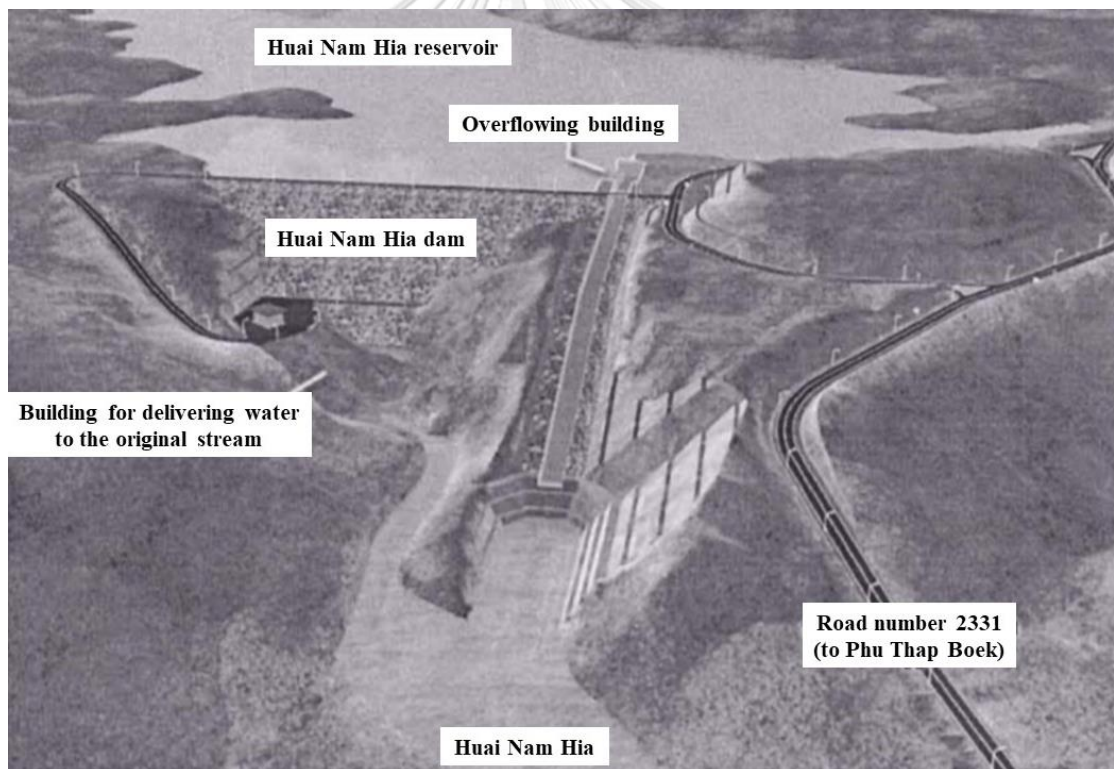


**Figure 3.15** Project of the Huai Nam Hia reservoir (Royal Irrigation Department Thailand, 2011)

## **3.2 Landslide survey**

This study conducted a satellite image analysis to survey the occurrence of landslides, especially in areas with a slope of 20 degrees or more, which is at risk of landslides. After completing the visual survey, a field survey was conducted to check whether the results were consistent. Next, a map showing landslides was created to be used as a database for evaluating landslides in the next step.

### **3.2.1 Imagery survey**

Satellite images are spatial data obtained from resource exploration satellites. Currently, there are a lot of resource exploration satellites orbiting to explore changes in the surface of the earth. The satellites that are popular for researches are Landsat satellites since the data from those satellite is easily accessible and are public information. However, the public data from Landsat satellites still has restrictions on resolution. The data has a resolution of  $30 \times 30$  meters. Therefore, it cannot be used to survey landslides smaller than 30 meters. Nevertheless, there are still high-resolution public image data such as photos provided by Google, which has been synthesized from satellite and aerial imagery from multiple sources. It can be used to explore the landslide area at a resolution of  $5 \times 5$  meters and can also be looked back at different times with Google Earth Pro.

### **3.2.2 Field survey**

The field survey was the validation of the visual survey data in order to check whether the landslides occurred in the surveyed area or not. However, due to the large size of the study area, the field survey could not be done thoroughly. Therefore, it was necessary to randomly select sample areas where landslides occurred.

## **3.3 Soil thickness mapping**

The soil thickness is a variable used to calculate the factor of safety in slope stability. It was also an important variable to calculate other variables such as the groundwater depth. This study brought the relationship between the topographic wetness index (TWI) and the observed soil thickness to generate the soil thickness map following the previous studies of Lee et al. (2009) and Ho et al. (2012) which were conducted in Taiwan. Those studies used the linear relationship to generate the soil thickness map in their study areas. Therefore, this study applied that theory to generate the soil thickness map in the Huai Nam Phung subbasin.

## **3.4 Meteorological data interpolation**

Rainfall data is one of the important data for the analysis with the TOPMODEL. However, the input data which can be imported to the model must be the average areal data of the study area for each timestep. With this reason, a single mean value must be calculated. Analysis by a geographic information system was used for this purpose. There are several interpolate methods, such as inverse distance weighting (IDW), spline, kriging, trend, etc. For the Huai Nam Phung subbasin, the terrain is mostly flat with mountains only in the western border and the north. IDW is

most suitable for that area since this method interpolates the data by averaging the data using a weight calculated from a distance between each station regardless of its location (Ikechukwu et al., 2017).

Apart from the rainfall data, an evaporation data is also required to be interpolated and calculated as a single mean value. However, for the Huai Nam Phung subbasin, there is only one station where the evaporation was measured. Therefore, the data from that station was used as the single mean value.

### 3.5 Observed streamflow data transferring

Observed streamflow was a very important data because it was used to calibrate the model to find the most suitable values of the parameters, which made the simulated streamflow as close as to the observed streamflow as possible. The process would be easier if there was a streamflow measurement station at the outlet of the study area. However, the Huai Nam Phung subbasin does not have a station. For this reason, it was necessary to estimate the data from the nearby station, S.3 station.

S.3 station is a streamflow measurement station of the Royal Irrigation Department that is located in the Pasak river. The catchment area of the S.3 station is next to the Huai Nam Phung subbasin in the eastern side. It is slightly larger than the Huai Nam Phung subbasin. The terrains of the Huai Nam Phung subbasin and the catchment area of the S.3 station is similar (**Figure 3.16**). With this reason, the observed streamflow data from the S.3 station was used to estimate the streamflow data of the Huai Nam Phung subbasin.

The transferring of the observed streamflow data was following the linear relationship between annual average streamflow and catchment area.

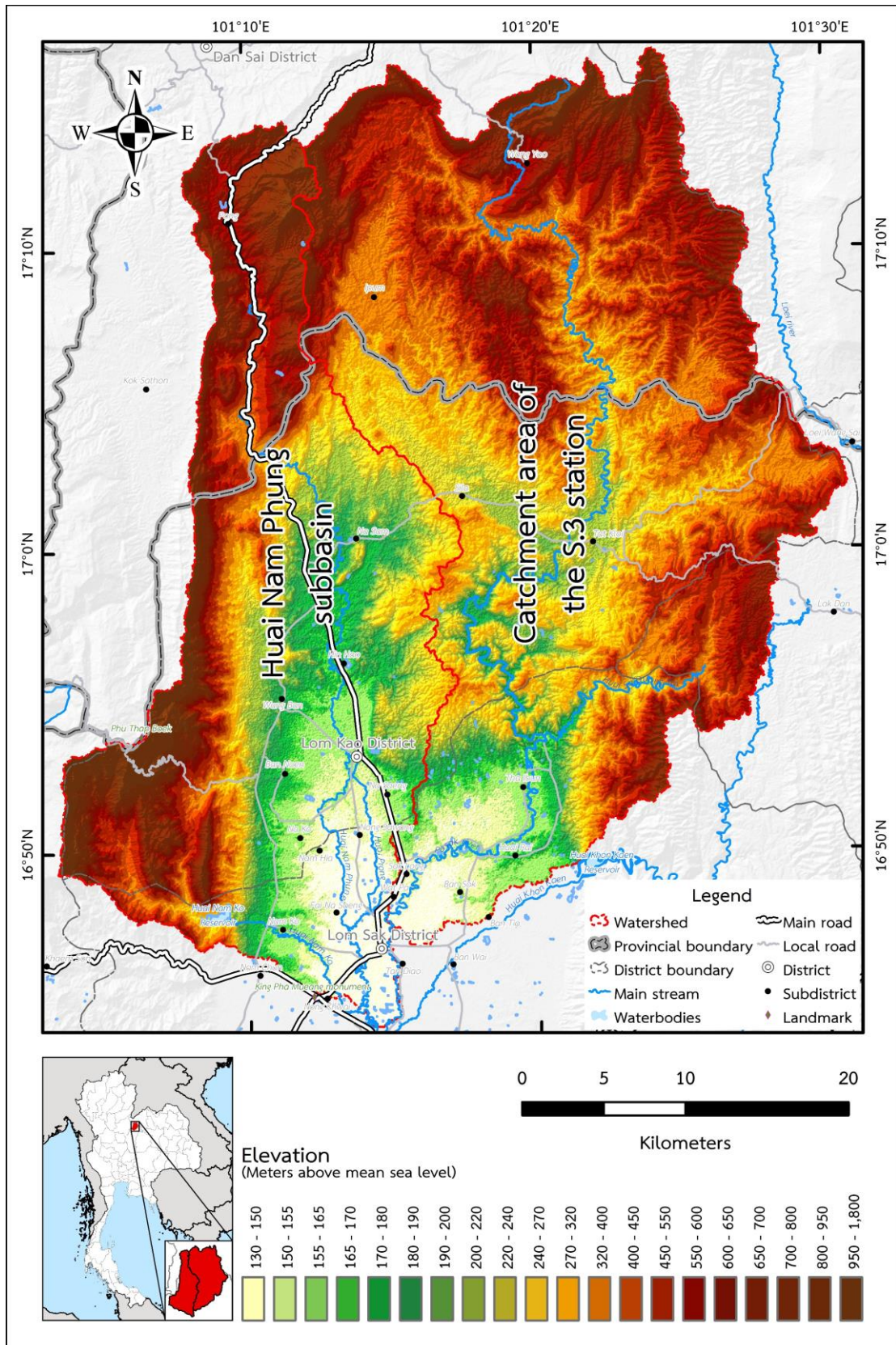


**Figure 3.16** Topographic map of the Huai Nam Phung subbasin and catchment area of the S.3 station

### 3.6 Streamflow simulation using the TOPMODEL

The analysis by the TOPMODEL requires calibrating to find the appropriate values of parameters for the study area. Therefore, streamflow data was very important for the comparison to get the simulation results that are closest to observed data. For this study, streamflow simulation was not the main content in landslides evaluation, but the average height between soil surface and groundwater level included in the streamflow simulation was important for calculation of the groundwater level, which was an important variable in evaluating the landslide occurrences.

#### 3.6.1 Data gathering

The data required for the analysis by the TOPMODEL consisted of the topographic wetness index (TWI), delay function, rain, and evaporation. The TWI was generated from the surface slope by using equation 2.3, it was an index that indicates the humidity of the area according to the topography. Next, the delay function was generated from the flow length in the catchment. This function would show the relationship between the stream length and the cumulative relative area. It could be generated by R program. The next one was rain data. It was generated as the mean values in the catchment. There were several raingauges in the study area. Therefore, an interpolation was required to get a single mean value for each timestep. The last one was the evaporation. There was only one meteorological station nearby the study area that had this data. Therefore, so the interpolated was not required.

#### 3.6.2 Model processing

In the simulation process, it was necessary to define parameters for the model to make it able to display the results. These parameters can be seen in the **Table 3.5**. This study used the default values in the TOPMODEL tutorial (Buytaert, 2009) for each parameter. Model processing of this study would explain in **Figures 3.17 to 3.19**.

#### 3.6.3 Model calibration

From the TOPMODEL tutorial, the Monte-Carlo method could be used to assign the values of parameters. Then, the Nash–Sutcliffe model efficiency coefficient (NSE) was calculated for each simulation with each set of random parameters. The set of the parameters which make the NSE closest to 1 was the most appropriate one to simulate the streamflow. In order to make the calibration easier, the sensitivity analysis was done to find the sensitivity index of each parameter. The parameters with higher sensitivity indices were calibrated before the parameters with lower sensitivity indices.



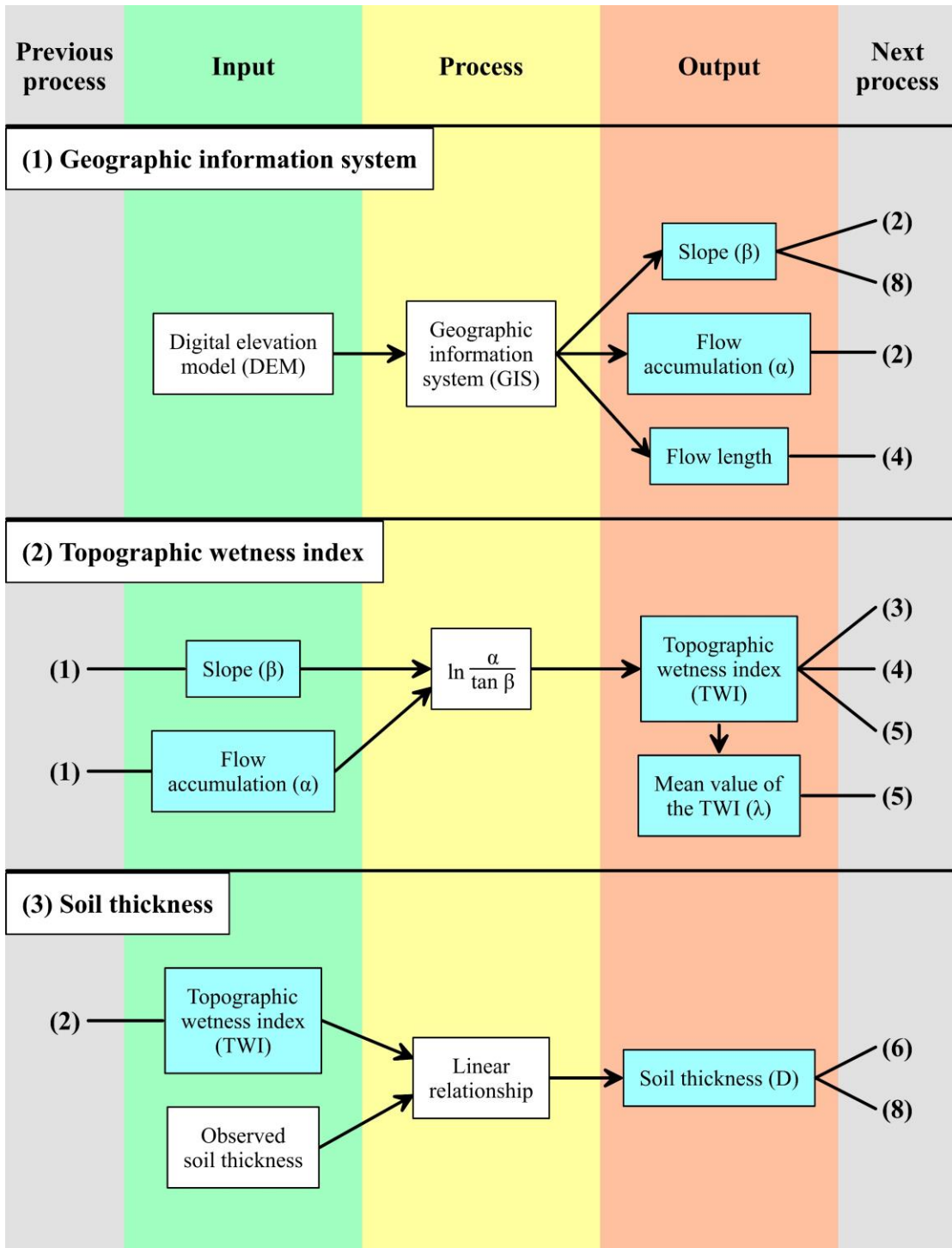


Figure 3.17 Flowchart of research procedure (page 1 of 3)

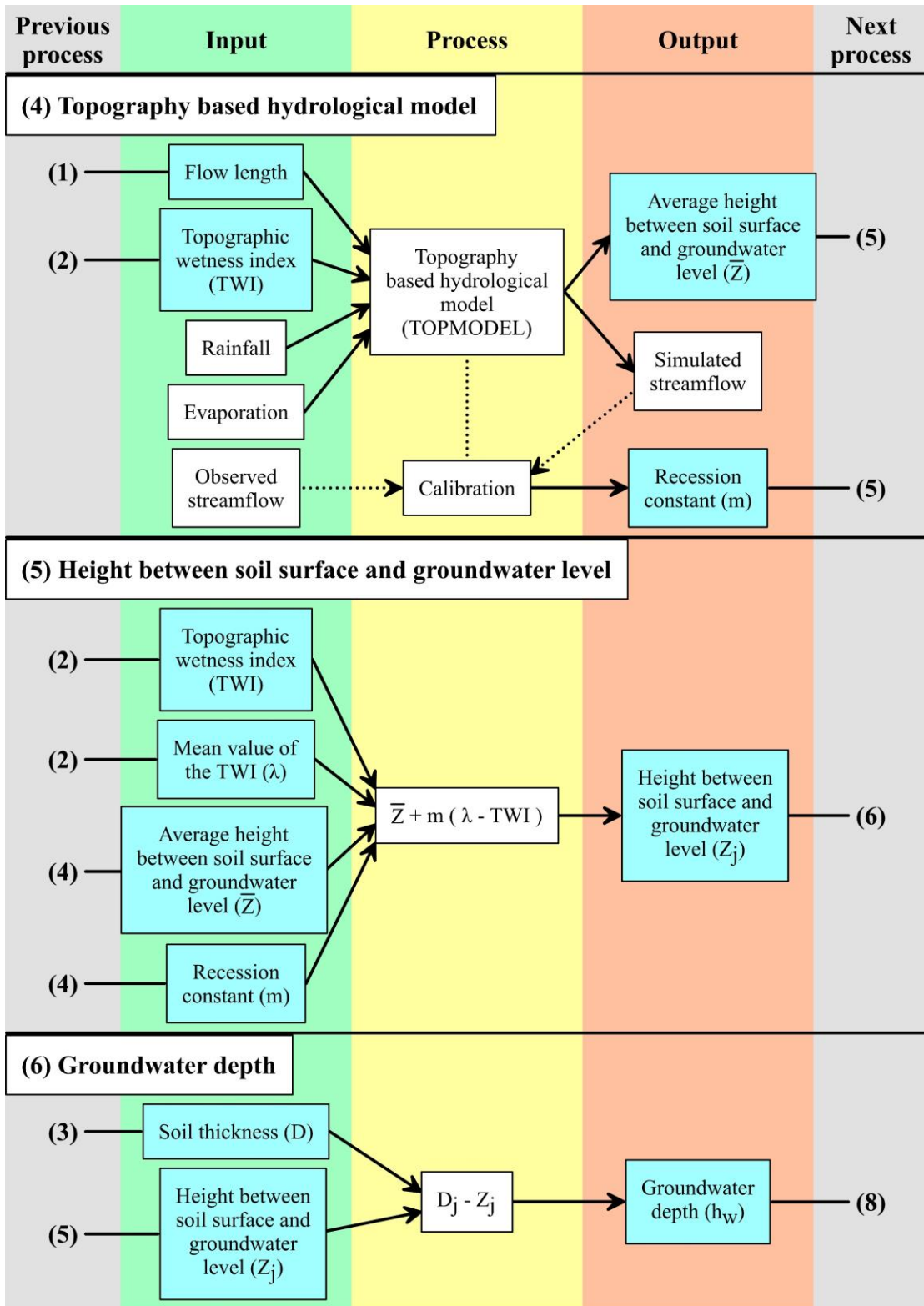
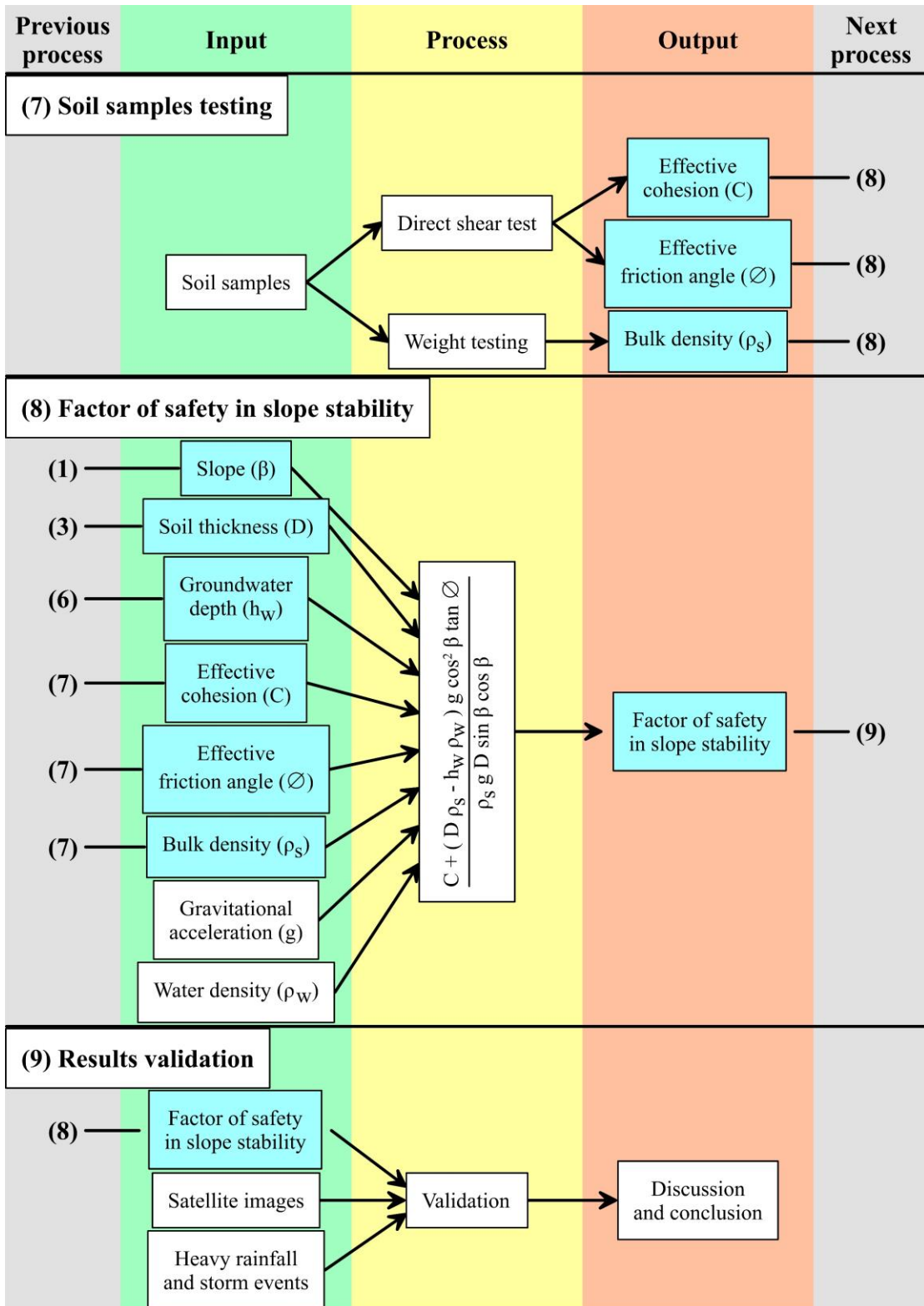


Figure 3.18 Flowchart of research procedure (page 2 of 3)



**Figure 3.19** Flowchart of research procedure (page 3 of 3)

**Table 3.5** Parameters in the TOPMODEL

| Character | Explanation  | Unit              |
|-----------|--|-------------------|
| qs0       | Initial subsurface flow per unit area  | m                 |
| lnTe      | Logarithm of the areal average of saturated soil transmissivity  | m <sup>2</sup> /h |
| m         | Model parameter controlling the rate of decline of transmissivity in the soil profile, see Beven, 1984 |                   |
| Sr0       | Initial root zone storage deficit  | m                 |
| Srmax     | Maximum root zone storage deficit  | m                 |
| td        | Unsaturated zone time delay per unit storage deficit   | h/m               |
| vch       | Channel flow outside the catchment (currently not used)  | m/h               |
| vr        | Channel flow inside catchment  | m/h               |
| k0        | Surface hydraulic conductivity   | m/h               |
| CD        | Capillary drive (Morel-Seytoux and Khanji, 1974)   |                   |
| dt        | The timestep   | h                 |

### 3.6.4 Sensitivity analysis of the model's parameters

The sensitivity analysis was used to find the sensitivity index which showed the most sensitive parameter in the model (Lenhart et al., 2002). This process was useful because calibrating the more sensitive parameters before the less sensitive parameters made the calibration easier. The sensitivity analysis was done by analyzing each event, especially, the events of heavy rainfall or storm. This study just analyzed the sensitivity index from the first peak of the hydrograph on May of each year that was the beginning of the rainy season. This peak was the beginning point of the model simulation that affected the subsequent results. The sensitivity analysis of the model's parameters could be analyzed by equation 3.2.

$$I = \frac{(y_2 - y_1)/y_0}{2\Delta x/x_0} \quad 3.2$$

when

$$\Delta x = x_0 - x_1$$

or

$$\Delta x = x_2 - x_0$$

where  $I$  was the sensitivity index

$x_0$  was the initial value of parameter  $x$

$y_0$  was the model output calculating with  $x_0$

$y_1$  was the model output calculating with  $x_1$

$y_2$  was the model output calculating with  $x_2$

### 3.7 Average height between soil surface and groundwater level simulation using the TOPMODEL

In the evaluation of the occurrence of landslides, it was necessary to know the depth of the groundwater, which was a variable in the calculation of factor of safety in slope stability. In order to obtain the groundwater depth variable, it was necessary to simulate the streamflow and average height between soil surface and groundwater level, which were results from the TOPMODEL. However, only the streamflow data was collected from the raingauges. Therefore, it is the only variable that could be used to calibrate to model.

The values of the heights between soil surface and groundwater level varies upon time and location. It could be calculated for all grids and times by equation 3.3.

$$Z_j = \bar{Z} + m(\lambda - TWI) \quad 3.3$$

|       |           |   |
|-------|-----------|---|
| where | $Z_j$     | was the height between soil surface and groundwater level each grid (meters)            |
|       | $\bar{Z}$ | was average height between soil surface and groundwater level in each timestep (meters) |
|       | $m$       | was a recession constant – generated from the calibration of the streamflow             |
|       | $\lambda$ | was a mean value of the topographic wetness index in the catchment                      |
|       | $TWI$     | was the topographic wetness index – calculated by equation 2.3                          |

After the height between soil surface and groundwater level had been obtained, the groundwater depth could be calculated from the difference between the soil thickness and that height as shown **Figure 3.20**.  $D_j$  is the soil thickness of each grid,  $Z_j$  is the height between soil surface and groundwater level of each grid, and  $h_w$  is the groundwater depth of each grid.

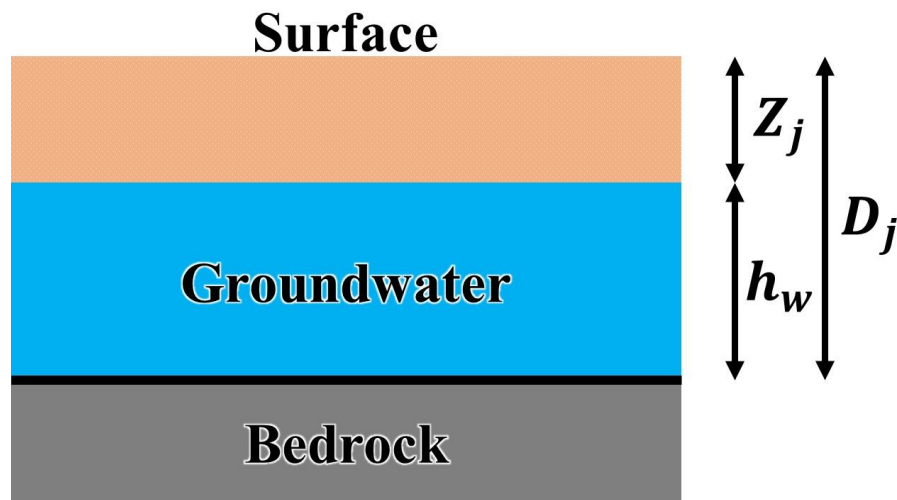


**Figure 3.20** Schematic diagrams showing the relationship between soil thickness and groundwater depth

### 3.8 Evaluation of landslide occurrence using factor of safety in slope stability

The generation of a factor of safety map was an application of the factor of safety in slope stability theory in equation 2.1 to assess the sensitivity of the study area. The variables calculated according to the above theory were generated from the TOPMODEL and the laboratory analysis of the soil samples in the study area. After obtaining that variables, the simulation results would be as close to the observed data as possible. The results of this study were shown in the form of a map showing the values of the factor of safety in slope stability at various times in the Huai Nam Phung subbasin.

### 3.9 Results validation

Finally, after a map showing the daily factor of safety values was generated, the timeline of the storms and the heavy rainfall periods was investigated with that map to check whether the factor of safety values were associated with each event. In addition, the factor of safety maps must be checked with the satellite images which showed the occurrence of the landslides to confirm the study results.

## CHAPTER IV RESULTS

This study has 5 parts such as physical data gathering, generating data for the model, field study, model calibration, and calculation of factor of safety in slope stability. The results of these processes are as the following:

### 4.1 Landslide occurrences

A field survey of landslides in the Huai Nam Phung subbasin was carried out to check landslide occurrences. This study focused on the areas where the slopes are higher than  $30^\circ$  because these areas were very sensitive (Soralump, 2010). This theory corresponds to the classification of landslide risk areas, which states that the landslides often occur on the areas with slopes greater than 30 degrees (Chen et al., 2016; Gökceoglu and Aksoy, 1996; Maharaj, 1993; Moreiras, 2005; Phien-Wej et al., 1993; Pourghasemi et al., 2014; Pourghasemi et al., 2013; Pourghasemi et al., 2012; Sassa et al., 2006; Shirzadi et al., 2017; Tsutsumi and Fujita, 2008; Zhang et al., 2009). In the study area, 3.9% of the total area (26.75 square kilometers) has slope higher than  $30^\circ$  and 10.55% of the total area (72.35 square kilometers) has the slope of  $20 - 30^\circ$  (**Figure 4.1**).

#### 4.1.1 Landslide occurrences by visible imagery analysis

Based on visible imagery analysis, landslides occurred at 59 points and most of them occurred in 2017. All of them are classified as the shallow landslides. Most of the landslides were in the western part of the catchment, especially in the area near the Phu Thap Boek, Ban Noen subdistrict, Lom Kao district, Phetchabun Province.

#### 4.1.2 Landslide occurrences by a field survey

The field survey was carried out to check the landslide occurrences in the Huai Nam Phung subbasin on 26 – 29 July 2018. However, since some parts of the area were too dangerous to access and/or heavily covered by trees which hide the traces of landslides, only 13 points out of 59 points were investigated. All of 13 points are matched with the results imagery analysis and there are additional 4 points that have been newly found following the interview with local residents. Totally, there are 17 points where landslide occurrences have been confirmed from the field survey.

#### 4.1.3 Landslides occurred in the Huai Nam Phung subbasin

Most of the landslides that occurred in the Huai Nam Phung subbasin were in the southwestern part of the subbasin. There are 2 big catchments in this area consisting of the Huai Nam Ko catchment and the Huai Nam Hia catchment. In these 2 catchments, occurrences of landslides have been found at 51 points or more. For the Huai Nam Ko catchment, the area is difficult to access because there is a reservoir in the area. Therefore, the landslide occurrences in Huai Nam Ko catchment have still not been confirmed in this field survey (**Figure 4.2**).

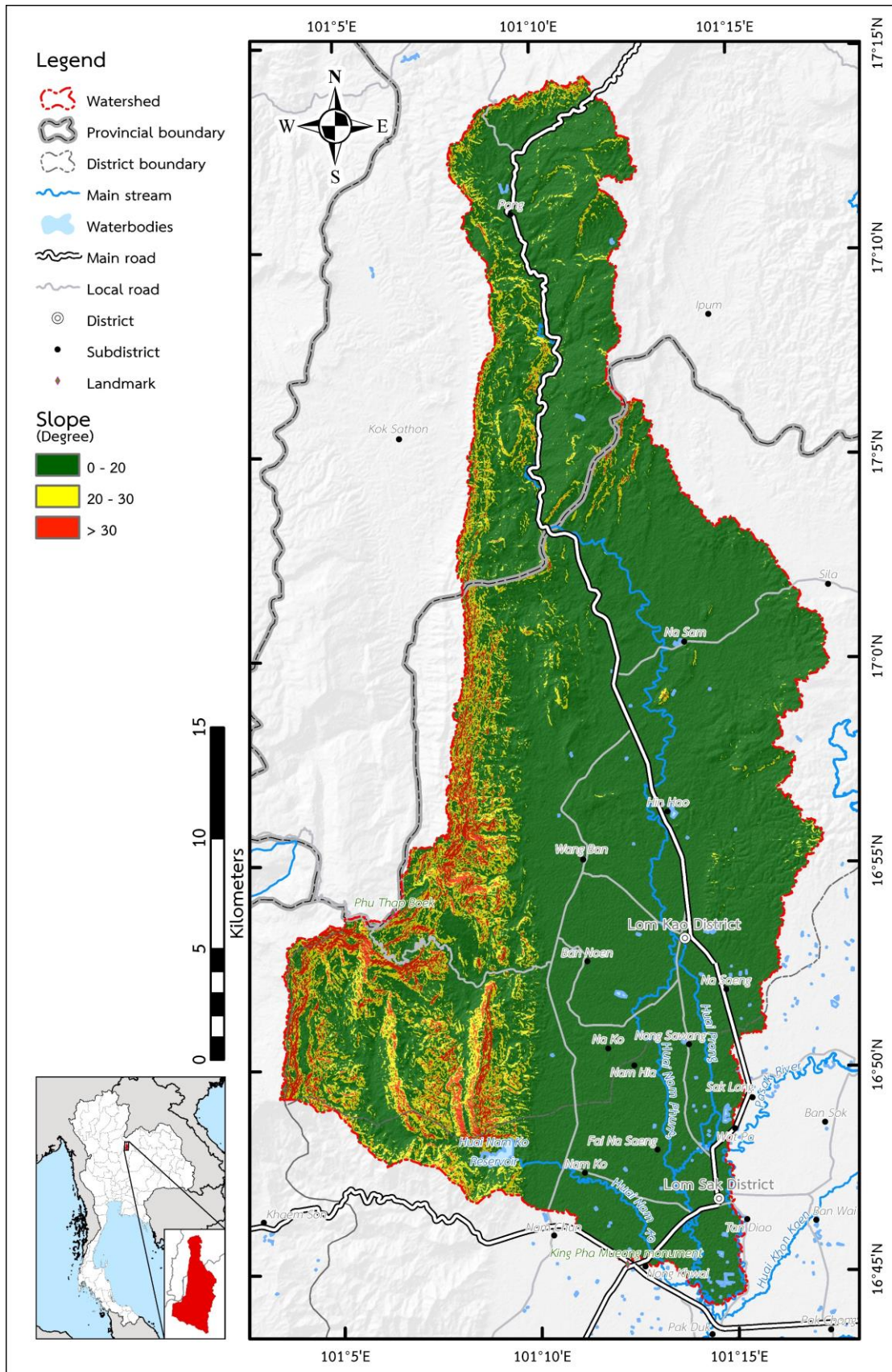


**Figure 4.1** Slope of the Huai Nam Phung subbasin showing in 3 classes



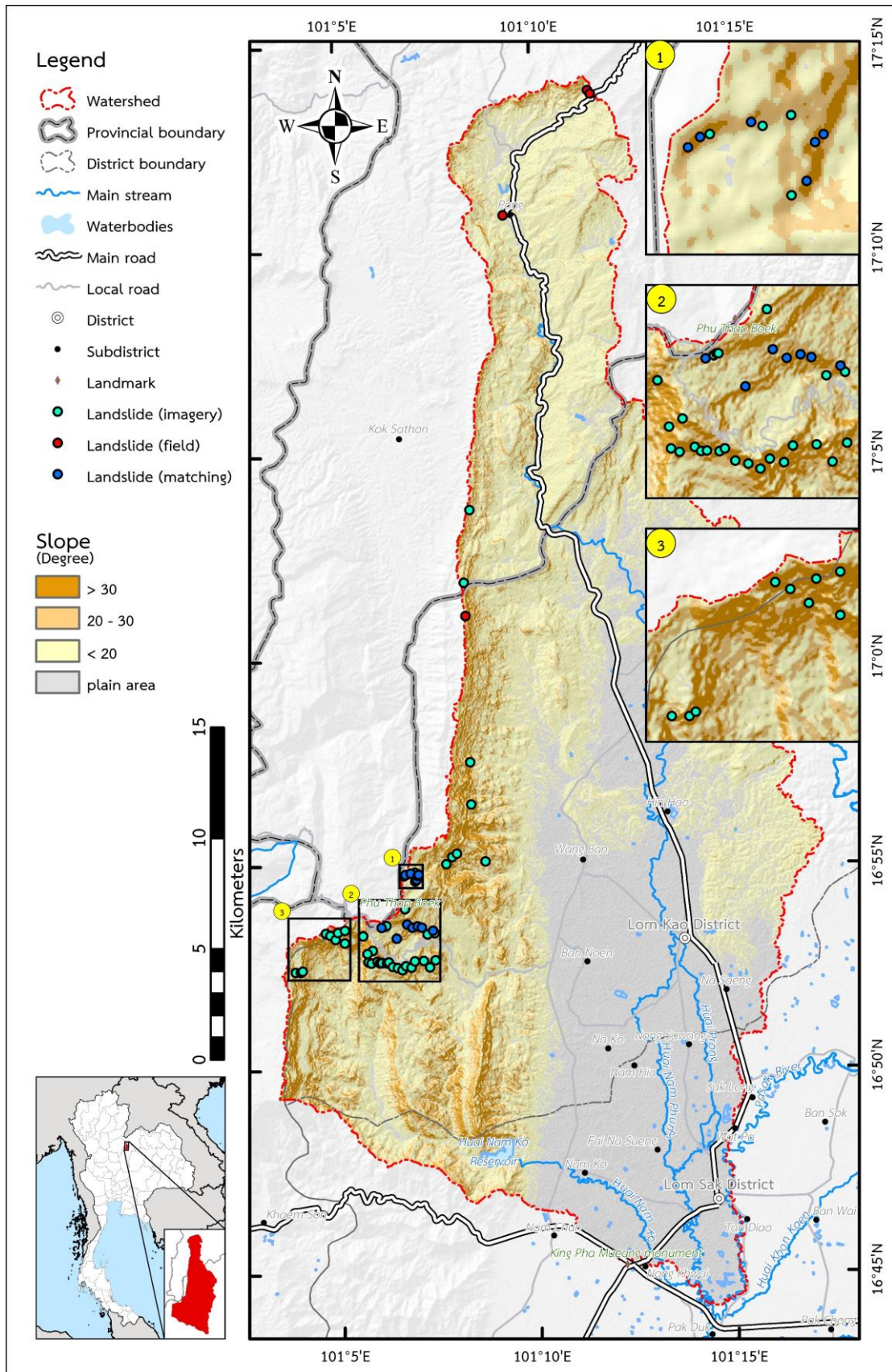


**Figure 4.2** Landslides occurrence in the Huai Nam Phung subbasin in 2017

As mentioned, based on visible imagery analysis and field survey, landslides in the Huai Nam Phung subbasin was probably occurred in 2017. Therefore, this study focused on the landslide occurrence from 2016 to 2017.

## 4.2 Physical data of the study area

This study used the streamflow data from the stream gauges of the Royal Irrigation Department Thailand (RID Thailand) as comparing with the simulated data from TOPMODEL. In addition, this study used the digital elevation model (DEM) from the earth database of the National Aeronautics and Space Administration (NASA). It was generated from ALOS PALSA Global Radar Imagery with a resolution of  $12.5 \times 12.5$  meters. All DEMs used in this study was generated in 2008, which is the most recent period. The DEM shows that Huai Nam Phung subbasin has the highest elevation of 1,768 meters above mean sea level (amsl) at the top of Phu Thap Boek in Ban Noen subdistrict, Lom Kao district, Phetchabun Province, at the longitude of  $101^\circ 05' 07''$  E and the latitude of  $16^\circ 53' 36''$  N and the lowest elevation of 131 meters amsl. in the plain area, which is the outlet of the Huai Nam Phung subbasin.

### 4.2.1 Slope map

The slope map has been generated from the DEM using the geographic information system (GIS) that operated on the software of ArcMap 10.5. The slope generated by GIS was in degree and was converted to radian by raster calculator in the GIS process. The slope of the Huai Nam Phung subbasin ranges from 0-1.35 radians. Most of the high slope areas are in the west of the subbasin (**Figure 4.3**).

### 4.2.2 Flow accumulation

The flow accumulation was a variable used to calculate the topographic wetness index (TWI), which was used further to generate several other parameters. The flow accumulation was generated from the digital elevation model (DEM) by the geographic information system (GIS) with the hydrological tools that operated on the software of ArcMap 10.5. The flow accumulation shows the runoff accumulation in the catchment and it reveals the streams in the catchment (**Figure 4.4**).

### 4.2.3 Topographic Wetness Index (TWI)

The topographic wetness index (TWI) is a steady state wetness index generated from slope in radians and flow accumulation using GIS. It shows the higher value in the area near the valley and lower value in the area near the ridge. In this study, the TWI was an important data to generate soil thickness map, which was used as an input data to generate the streamflow and the average height ( $\bar{Z}$ ) between soil surface and groundwater level in the TOPMODEL. The TWI of the Huai Nam Phung subbasin has the highest value of 16.39 and the lowest value of 0. However, the TWI cannot be generated in some parts of the plain terrain since the plains are not clearly ridges and valleys (**Figure 4.5**).

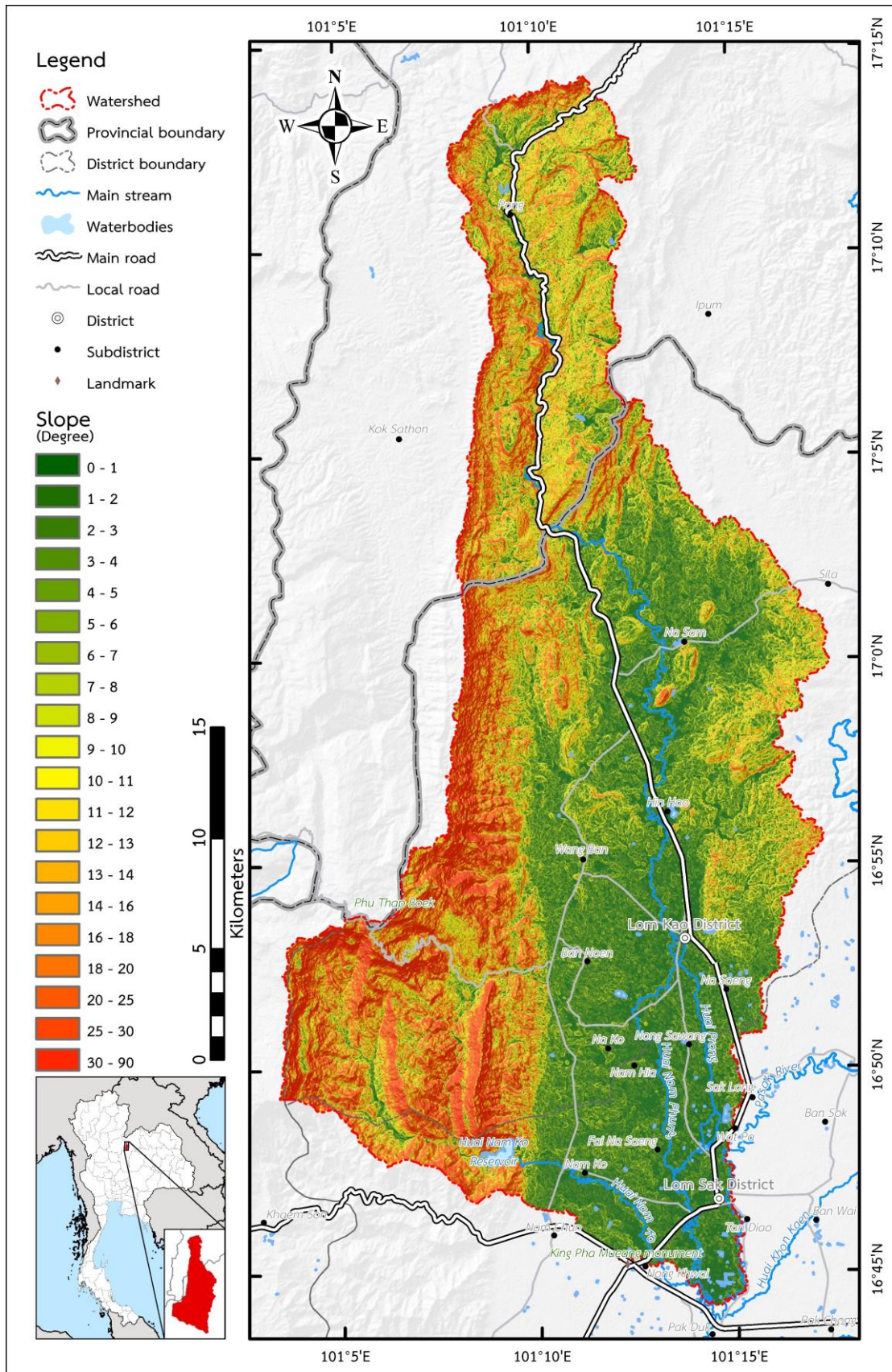
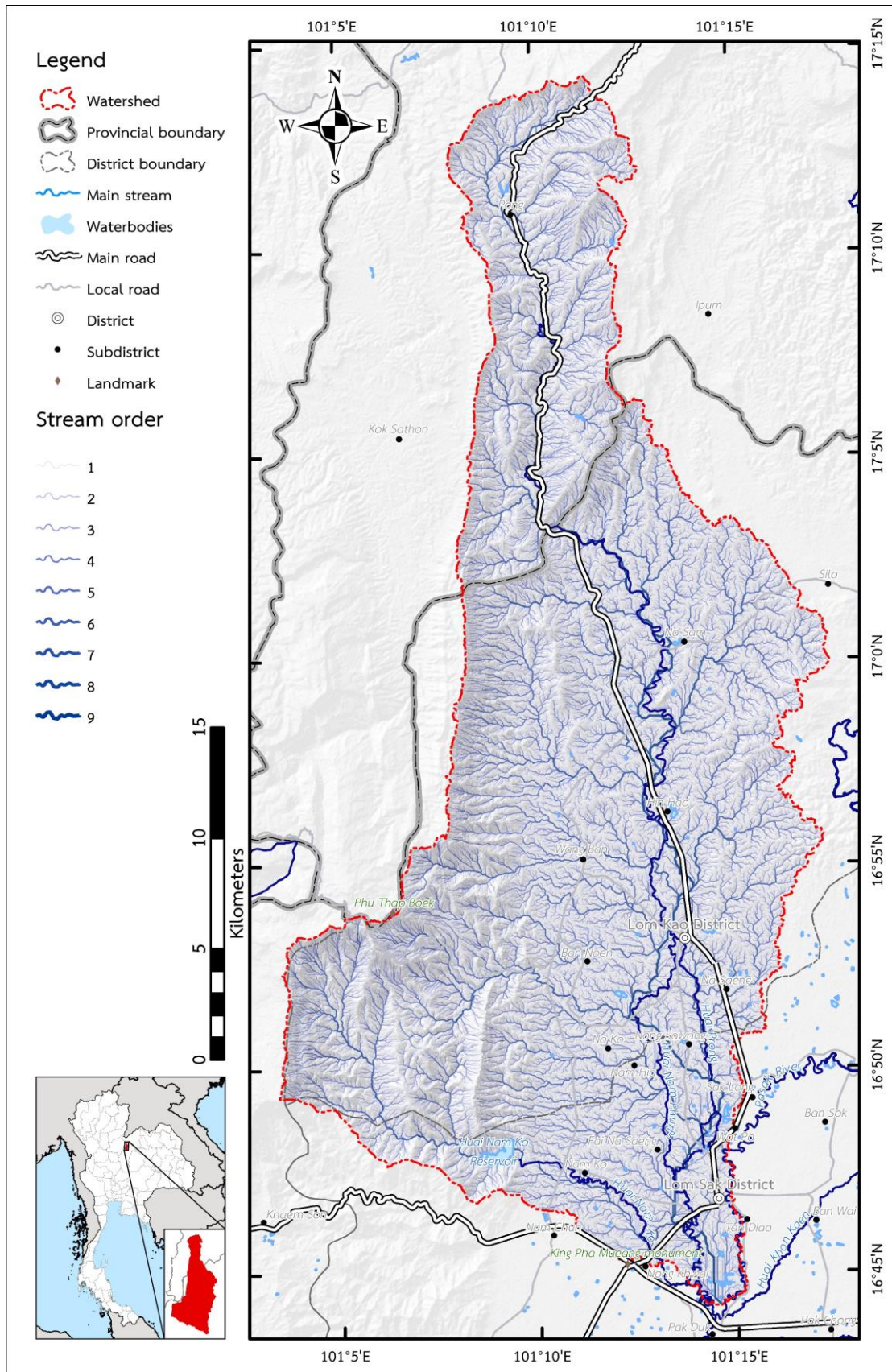
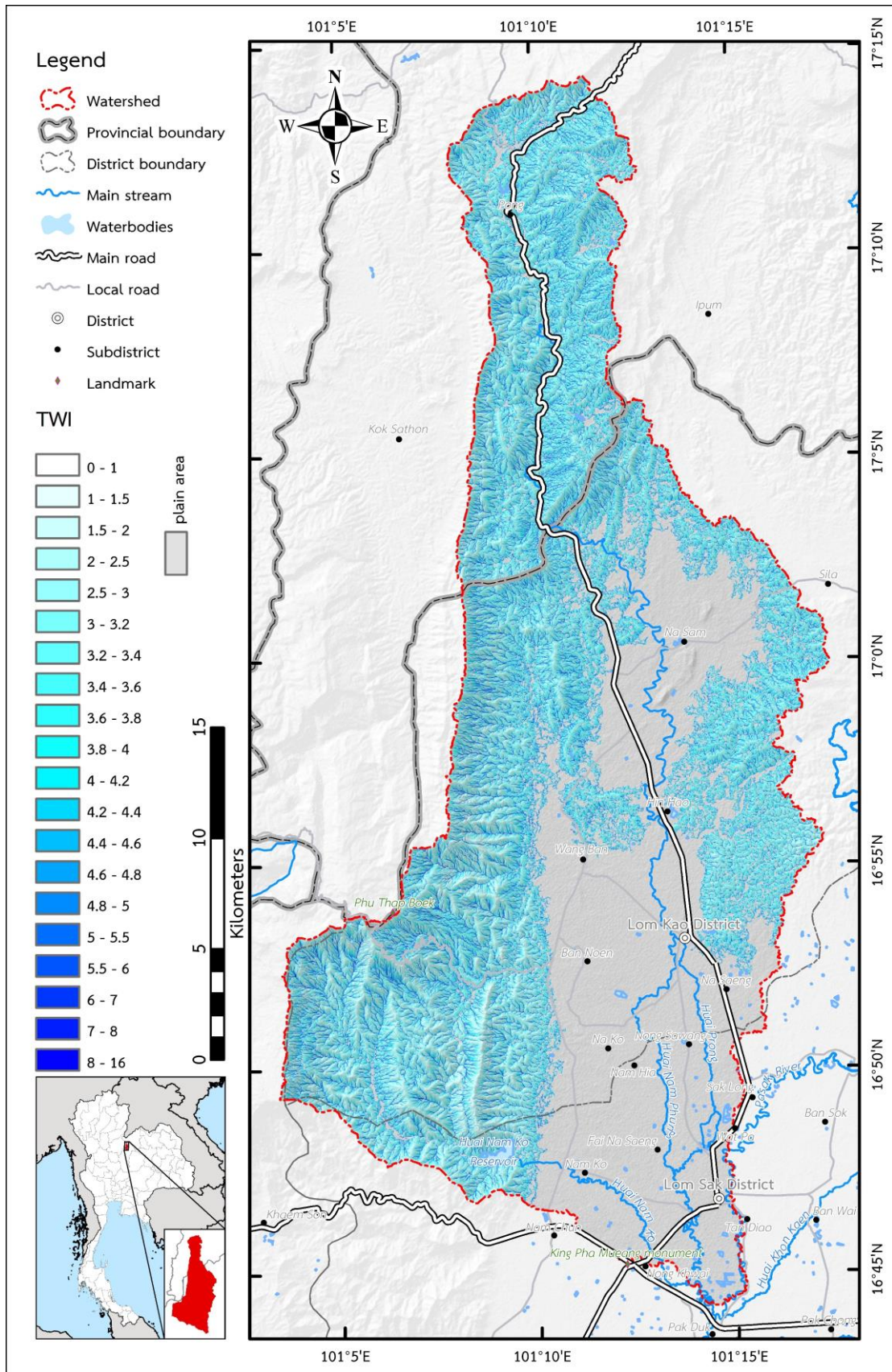


Figure 4.3 Slope of the Huai Nam Phung subbasin



**Figure 4.4** Streams in the Huai Nam Phung subbasin generated by flow accumulation



#### 4.2.4 Soil thickness

In this study, the soil sampling was done at only 13 points on the ridge near the outcrops area (**Figure 4.6**). The linear relationship between the TWI and soil thickness in the study area is similar to the results from Lee et al. (2009) and Ho et al. (2012), but the  $R^2$  value of 0.59 is fair due to less sampling points (**Table 4.1 and Figure 4.7**). Soil thickness of the Huai Nam Phung subbasin with the slope more than 6%, ranges from 0 – 1.64. In some parts of the plain terrain, the soil thickness cannot be generated because the TWI was not available (**Figure 4.8**).

#### 4.2.5 Flow length

The flow length shows the distance from each grid to the outlet of the catchment according to the flow accumulation. It must be used for delay data generating in the TOPMODEL. The flow length was generated from the DEM using GIS. The maximum flow length of the Huai Nam Phung subbasin is 83,809.35 meters, which is the flow length from the area of Pong subdistrict, Dan Sai district, Loei Province to the outlet. (**Figure 4.9**).

### 4.3 Meteorological data

This study used the meteorological data in 2016 and 2017 because the investigation suggests that most of the landslides occurred in 2017. Meteorological data used in the TOPMODEL consists of rainfall and evaporation rate. These meteorological data were obtained from Thai Meteorological Department (TMD).

#### 4.3.1 Interpolated rainfall

This study used the rainfall data from TMD. The data was interpolated from several stations around the Huai Nam Phung subbasin. In 2016, the maximum daily rainfall was 36.12 mm. on 14 September, 2016 (**Figure 4.10**). In 2017, the maximum daily rainfall was 43.10 mm. on 16 October, 2017 (**Figure 4.11**).

#### 4.3.2 Evaporation rates

This study used the evaporation data collected by TMD using the American class A pan. There was only one evaporation station (379401) where is located in Lom Sak district, Phetchabun province. In 2016, the average evaporation rate was 0.18 mm per day (**Figure 4.12**). In 2017, the average evaporation rate was 0.17 mm per day (**Figure 4.13**).

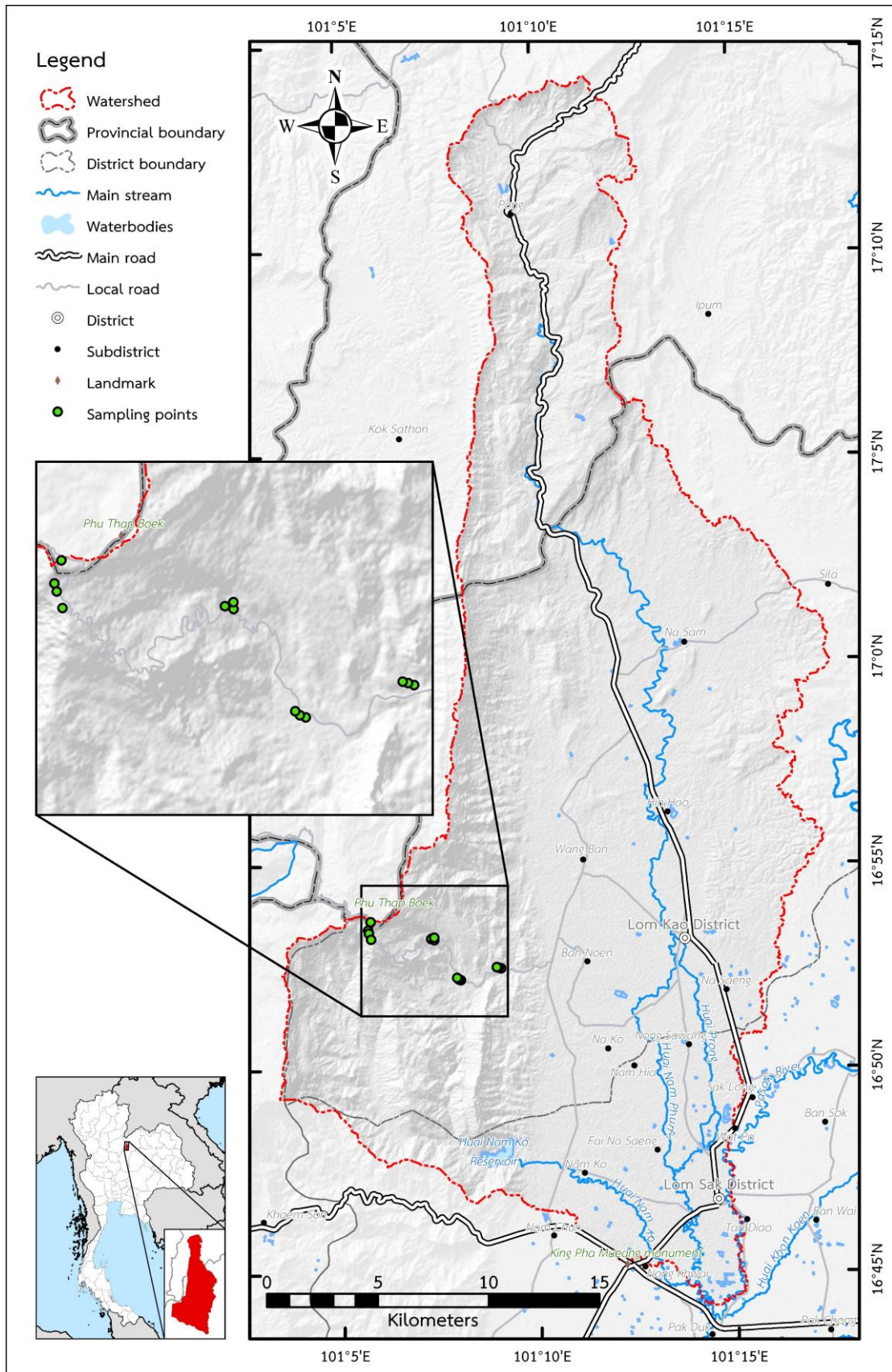


**Figure 4.6** Sampling points of soil thickness in the Huai Nam Phung subbasin

**Table 4.1** The relationship between soil thickness and TWI in the Huai Nam Phung subbasin with the slope of higher than 6%

| No. | Longitude        | Latitude        | TWI  | Soil thickness (meters) |
|-----|------------------|-----------------|------|-------------------------|
| 1   | 101° 09' 03.2" E | 16° 52' 28.1" N | 4.05 | 0.30                    |
| 2   | 101° 08' 59.8" E | 16° 52' 29.2" N | 1.61 | 0.25                    |
| 3   | 101° 08' 57.0" E | 16° 52' 30.2" N | 2.42 | 0.25                    |
| 4   | 101° 08' 01.9" E | 16° 52' 11.2" N | 2.87 | 0.30                    |
| 5   | 101° 07' 58.6" E | 16° 52' 12.4" N | 2.90 | 0.30                    |
| 6   | 101° 07' 56.5" E | 16° 52' 14.6" N | 4.26 | 0.40                    |
| 7   | 101° 07' 17.1" E | 16° 53' 12.0" N | 2.63 | 0.25                    |
| 8   | 101° 07' 21.9" E | 16° 53' 10.4" N | 2.15 | 0.25                    |
| 9   | 101° 07' 21.6" E | 16° 53' 14.2" N | 4.37 | 0.45                    |
| 10  | 101° 05' 41.2" E | 16° 53' 25.3" N | 1.83 | 0.20                    |
| 11  | 101° 05' 42.4" E | 16° 53' 21.0" N | 1.16 | 0.20                    |
| 12  | 101° 05' 45.8" E | 16° 53' 12.0" N | 1.61 | 0.20                    |
| 13  | 101° 05' 45.2" E | 16° 53' 37.8" N | 3.66 | 0.50                    |

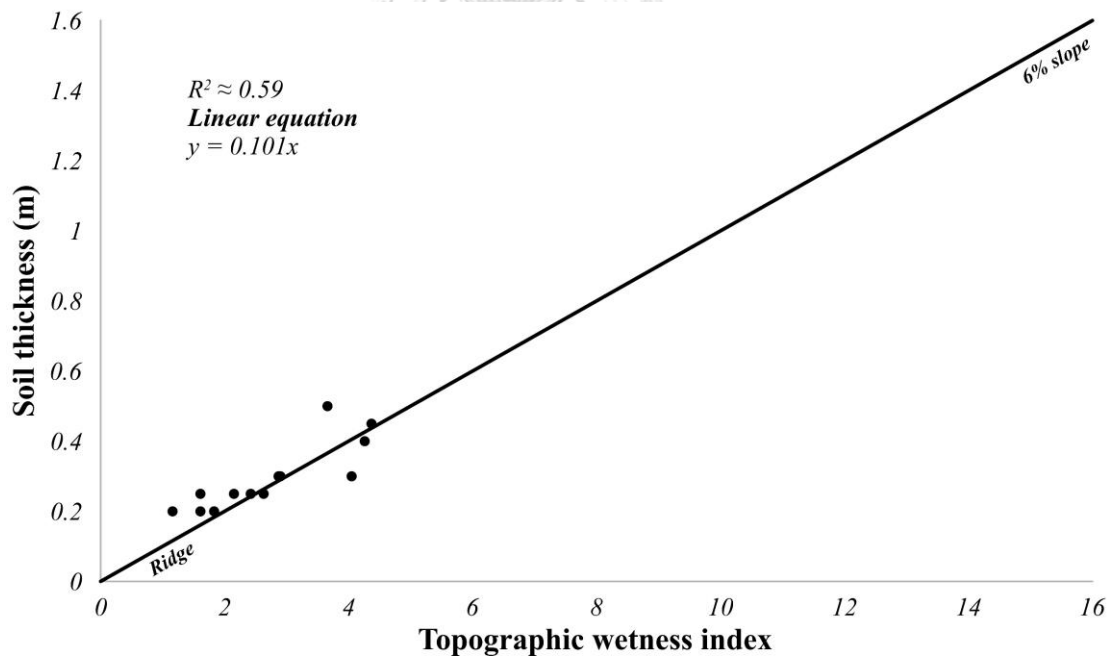


**Figure 4.7** Linear relationship between soil thickness and the topographic wetness index in the Huai Nam Phung subbasin with the slope of higher than 6%



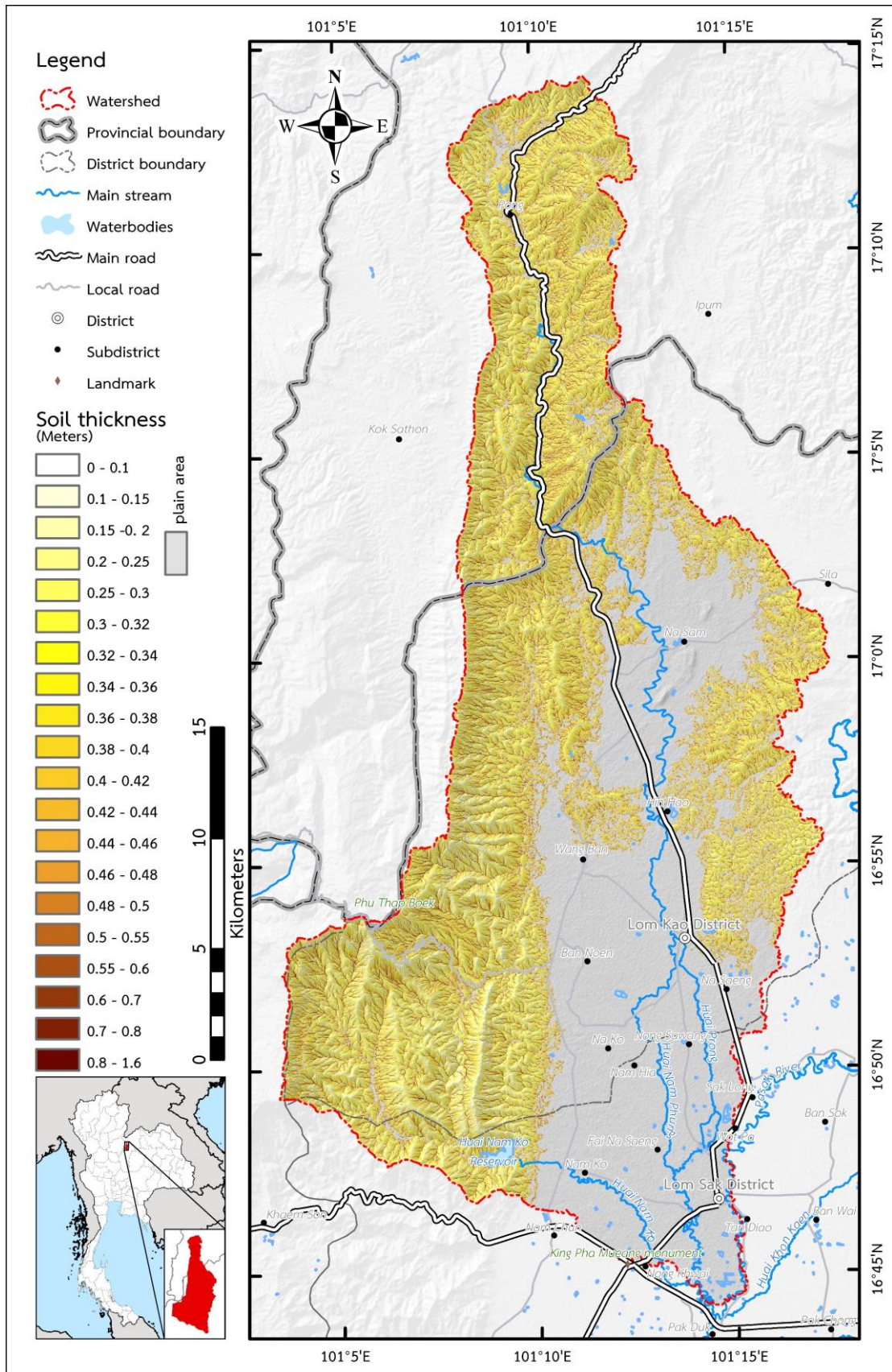
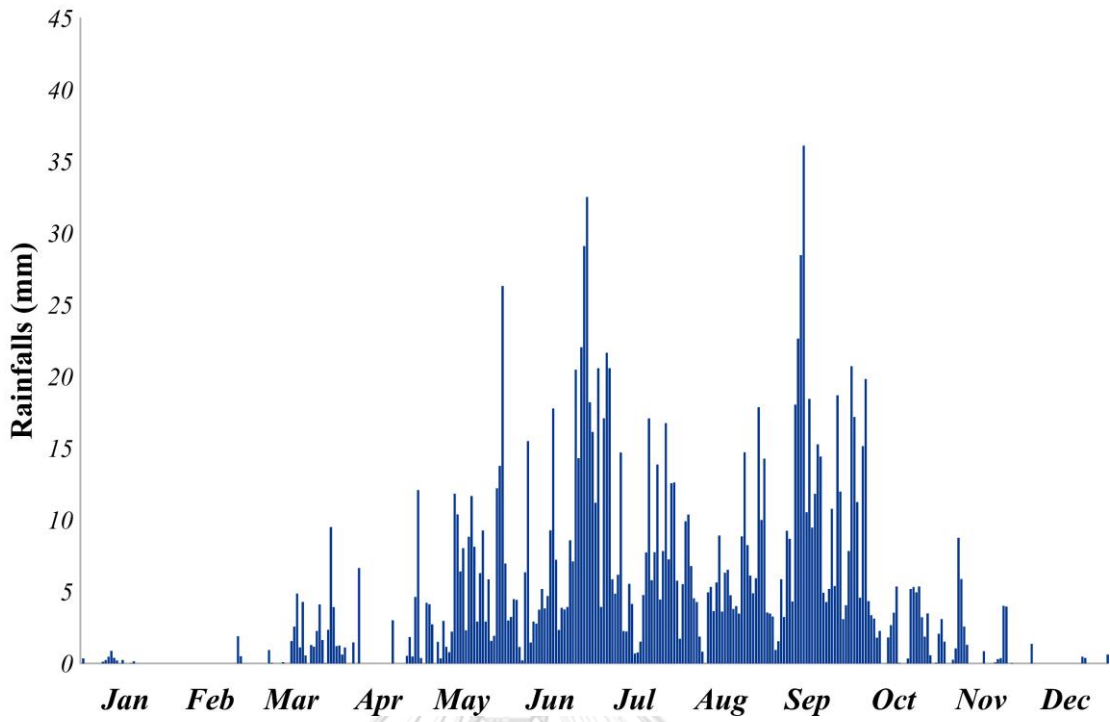
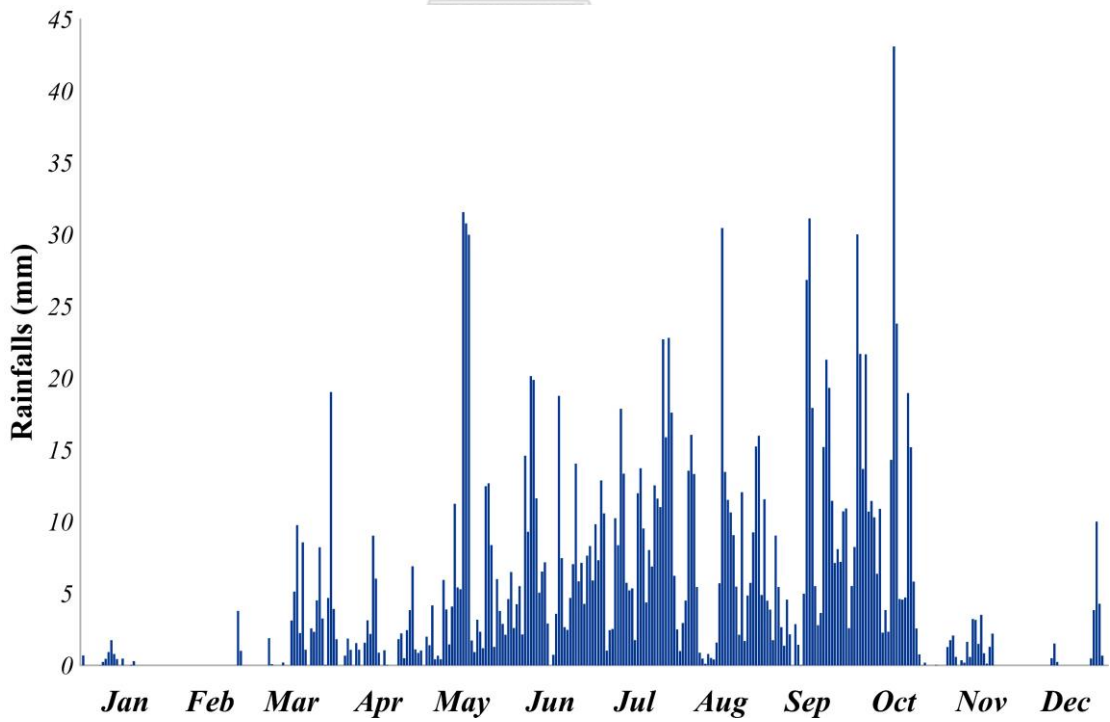


Figure 4.8 Soil thickness of the Huai Nam Phung subbasin





**Figure 4.10** Daily rainfall in the Huai Nam Phung subbasin in 2016



**Figure 4.11** Daily rainfall in the Huai Nam Phung subbasin in 2017

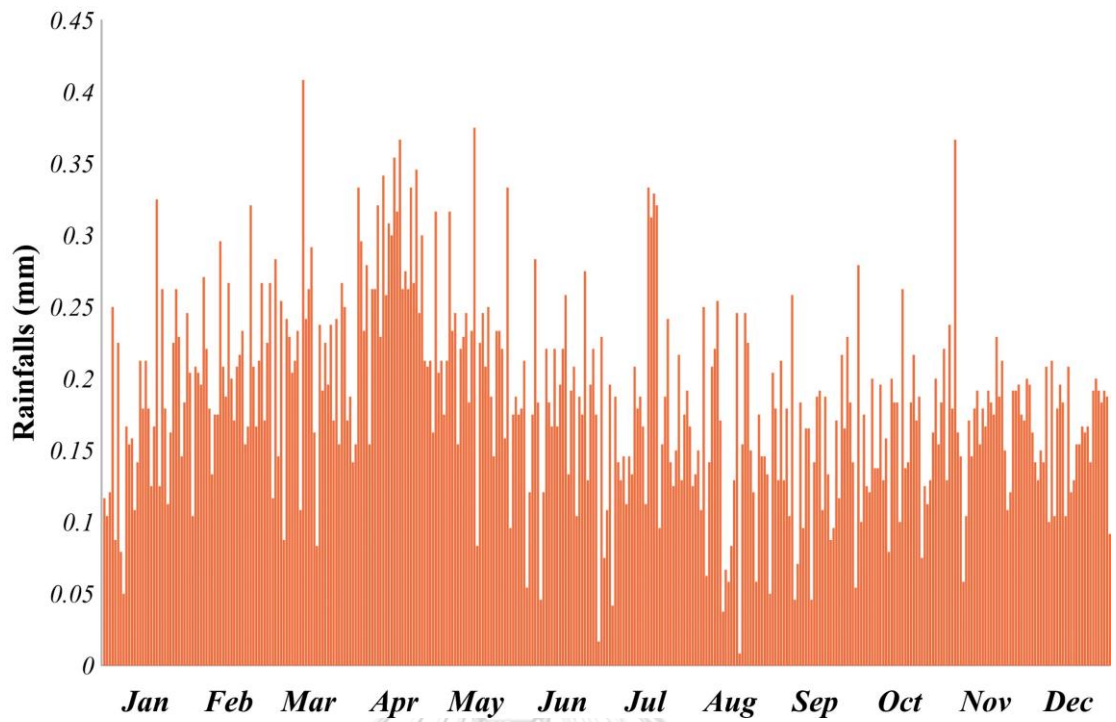


**Figure 4.12** Daily evaporation in the Huai Nam Phung subbasin in 2016

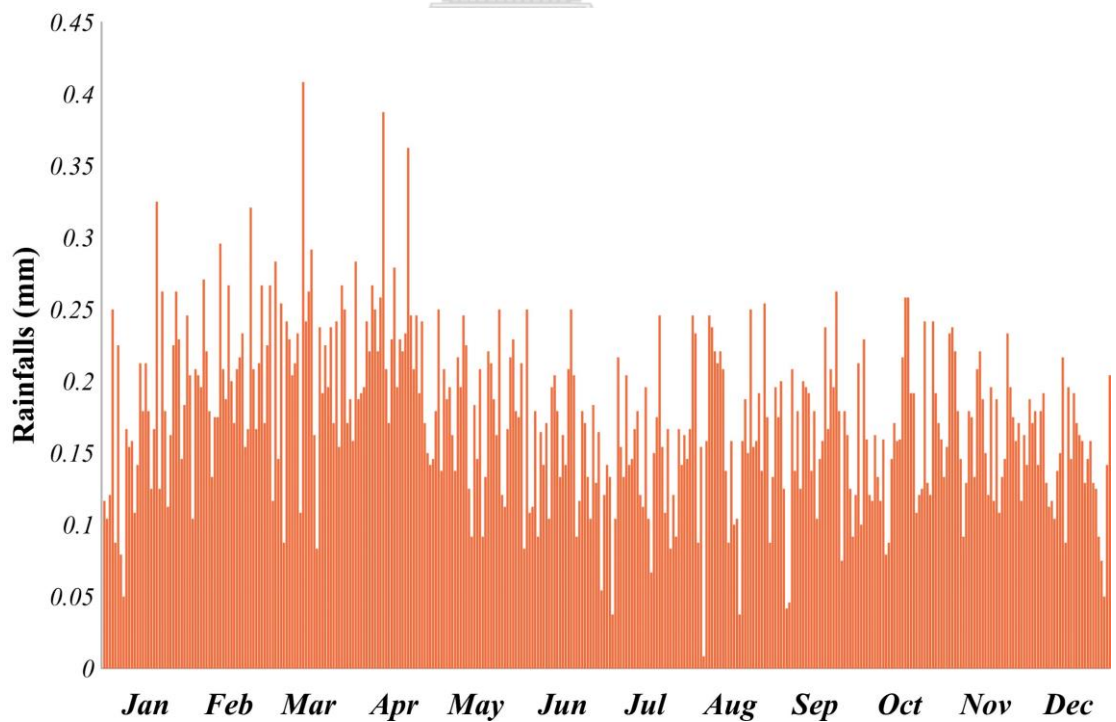


**Figure 4.13** Daily evaporation in the Huai Nam Phung subbasin in 2017

#### 4.4 Streamflow calculation

There were 4 streamflow gauging stations (S.3, S.10, S.36 and S.41) nearby the Huai Nam Phung subbasin, but the streamflow data during the 2016-2017 was available only at the station S.3. At the station, the highest streamflow in 2016 was 126.91 m<sup>3</sup>/s on 15 September, 2016 and the highest streamflow in 2017 was 127.66 m<sup>3</sup>/s on 30 July, 2017. For the S.36 station, it has been closed. For the stations S.10 and S.41, only the water levels were recorded. Therefore, this study used the linear relationship between the annual average streamflow and catchment area to estimate the streamflow in Huai Nam Phung subbasin. The linear equation of 2016 is  $y = 0.16x + 58.79$ , while the linear equation of 2017 is  $y = 0.25x + 280.58$ . From that linear relationship, the annual average streamflow of the Huai Nam Phung subbasin in 2016 was 167.31 MCM (**Figure 4.14**) and that in 2017 was 451.21 MCM (**Figure 4.15**). After using the observed streamflow at the station S.3 to calculate the streamflow of the Huai Nam Phung subbasin, it is found that the peak of streamflow in the Huai Nam Phung subbasin in 2016 was 63.02 m<sup>3</sup>/s which occurred on 15 September 2016 (**Figure 4.16**) while the peak in 2017 was 103.44 m<sup>3</sup>/s which occurred on 30 July 2017 (**Figure 4.17**).

#### 4.5 Parameters of the topography based on hydrological model

The calibration results show the fitted parameters with the highest NSE in 2016 and 2017 of 0.73 and 0.79, respectively (**Table 4.2**). According to the sensitivity analysis, there are 3 classes as follows: highly sensitive (3 parameters), moderately sensitive (3 parameters), and low sensitive (3 parameters). The highly sensitive parameters were transmissivity (lnTe), lnTe followed by surface hydraulic conductivity (k0) and capillary drive (CD). The moderately sensitive parameters consist of initial subsurface flow per unit area (qs0), channel flow inside catchment (vr), and model parameter controlling the rate of decline of transmissivity in the soil profile (m). The last group consists of maximum root zone storage deficit (Srmax), unsaturated zone time delay per unit storage deficit (td), and initial root zone storage deficit (Sr0). While channel flow outside the catchment (vch) was not used in the simulation. The timestep for the simulation was 1 hour.

**Table 4.2** The values and sensitivity index of parameters used in the TOPMODEL

| Parameters | Values                  |                        | Sensitivity index |
|------------|-------------------------|------------------------|-------------------|
|            | 2016 (NSE = 0.73)       | 2017 (NSE = 0.79)      |                   |
| qs0        | $5.04 \times 10^{-6}$   | $1.85 \times 10^{-6}$  | 0.98              |
| lnTe       | -6.45                   | -7.87                  | 7.09              |
| m          | $8.47 \times 10^{-2}$   | $2.62 \times 10^{-2}$  | 0.56              |
| Sr0        | $-10.82 \times 10^{-4}$ | $-9.38 \times 10^{-4}$ | 0.00              |
| Srmax      | $11.95 \times 10^{-2}$  | $3.99 \times 10^{-2}$  | 0.14              |
| td         | 8.53                    | 236.66                 | 0.05              |
| vr         | 639.87                  | 580.55                 | 0.61              |
| k0         | $2.64 \times 10^{-3}$   | $4.16 \times 10^{-3}$  | 3.35              |
| CD         | $2.40 \times 10^{-2}$   | $4.56 \times 10^{-2}$  | 2.53              |

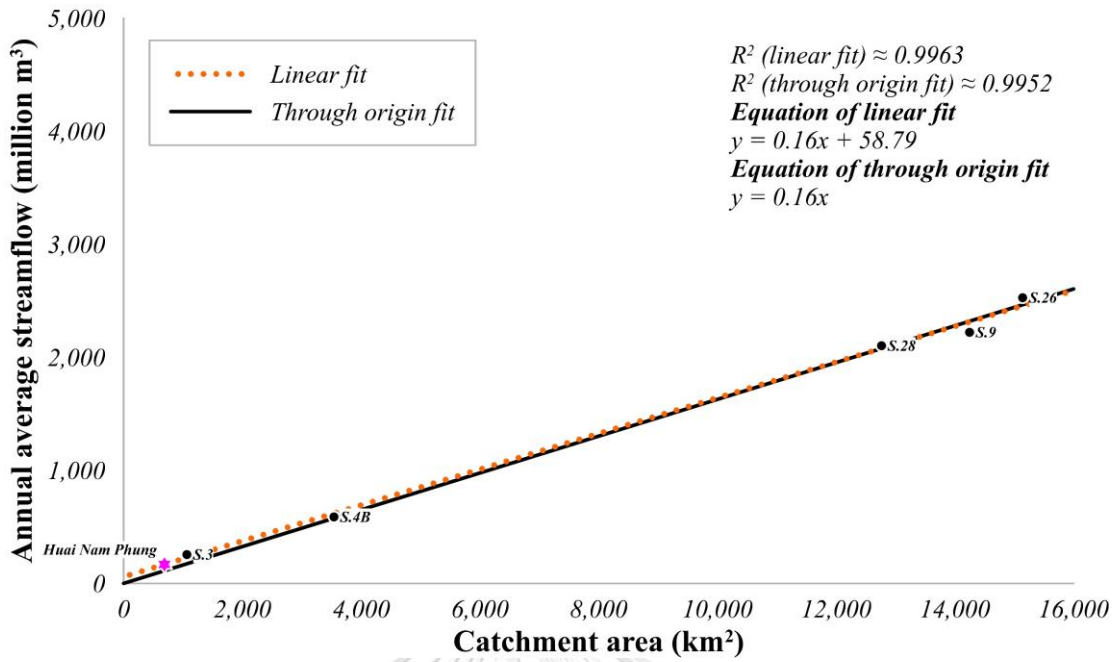


**Figure 4.14** Relationship between annual average streamflow and catchment area in the Pasak river basin in 2016

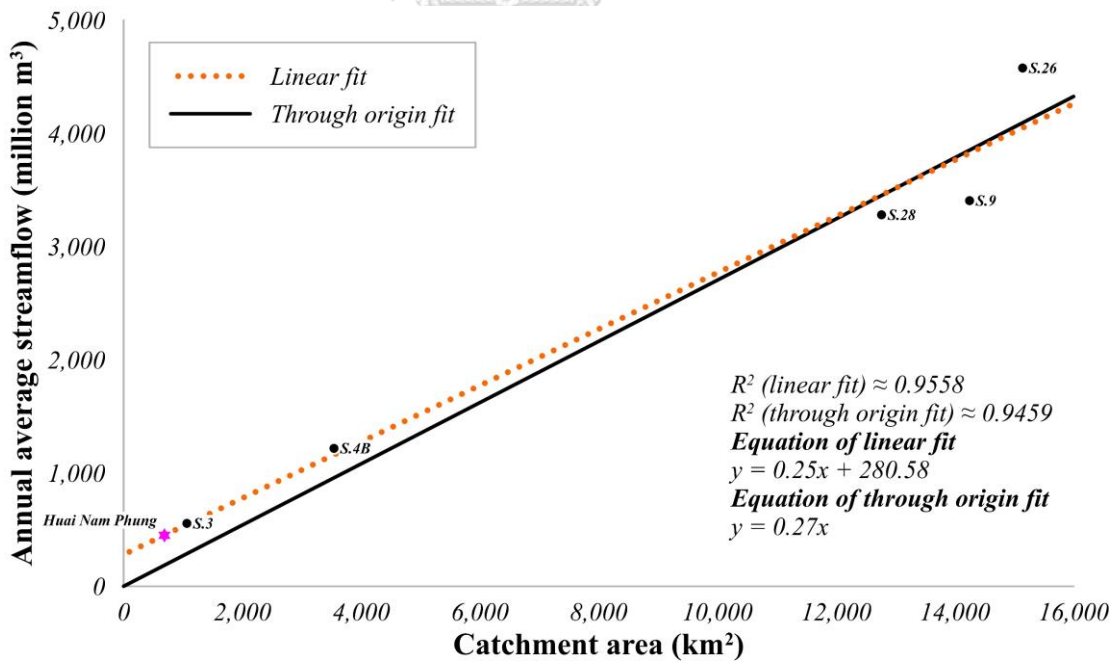


**Figure 4.15** Relationship between annual average streamflow and catchment area in the Pasak river basin in 2017

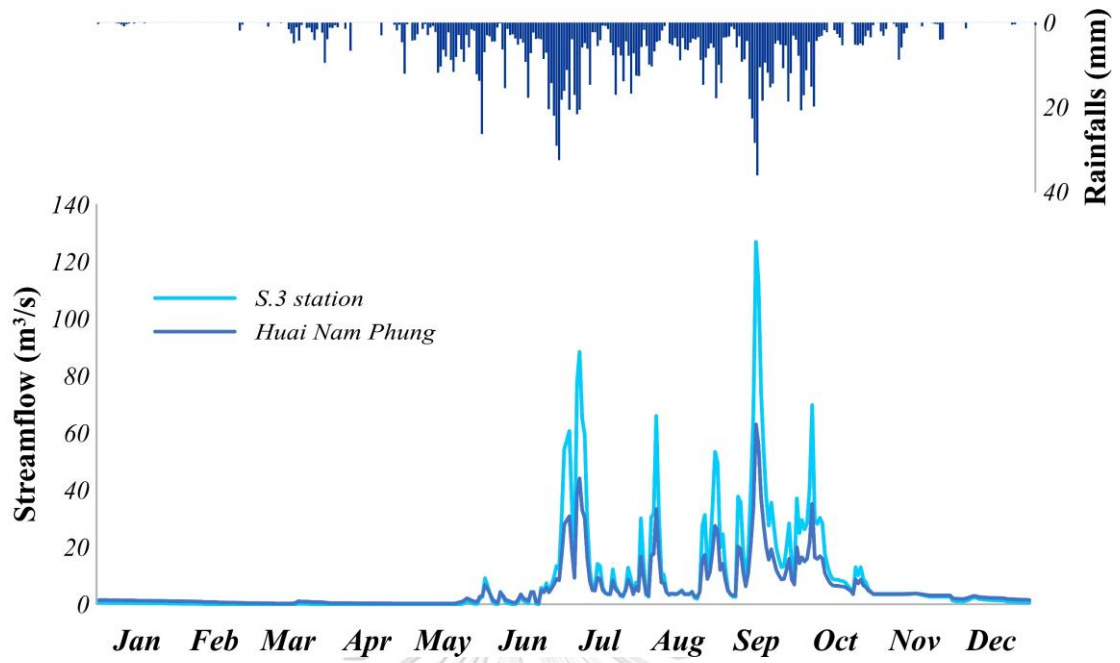


**Figure 4.16** Comparison between the observed streamflow at the S.3 station and the calculated streamflow of the Huai Nam Phung subbasin in 2016

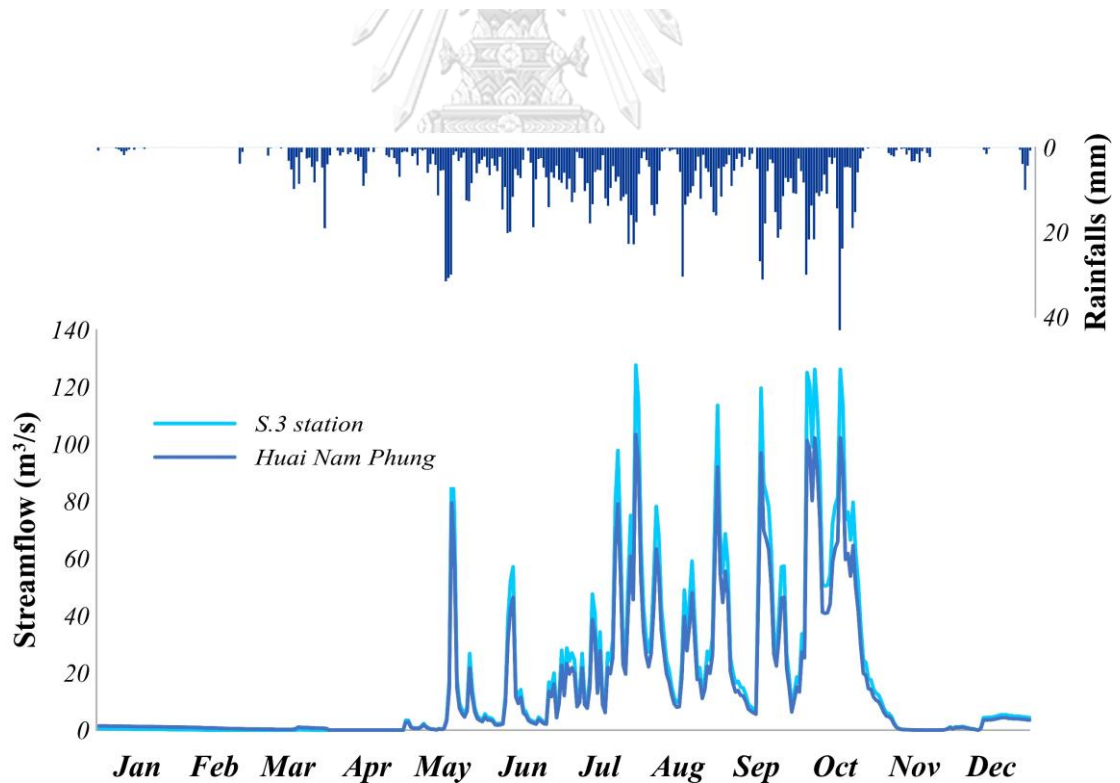


**Figure 4.17** Comparison between the observed streamflow at the S.3 station and the calculated streamflow of the Huai Nam Phung subbasin in 2017

#### 4.6 Simulated streamflow

This study focused on simulation of the streamflow at the outlet of the Huai Nam Phung subbasin in 2017 because there were many landslides occurred in that year. The data in 2016 was used to compare the simulation result with the observed data.

The simulation of the Huai Nam Phung subbasin was done by its own physical data. The observed streamflow calculated from the data at the station S.3 was used to calibrate the unknown parameters. The streamflow hydrograph simulated from the topography based hydrological model (TOPMODEL) shows that the discharge is associated with the rainfall data. The values of  $R^2$  in 2016 and 2017 are 0.73 and 0.79, respectively. The simulation results suggest that the streamflow in 2016 had the highest value of is 54.50 m<sup>3</sup>/s on 16 September, 2016 (**Figure 4.18**) and the streamflow in 2017 had the highest value of 118.05 m<sup>3</sup>/s on 19 October, 2017 (**Figure 4.19**).

#### 4.7 Simulated average height between soil surface and groundwater level

The average height between soil surface and groundwater level was denoted to  $\bar{Z}$ . This variable was simulated with the streamflow. Then, the map showing the height between soil surface and groundwater level ( $Z_j$ ) was generated. After that, the  $Z_j$  was deducted from the soil thickness to obtain the groundwater depth, which was an important variable for calculation the factor of safety in slope stability.

The simulation results in the Huai Nam Phung subbasin showed that the  $\bar{Z}$  graph was consecutively decreasing with the accumulation of groundwater. In 2016, the lowest value was 0.91 meters on 9 October, 2016 (**Figure 4.20**). In 2017, the lowest value was -0.17 meters on 30 October, 2017 (**Figure 4.21**). The simulated values in 2016 and 2017 are difference because the extreme drought occurred in 2016, while many heavy rainfall and storms was found in 2017. The negative lowest value of  $Z_j$  in 2017 indicated that the groundwater level was high enough to cause an overland flow.

#### 4.8 Height between soil surface and groundwater level

By calculating with equation 3.3, it is found that the heights between soil surfaces and groundwater levels in 2016 and 2017 were largely different. The results varied upon the meteorological data in these 2 consecutive years, which were relatively different rainfall amounts.

In 2016, the amounts of rainfall and runoff were very low. With this reason, the simulated value of height between soil surface and groundwater level was relatively high. It was greater than 2 meters in the ridge area. In the rainy season (May to October, 2016) (**Figure 4.22**), it found that the groundwater level was very low. Even in the rainy season, for example, on 9 October 2016, the  $Z_j$  value in the ridge area was still high (greater than 2 meters).



In 2017, both rainfall and runoff were much higher than those in 2016. Therefore, the values of simulated height between soil surface and groundwater level was very low. There were no any locations with the  $Z_j$  value of higher than 2 meters (Figure 4.23). The lowest value appeared on 30 October, 2017. Many parts of the area were found the  $Z_j$  values were lower than 0, indicating that groundwater level was very high and generate the surface runoff.

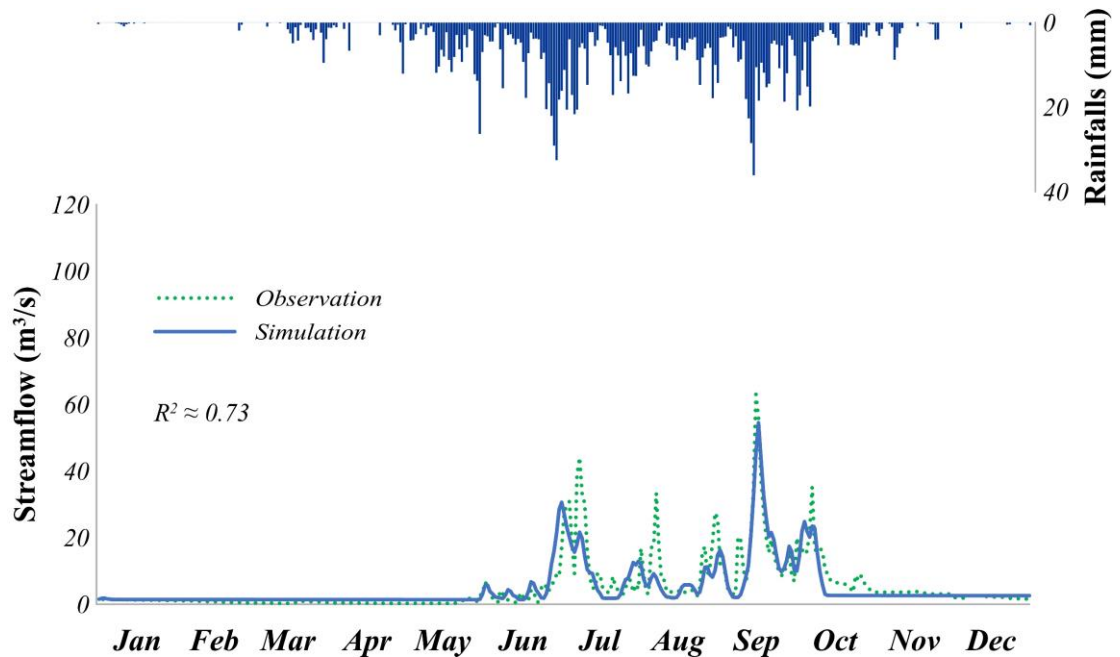


**Figure 4.18** Comparison between the observed streamflow and the simulated streamflow in the Huai Nam Phung subbasin in 2016

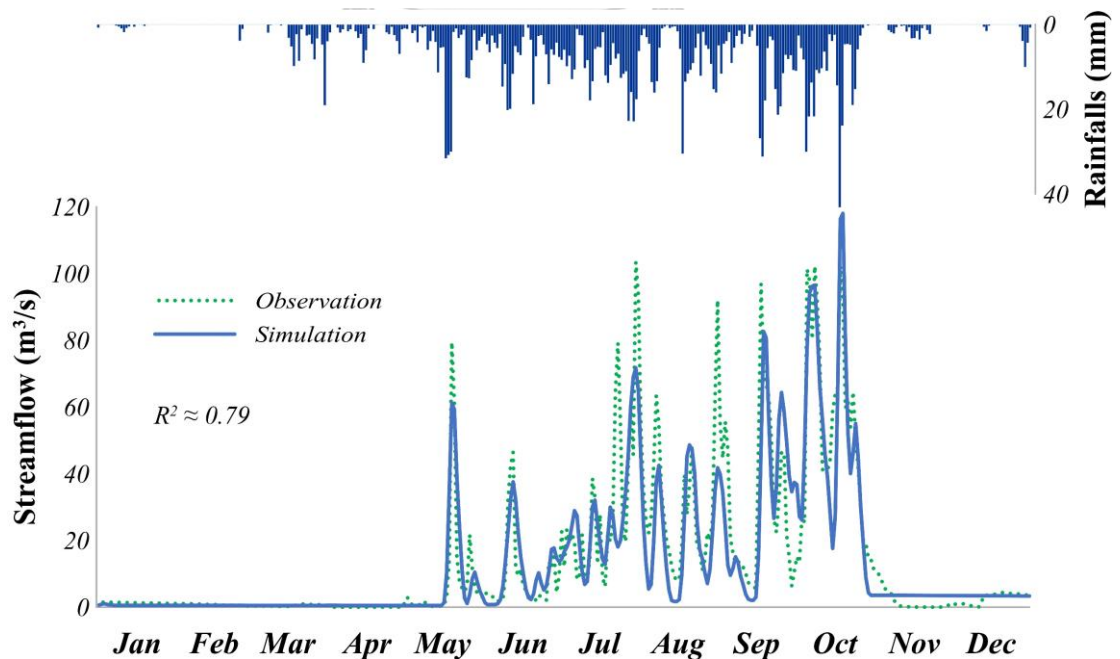


**Figure 4.19** Comparison between the observed streamflow and the simulated streamflow in the Huai Nam Phung subbasin in 2017

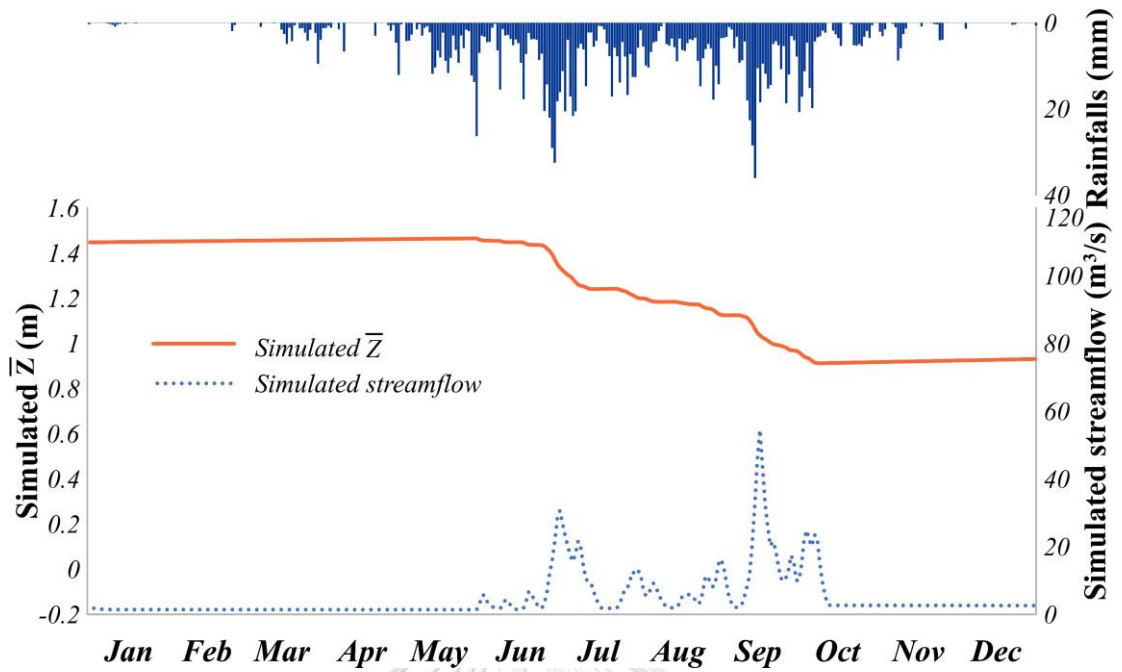


**Figure 4.20** The simulated average height ( $\bar{Z}$ ) between soil surface and groundwater level in the Huai Nam Phung subbasin in 2016

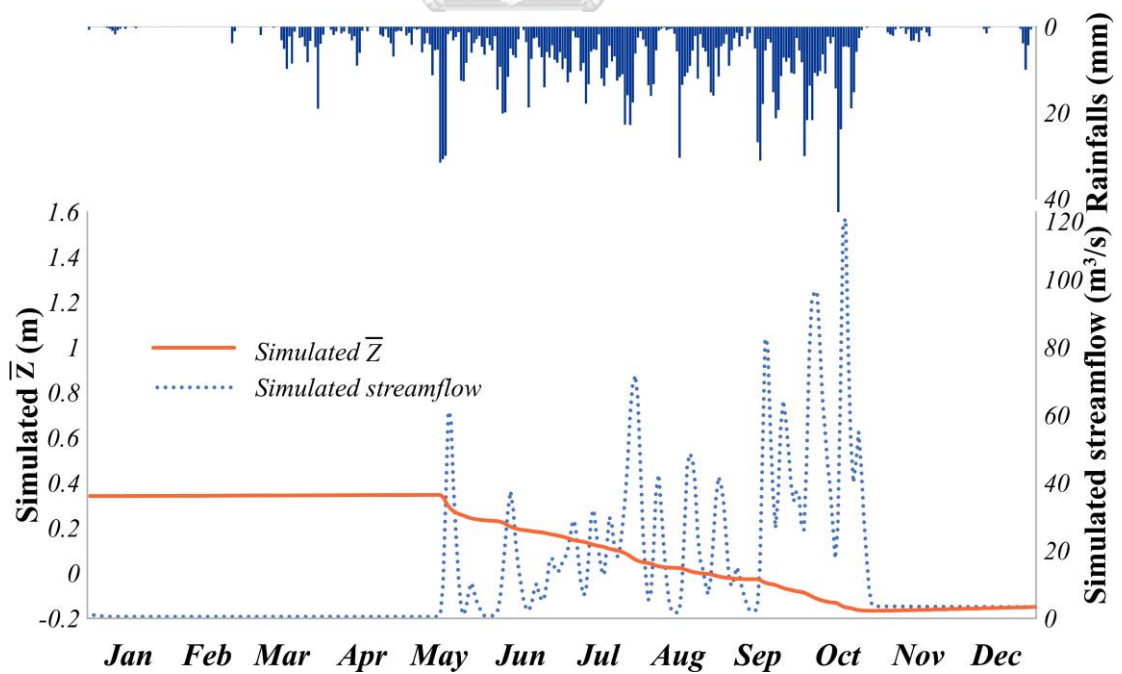


**Figure 4.21** The simulated average height ( $\bar{Z}$ ) between soil surface and groundwater level in the Huai Nam Phung subbasin in 2017

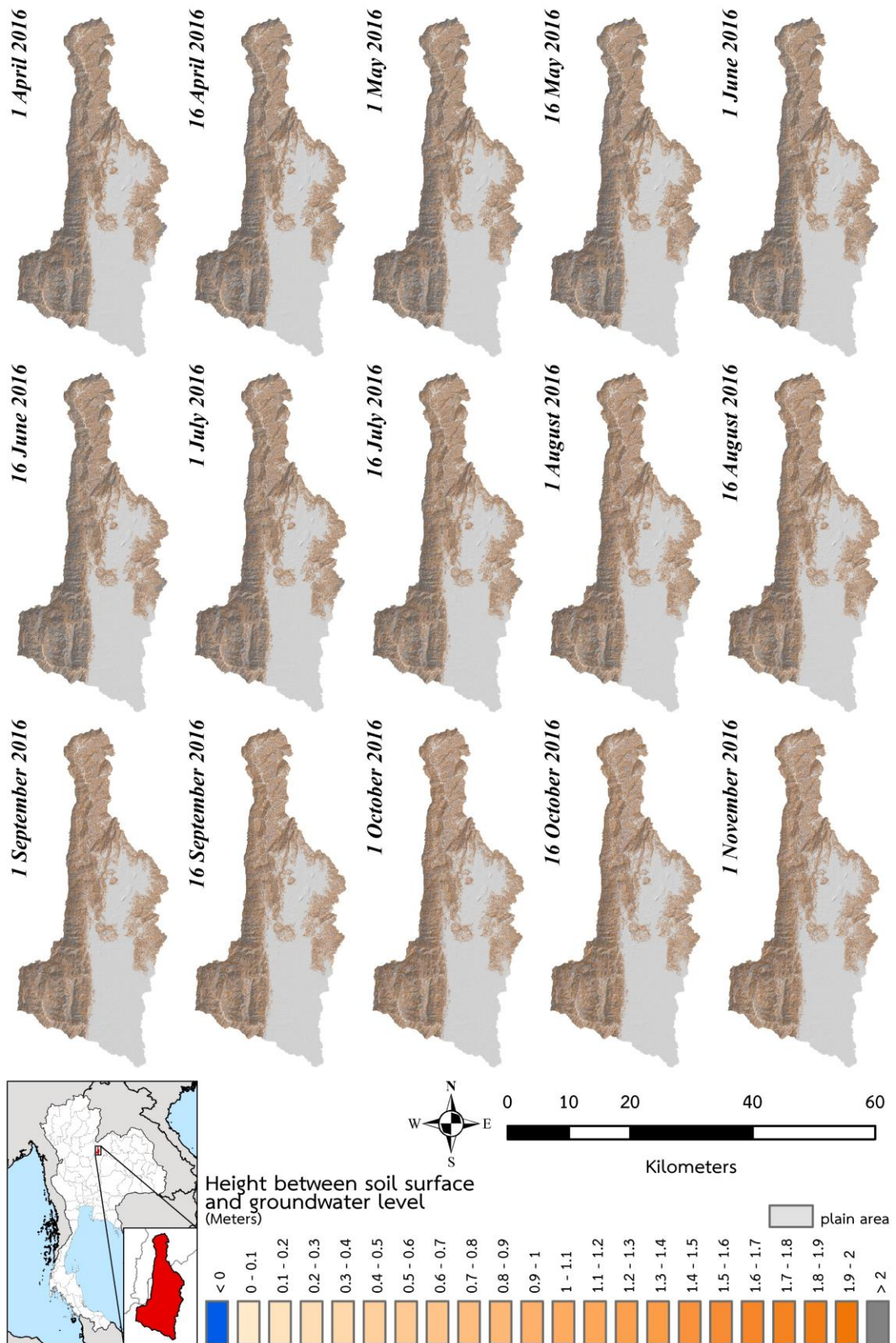


**Figure 4.22** Comparison of the height between soil surface and groundwater level of the Huai Nam Phung subbasin from 1 April to 1 November, 2016

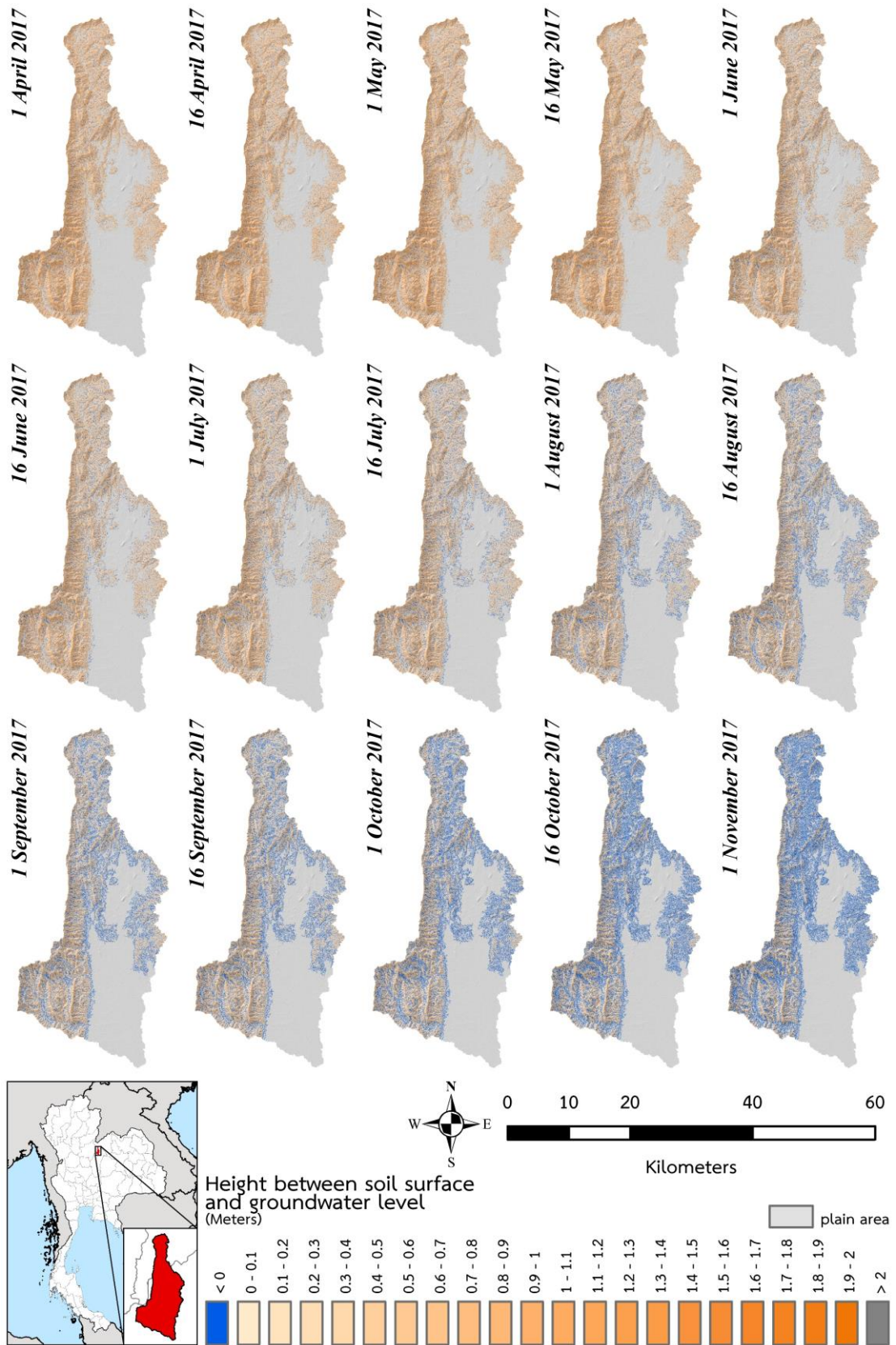


**Figure 4.23** Comparison of the height between soil surface and groundwater level of the Huai Nam Phung subbasin from 1 April to 1 November, 2017

#### 4.9 Groundwater depth determination

Following the previous process, after the height between soil surface and groundwater level was generated, this height was deducted from the soil thickness to obtain the groundwater depth following **Figure 3.17**. Theoretically, the obtained groundwater depth negatively varies with the height between soil surface and groundwater level. The heights and groundwater depths in these two years were shown in **Figures 4.24 and 4.25**, respectively. The high value of groundwater depth indicates that the soil is moist and flooding on the soil surface may occur. The groundwater depth in 2017 was associated with landslide occurrences, which were found during the field survey. Furthermore, the generated groundwater depth is a very important data for the calculation of the factor of safety in slope stability to evaluate the landslide occurrence.

#### 4.10 Estimation of factor of safety in slope stability

Based on the equation of factor of safety (FS) in slope stability (Equation 2.1), it showed that all 63 points of landslide occurrence found in the field was unstable ( $FS < 1.2$ ) (**Figure 4.1**). It is found that many grids in the western side of the basin become unstable ( $FS < 1.2$ ). In 2016, there were few unstable grids, interpreting that there were little chances of landslide occurrences. On the contrary, there were lots of chances of landslide occurrences in 2017. The factor of safety became less than 1.2, indicating the instability, which was found in May and consecutively increased to the peak in late October (**Figure 4.26**). The unstable grids began to appear clearly in July and gradually became clearer until October. The western side of the area along the mountain ranges has more unstable grids than the northeastern side consisting of few unstable grids. In addition, there were no unstable grids in valleys and plain areas.

The most unstable grids were found in 30 October, 2017 (**Figure 4.27**). There were 323.76 km<sup>2</sup> of unstable area which was accounting for 47.22% of the total area. Most of the unstable areas are along mountain ranges in the western and northern parts of the basin, especially in the area of Phu Thap Boek and Nam Ko catchment in the southwestern part of basin. On the other hand, the plain areas in the central part of the basin were still stable. All of the areas with a high slope of more than 30 degrees were unstable.

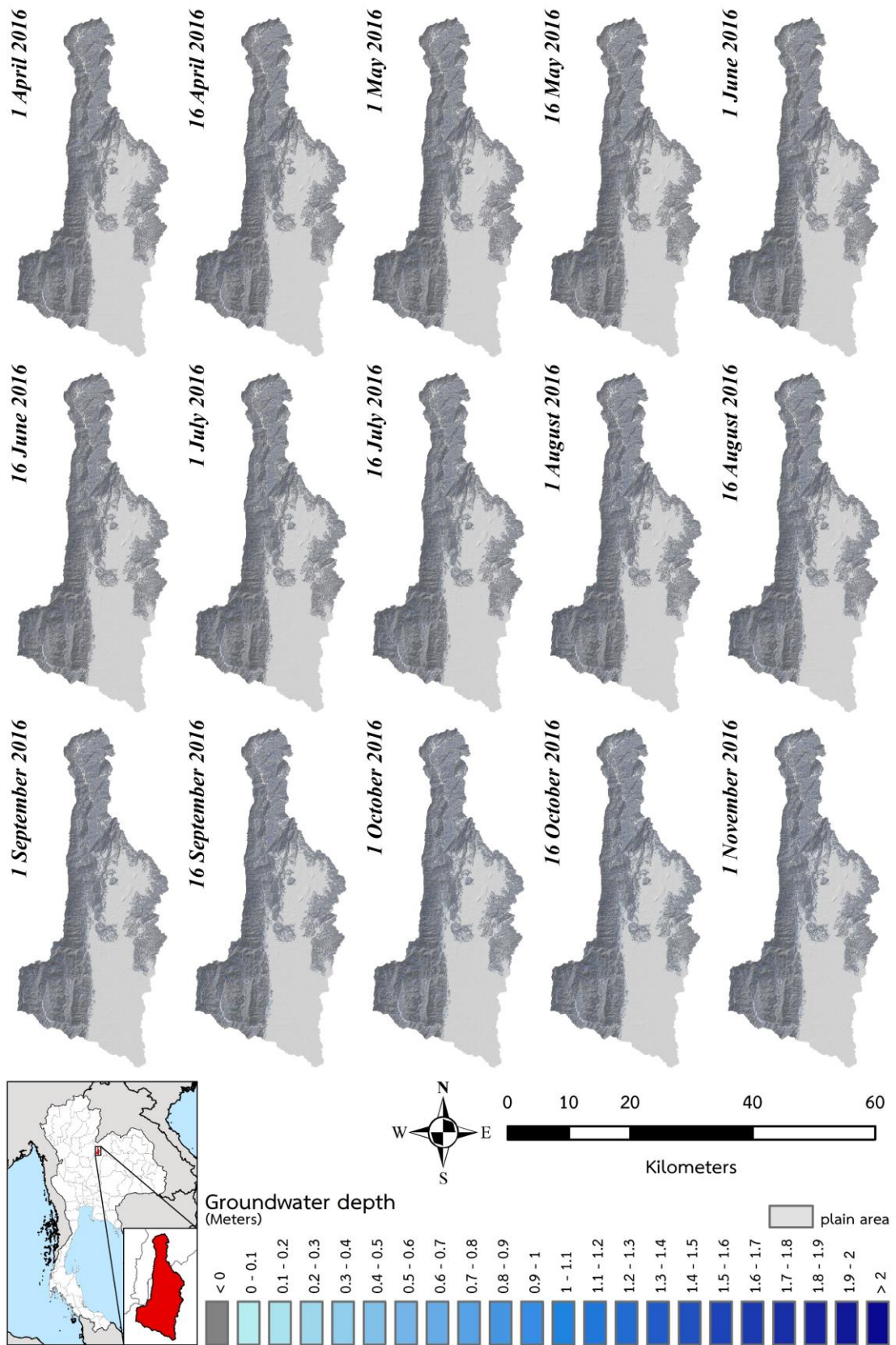


**Figure 4.24** Comparison of groundwater depths of the Huai Nam Phung subbasin from 1 April to 1 November, 2016

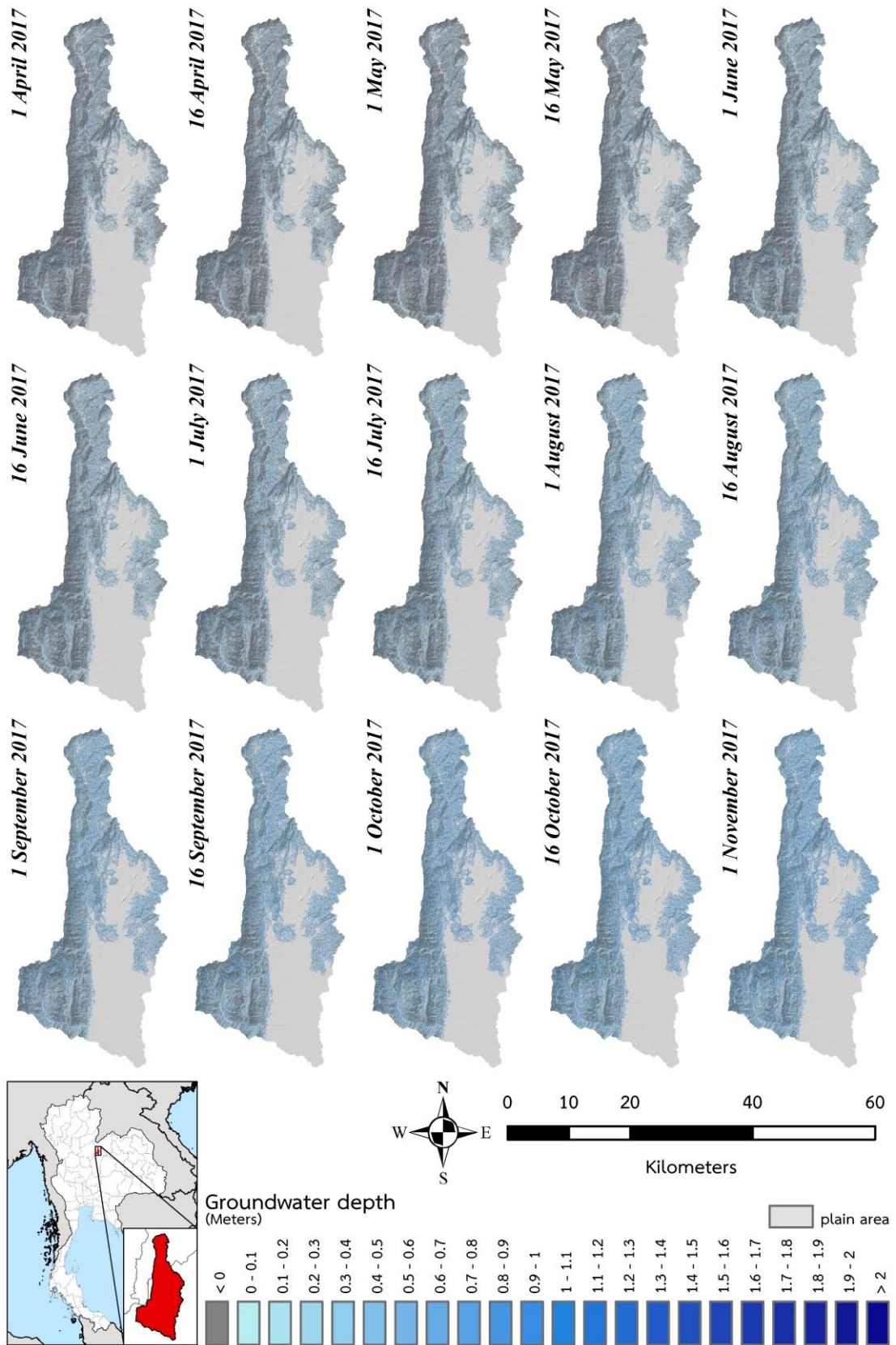


**Figure 4.25** Comparison of groundwater depths of the Huai Nam Phung subbasin from 1 April to 1 November, 2017

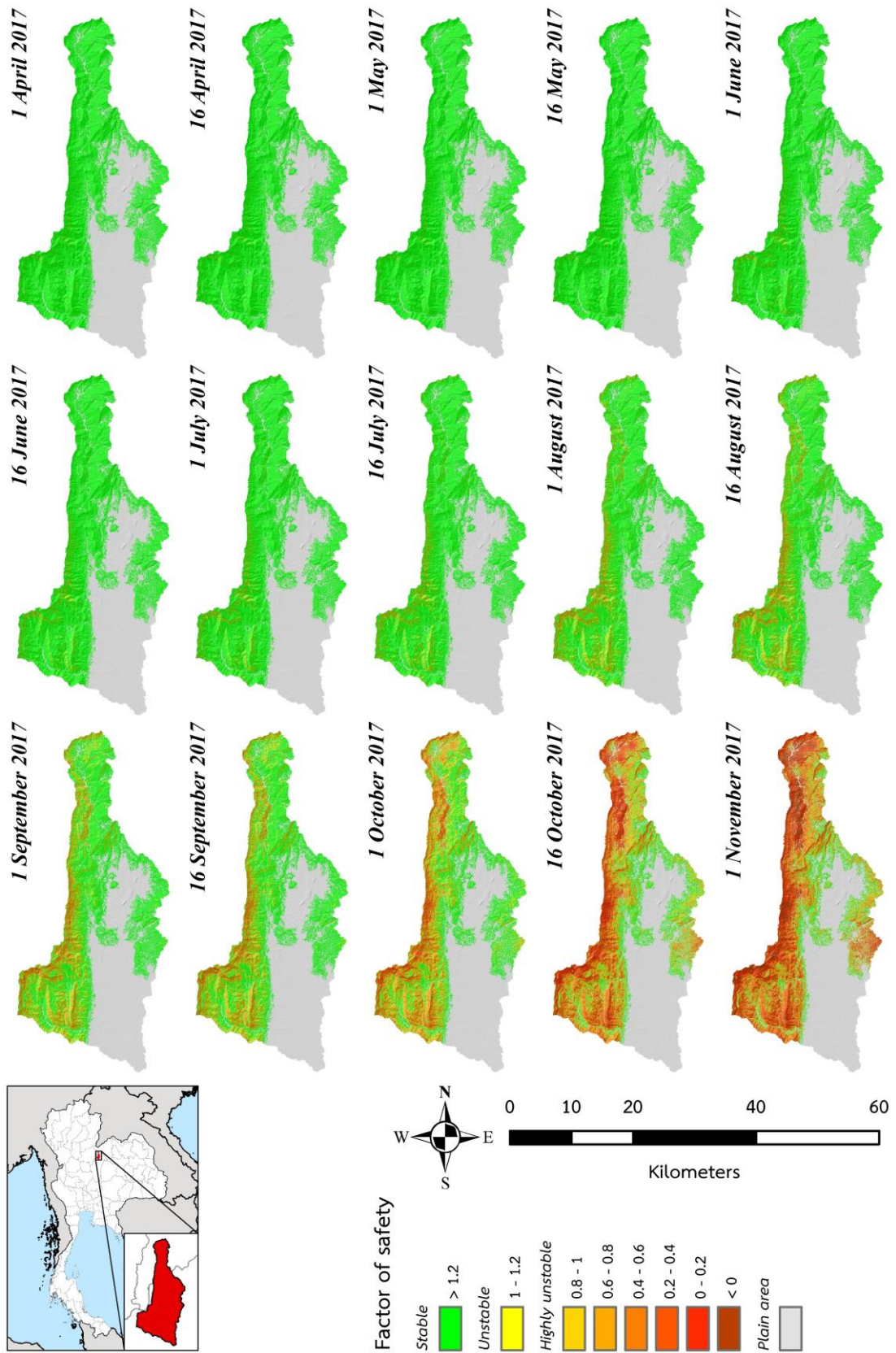


**Figure 4.26** Factor of safety in slope stability of the Huai Nam Phung subbasin from 1 April to 1 November, 2017



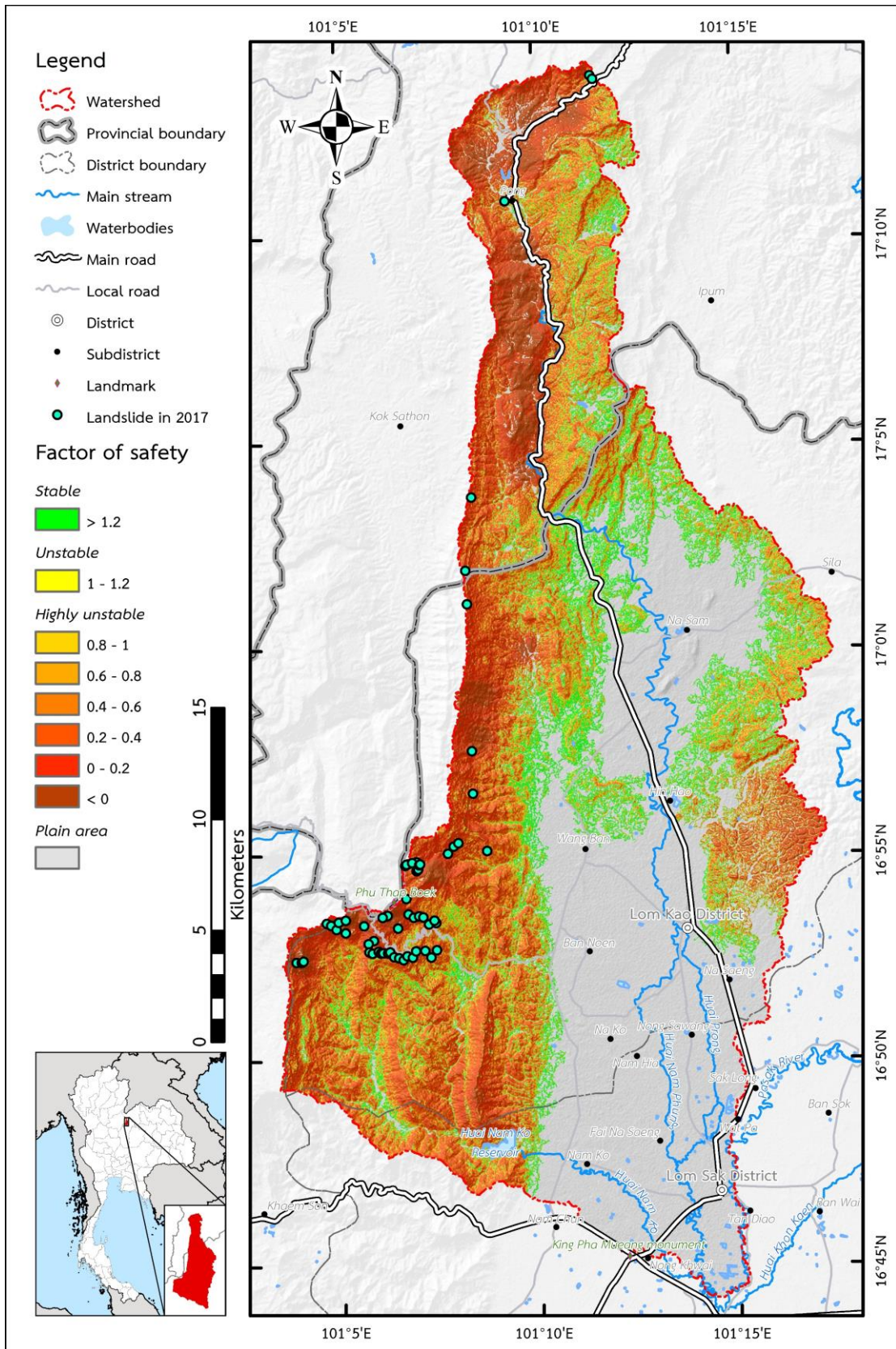


**Figure 4.27** Factor of safety in slope stability of the Huai Nam Phung subbasin on 30 October, 2017

#### 4.11 Validation of landslide occurrence

There were 63 points where landslides occurred in the Huai Nam Phung subbasin in 2017. The value of factor of safety at each point indicated the area just became unstable in the rainy season of 2017 (**Table 4.3**). In 2016, there were very little rainfall and streamflow. Therefore, those points where landslide occurred in 2017 were stable throughout the year.

The factor of safety in slope stability shows that each grid just become highly unstable when the factor of safety is lower than 1. The unstable grids during the rainy season of 2017 were 6 grids, 13 grids, 19 grids, 4 grids and 4 grids in May, June, July, August and September, respectively. From the results, it is possible that landslides may occur in the middle of the rainy season, which is around July – September. It is possible that landslides may occur after the soils in slope areas become unstable.

**Table 4.3** Times of the beginnings of instabilities at the points of landslides in the Huai Nam Phung subbasin

| No.   | Longitude     | Latitude     | Slope (radians) | Soil thickness (meters) | Time of beginning of instability (date) |
|---|---------------|--------------|-----------------|-------------------------|---|
| <i>Matching between imagery survey and field survey</i> |               |              |                 |                         |   |
| 1   | 101°06'01.8"E | 16°53'29.1"N | 0.60            | 0.11                    | 27-08-17                                |
| 2   | 101°06'24.8"E | 16°53'13.1"N | 0.63            | 0.14                    | 06-08-17                                |
| 3   | 101°06'40.9"E | 16°53'33.8"N | 0.55            | 0.16                    | 11-08-17                                |
| 4   | 101°06'48.9"E | 16°53'28.8"N | 0.60            | 0.30                    | 18-06-17                                |
| 5   | 101°06'57.0"E | 16°53'30.7"N | 0.70            | 0.09                    | 22-08-17                                |
| 6   | 101°07'03.3"E | 16°53'29.1"N | 0.60            | 0.30                    | 20-06-17                                |
| 7   | 101°07'20.2"E | 16°53'24.2"N | 0.74            | 0.19                    | 22-06-17                                |
| 8   | 101°06'36.6"E | 16°54'44.6"N | 0.56            | 0.19                    | 01-08-17                                |
| 9   | 101°06'38.7"E | 16°54'46.2"N | 0.59            | 0.20                    | 28-07-17                                |
| 10  | 101°06'47.2"E | 16°54'48.6"N | 0.58            | 0.22                    | 25-07-17                                |
| 11  | 101°06'56.3"E | 16°54'39.0"N | 0.64            | 0.24                    | 05-07-17                                |
| 12  | 101°06'57.8"E | 16°54'45.2"N | 0.56            | 0.34                    | 18-06-17                                |
| 13  | 101°06'59.2"E | 16°54'46.5"N | 0.60            | 0.26                    | 06-07-17                                |

| No.                        | Longitude     | Latitude     | Slope (radian) | Soil thickness (m) | Time of beginning of instability (date) |
|----------------------------|---------------|--------------|----------------|--------------------|---|
| <i>Field survey only</i>   |               |              |                |                    |   |
| 14                         | 101°11'29.0"E | 17°13'56.0"N | 0.38           | 0.25               | 28-08-17                                |
| 15                         | 101°11'33.2"E | 17°13'50.8"N | 0.36           | 0.10               | 28-09-17                                |
| 16                         | 101°09'18.1"E | 17°10'53.4"N | 0.16           | 0.36               | 10-10-17                                |
| 17                         | 101°08'14.6"E | 17°01'05.6"N | 0.53           | 0.05               | 27-09-17                                |
| <i>Imagery survey only</i> |               |              |                |                    |   |
| 18                         | 101°03'50.5"E | 16°52'24.4"N | 0.63           | 0.19               | 24-07-17                                |
| 19                         | 101°03'58.3"E | 16°52'24.4"N | 0.83           | 0.17               | 29-06-17                                |
| 20                         | 101°04'01.1"E | 16°52'26.1"N | 0.84           | 0.15               | 09-07-17                                |
| 21                         | 101°04'36.9"E | 16°53'21.2"N | 0.75           | 0.08               | 26-08-17                                |
| 22                         | 101°04'43.5"E | 16°53'18.2"N | 0.66           | 0.14               | 04-08-17                                |
| 23                         | 101°04'51.7"E | 16°53'12.1"N | 0.85           | 0.06               | 31-08-17                                |
| 24                         | 101°04'55.1"E | 16°53'22.4"N | 0.70           | 0.30               | 22-05-17                                |
| 25                         | 101°05'05.8"E | 16°53'25.4"N | 0.83           | 0.23               | 22-05-17                                |
| 26                         | 101°05'33.2"E | 16°53'17.0"N | 1.06           | 0.01               | 04-10-17                                |
| 27                         | 101°05'05.6"E | 16°53'06.8"N | 0.86           | 0.09               | 30-07-17                                |
| 28                         | 101°05'48.0"E | 16°52'55.4"N | 0.83           | 0.06               | 29-08-17                                |
| 29                         | 101°05'40.1"E | 16°52'51.0"N | 0.87           | 0.12               | 15-07-17                                |
| 30                         | 101°05'41.1"E | 16°52'38.7"N | 0.88           | 0.21               | 18-05-17                                |
| 31                         | 101°05'46.0"E | 16°52'36.8"N | 0.60           | 0.20               | 28-07-17                                |
| 32                         | 101°05'54.9"E | 16°52'39.5"N | 0.64           | 0.39               | 20-05-17                                |
| 33                         | 101°05'58.6"E | 16°52'37.1"N | 0.70           | 0.02               | 04-10-17                                |
| 34                         | 101°06'02.0"E | 16°52'37.4"N | 0.80           | 0.19               | 21-06-17                                |
| 35                         | 101°06'09.3"E | 16°52'37.0"N | 0.67           | 0.28               | 18-06-17                                |
| 36                         | 101°06'12.5"E | 16°52'38.4"N | 0.79           | 0.14               | 26-07-17                                |
| 37                         | 101°06'18.4"E | 16°52'31.5"N | 0.72           | 0.32               | 22-05-17                                |
| 38                         | 101°06'25.9"E | 16°52'29.8"N | 0.79           | 0.16               | 15-07-17                                |
| 39                         | 101°06'32.9"E | 16°52'26.9"N | 0.69           | 0.21               | 11-07-17                                |
| 40                         | 101°06'38.6"E | 16°52'32.5"N | 0.83           | 0.06               | 29-08-17                                |
| 41                         | 101°06'46.8"E | 16°52'30.3"N | 0.78           | 0.24               | 22-05-17                                |

| No. | Longitude     | Latitude     | Slope<br>(radian) | Soil<br>thickness<br>(m) | Time of<br>beginning of<br>instability<br>(date) |
|-----|---------------|--------------|-------------------|--------------------------|--|
| 42  | 101°06'52.0"E | 16°52'39.7"N | 0.77              | 0.20                     | 13-06-17   |
| 43  | 101°07'05.8"E | 16°52'40.2"N | 0.57              | 0.29                     | 05-07-17   |
| 44  | 101°07'23.6"E | 16°52'40.9"N | 0.66              | 0.27                     | 11-06-17   |
| 45  | 101°07'15.0"E | 16°52'30.4"N | 0.67              | 0.09                     | 21-08-17   |
| 46  | 101°06'37.7"E | 16°53'56.3"N | 0.75              | 0.01                     | 06-10-17   |
| 47  | 101°07'41.5"E | 16°55'01.7"N | 0.86              | 0.16                     | 14-06-17   |
| 48  | 101°07'50.5"E | 16°55'12.1"N | 0.71              | 0.22                     | 26-06-17   |
| 49  | 101°07'57.7"E | 16°55'17.0"N | 0.97              | 0.03                     | 18-09-17   |
| 50  | 101°08'41.2"E | 16°55'05.2"N | 0.63              | 0.17                     | 29-07-17   |
| 51  | 101°08'20.5"E | 16°56'29.0"N | 0.67              | 0.09                     | 31-08-17   |
| 52  | 101°08'19.6"E | 16°57'31.0"N | 0.67              | 0.30                     | 08-06-17   |
| 53  | 101°08'12.6"E | 17°01'54.5"N | 0.67              | 0.24                     | 04-07-17   |
| 54  | 101°08'22.6"E | 17°03'41.4"N | 0.63              | 0.14                     | 08-08-17   |
| 55  | 101°06'06.6"E | 16°53'30.7"N | 0.41              | 0.48                     | 24-06-17   |
| 56  | 101°06'08.0"E | 16°53'31.8"N | 0.43              | 0.30                     | 27-07-17   |
| 57  | 101°06'09.2"E | 16°53'31.8"N | 0.55              | 0.27                     | 13-07-17   |
| 58  | 101°07'11.9"E | 16°53'18.9"N | 0.35              | 0.35                     | 08-09-17   |
| 59  | 101°07'22.8"E | 16°53'20.6"N | 0.52              | 0.32                     | 14-07-17   |
| 60  | 101°06'40.3"E | 16°54'46.7"N | 0.53              | 0.23                     | 28-07-17   |
| 61  | 101°06'49.1"E | 16°54'47.9"N | 0.37              | 0.35                     | 04-08-17   |
| 62  | 101°06'53.8"E | 16°54'49.6"N | 0.49              | 0.20                     | 08-08-17   |
| 63  | 101°06'53.8"E | 16°54'36.7"N | 0.45              | 0.23                     | 06-08-17   |

## CHAPTER V DISCUSSIONS

The evaluation of landslides occurrence using TOPMODEL in the Huai Nam Phung subbasin was employed to assess the occurrence of landslides in the mountain areas. The risk areas for landslides are steep slope areas, especially those with slopes of 20 degrees or more. However, those areas can be divided by levels of risks into 2 categories as follows: 1) the low risk area with a slope of around 20 – 30 degrees and 2) the high-risk area with a slope of more than 30 degrees as mentioned in chapter 4. The Huai Nam Phung subbasin has high risk areas on the western part, consisting of ranges of hills stretching in the north-south direction. Therefore, this study conducted an evaluation of landslides in this area. The above-mentioned area is located in Lom Kao District and Lom Sak District of Phetchabun Province. The area is on the border of the Phetchabun Province connected to Phitsanulok Province, which is known as Phu Thap Boek.

### 5.1 Landslides occurrence

According to the investigation of landslides by visual analysis combined with the field surveys, there were landslides occurred in the Huai Nam Phung subbasin, especially near Phu Thap Boek, where is located on the southwest part of the catchment. Shape of landslide scars is sharper than deforested areas because the covered soil had collapsed to the bedrock layer (Akkrawintawong et al., 2008; Singhroy et al., 1998). From the digital elevation model (DEM), it is found that the area has a steep slope terrain, with the highest peak at the Phu Thap Boek approximately 1,768 meters amsl. There are steep cliffs in with traces of landslides throughout the area. The Huai Nam Phung subbasin can be separated into 2 sub-catchments consisting of the Phu Thap Boek, Nam Hia catchment and Nam Ko catchment. Both sub-catchments appeared to have a lot of landslides. Many of them were scattered around the mountain ranges in the western part of the Huai Nam Phung subbasin (**Figure 5.1**). All of landslides occurred in the areas with slopes of higher than 30 degrees or 20 – 30 degrees. This is in line with the theory of landslide occurrence, which has explained that the landslide occurs in an area with a slope of more than 30 degrees. Furthermore, almost all landslides occurred in Thailand were in areas with slopes of higher than 30 degrees (Soralump, 2010).

From the data analysis by remote sensing during 2016 and 2017, landslides occurred between 5 April 2016 and 17 December 2017 (**Figure 5.2**). The satellite imagery from Google Earth can investigate backward for some periods. The landslides may occur in the rainy seasons of 2016 or 2017. However, since the landslides often occur due to heavy rainfalls (Casagli et al., 2006; Guthrie and Evans, 2004; Keefer et al., 1987), it can infer that landslides in the Huai Nam Phung subbasin occurred in the rainy seasons of 2017 since the rainfall in 2016 is quite relatively lower than that in 2017. Therefore, landslide surveys would be better if satellite imagery data was with more detailed and the field survey could reach more landslide areas.

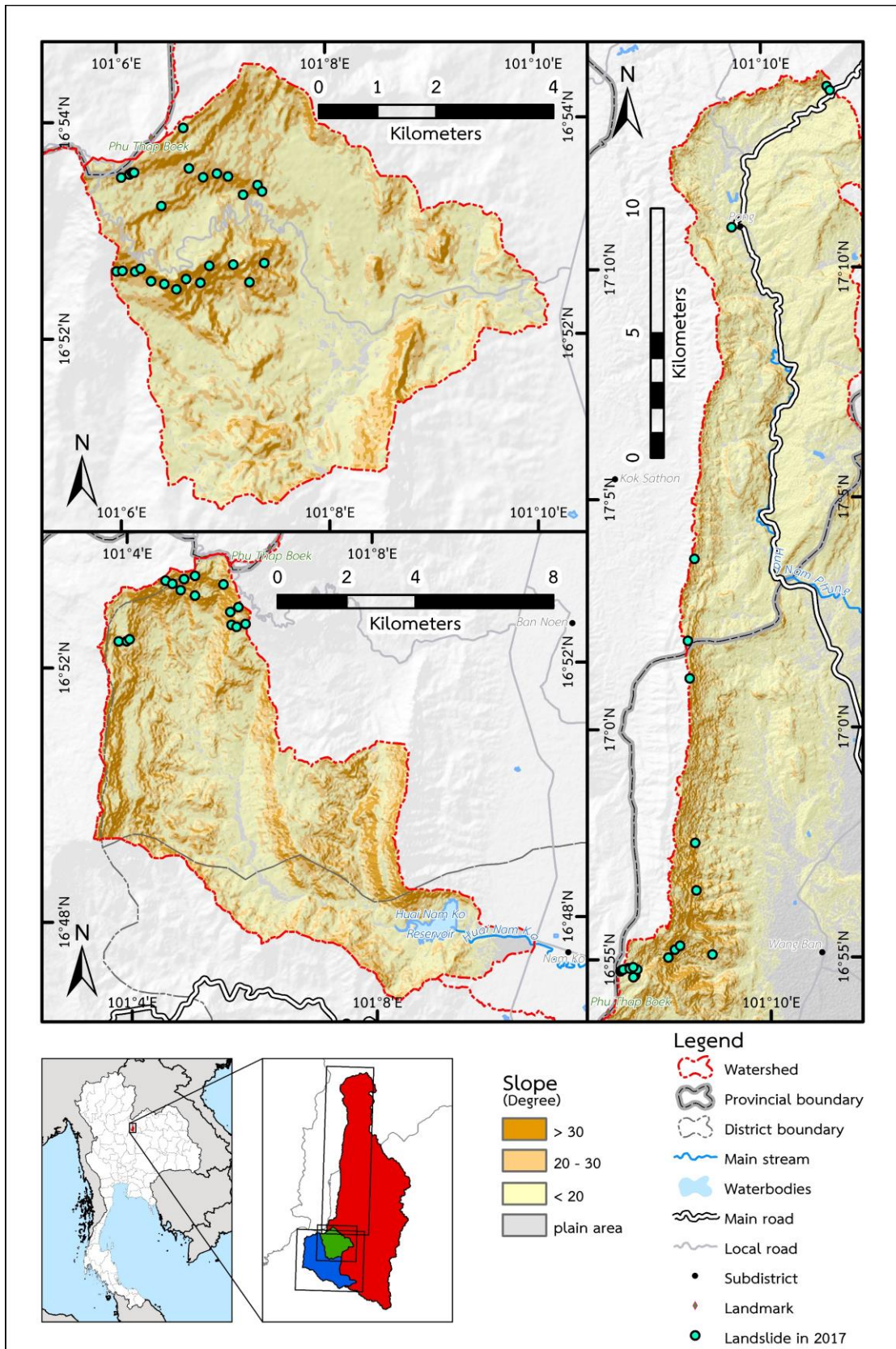


**Figure 5.1** Landslides occurred in the Huai Nam Phung subbasin in 2017 in each sub-catchment

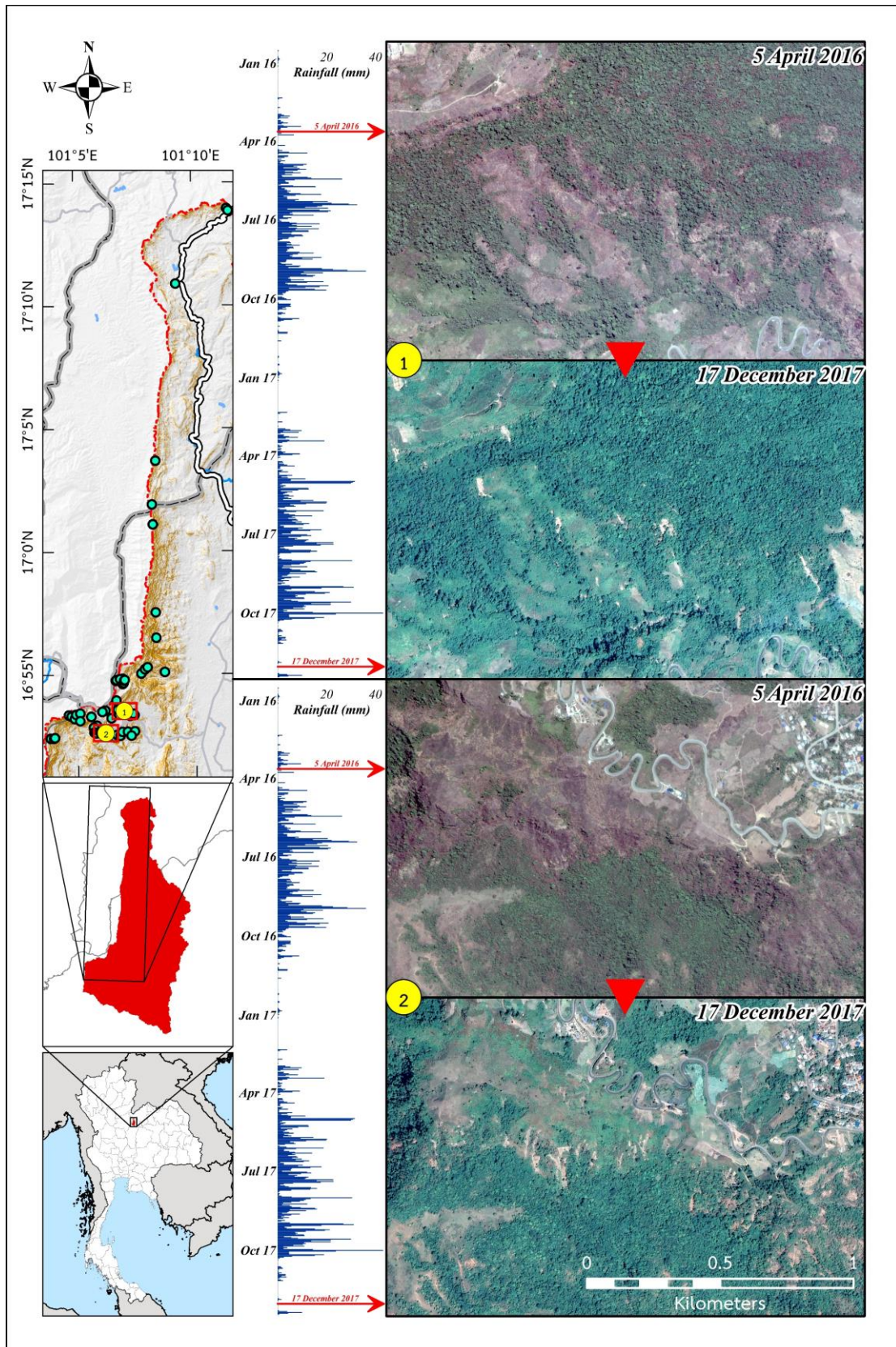


**Figure 5.2** Comparison of satellite imageries in the Huai Nam Phung subbasin between 2016 and 2017 in areas of the Phu Thap Boek

## 5.2 Soil thickness

The soil thickness is a variable used to calculate the factor of safety (FS) in slope stability. However, the complete map of the soil thickness is not available (Farshad et al., 2013). Therefore, a relationship between topographic wetness index (TWI) and observed soil thickness (D) was established to generate the soil thickness map for the areas with slope of higher than 6%. Thirteen points of the soil thickness was observed during the field survey on 16 – 19 February, 2019 in the area near the Phu Thap Boek.

The result of data analysis shows a linear relationship between the TWI and D that soil thickness 0.101 meters per TWI with the  $R^2$  of 0.59 (**Figure 4.7**). The results of this study correspond to the studies of Lee et al. (2009) and Ho et al. (2012) that studies about the prediction of the shallow landslide occurrence in Taiwan. The value of the TWI is higher near the valley and lower near the ridge. For the Phu Thap Boek, the maximum TWI value is 16.39 and the minimum TWI value is 0. These values are consistent with those in the previous studies (Lee et al., 2009; Ho et al., 2012). The previous study of Lee et al. (2009) has showed that soil thickness 0.1 meters per TWI with the  $R^2$  of 0.85 and the previous study of Ho et al. (2012) has showed that soil thickness 0.1 meters per TWI with the  $R^2$  of 0.85 as well. In addition, Sørensen et al. (2005) found that the higher soil moisture is associated with the higher value of TWI in the valley and the lower moisture is associated with the lower value of TWI on the ridge also supports our generated TWI. The result of the mapping by the linear relationship suggests that the highest soil thickness is 1.64 meters, which can be found near the 6% slope areas and lowest soil thickness is close to 0 meter, which can be found near the ridge.

However, the linear relationship used to fit the TWI and soil thickness (D) is moderately correlated with  $R^2$  of 0.59 because the number of observed soil thickness data used in this study was only 13 points. Only samples the areas near the outcrops were collected because of the limitation of digging tools. The other limitation is that the resolution of TWI map was too low. This caused large grid size, leading there are several thickness values in each grid. Gathering more soil thickness data and generating the TWI map with higher resolution can lead to more reliable results of soil thickness mapping.

The theory of the slope of the land stated that the hill must have the slope of higher 6% (DeYoung, 2018). Therefore, the areas with slope lower than 6% are the plain terrain. The relationship of the soil thicknesses of the Huai Nam Phung subbasin showed that the soil thickness in plain area is higher than that in the hill slope (**Figure 5.3**). Furthermore, this result confirmed that D can be explained by the TWI at the high slope areas. The TWI is good for the analysis in the high slope area but not suitable for the analysis in the plain terrain. In the high slope area, the generated TWI can show the locations of ridges and valleys. In the plain terrain, the generated TWI and soil thickness may be distorted by the very high values. However, this study focusses only the high slope area because it is the study of landslide occurrence. Therefore, the distort values of the TWI and D in the plain can be ignored.



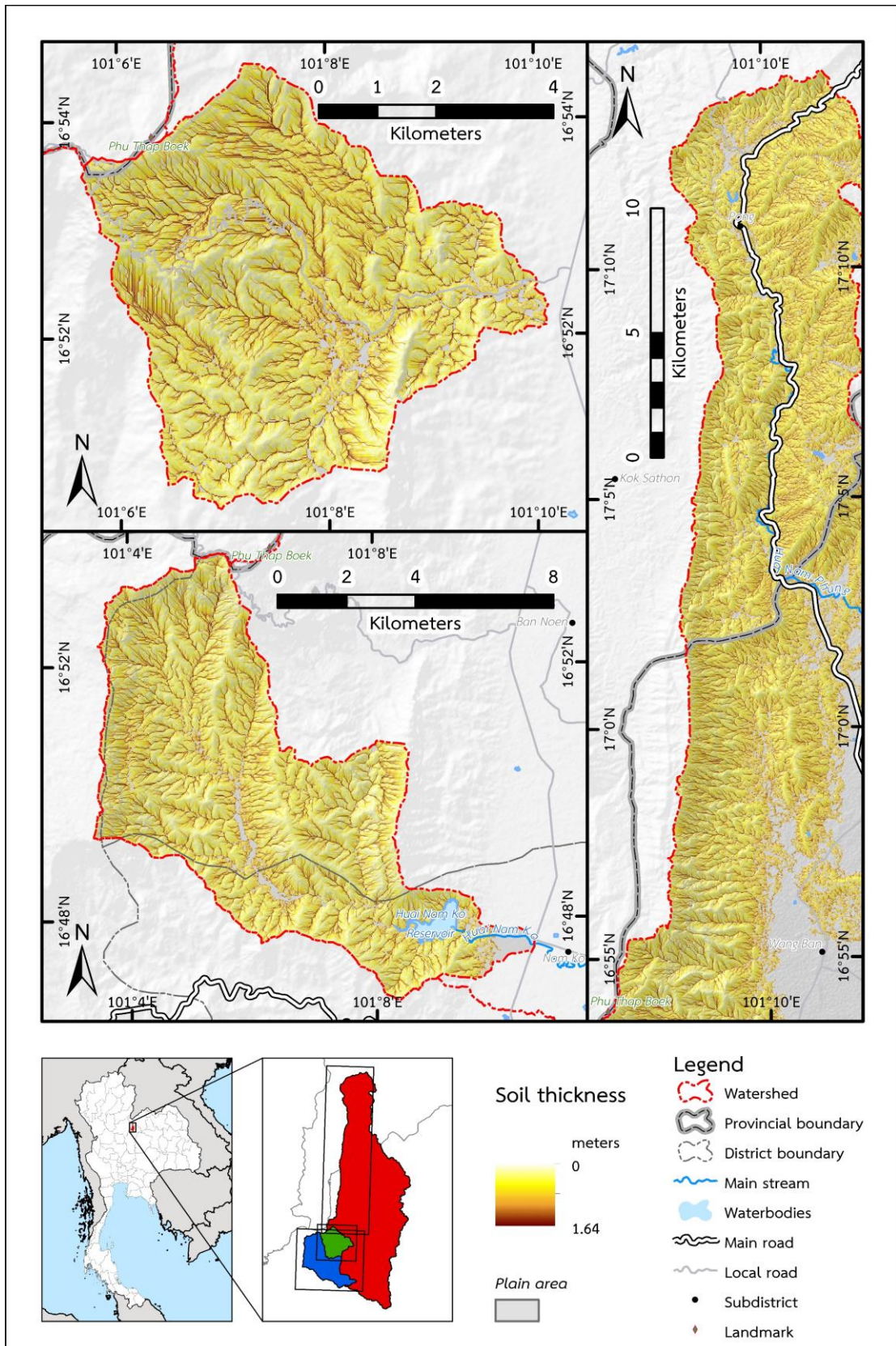


**Figure 5.3** Soil thickness in the Huai Nam Phung subbasin in each sub-catchment

### 5.3 Model simulation

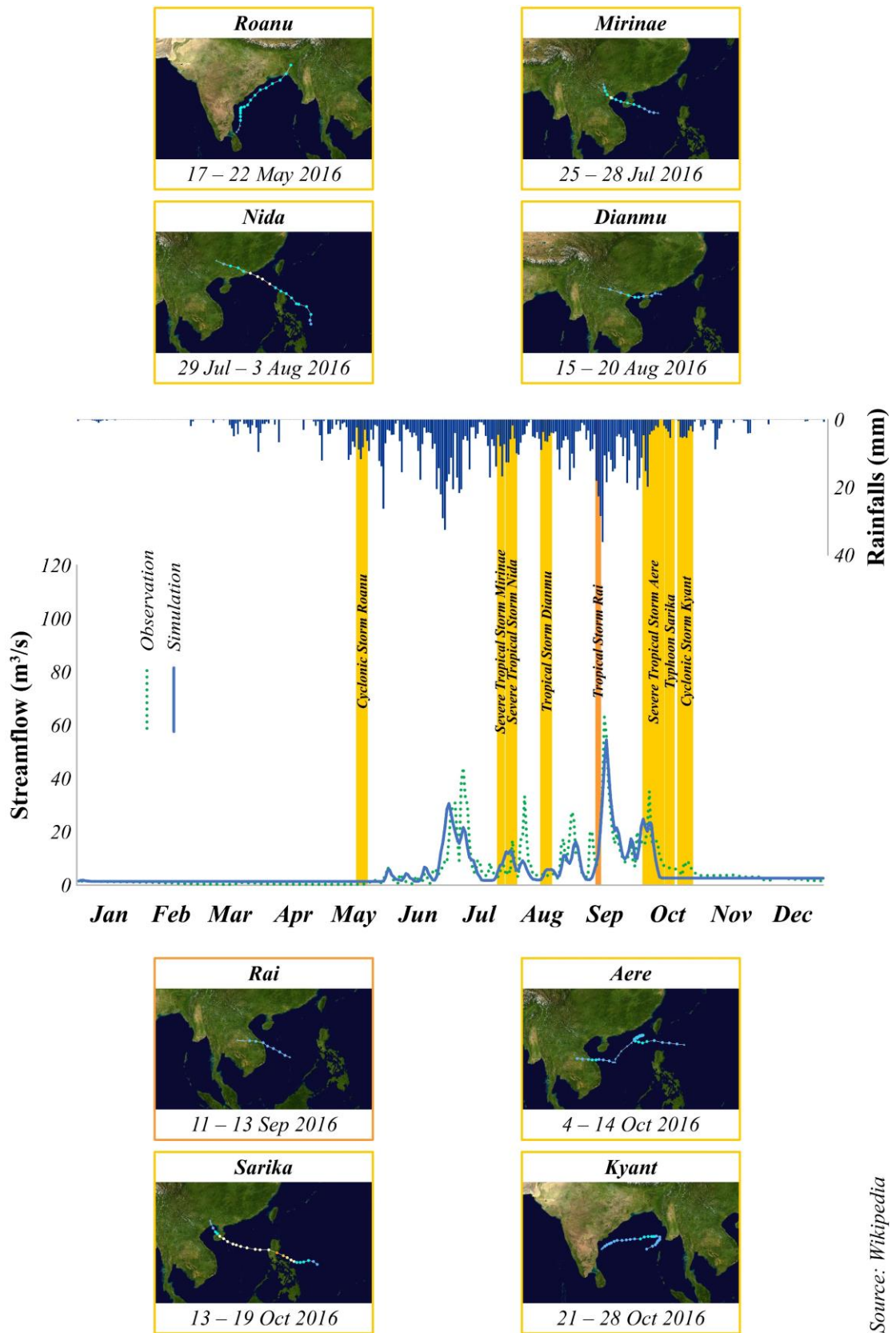
This study obtained the values of height between soil surface and groundwater level from the topography based on the hydrological model (TOPMODEL). It is an important variable to calculate groundwater depth that is a variable to generate factor of safety in slope stability. In the calibration process, the observed streamflow is required to compare with generated streamflow by the TOPMODEL. Finally, the appropriate parameters could be estimated. The simulated streamflow must correspond closely to the observed streamflow. The results of the study were discussed as follows:

#### 5.3.1 Streamflow

Based on the investigation of the rainfall and streamflow in the Huai Nam Phung subbasin and records of storm events in Thailand and surrounding regions, we found that landslide occurrence associated with some storm events caused heavy rainfall and high runoff amount. However, some storms had little or no effect on rainfall and runoff in the study area. The different effects depend upon the different sizes and strengths of those storms. In addition, the other factor is the distance between the storm and the study area, which can affect rainfall and runoff. In other word, the storm may have a little effect if it is far from the study area.

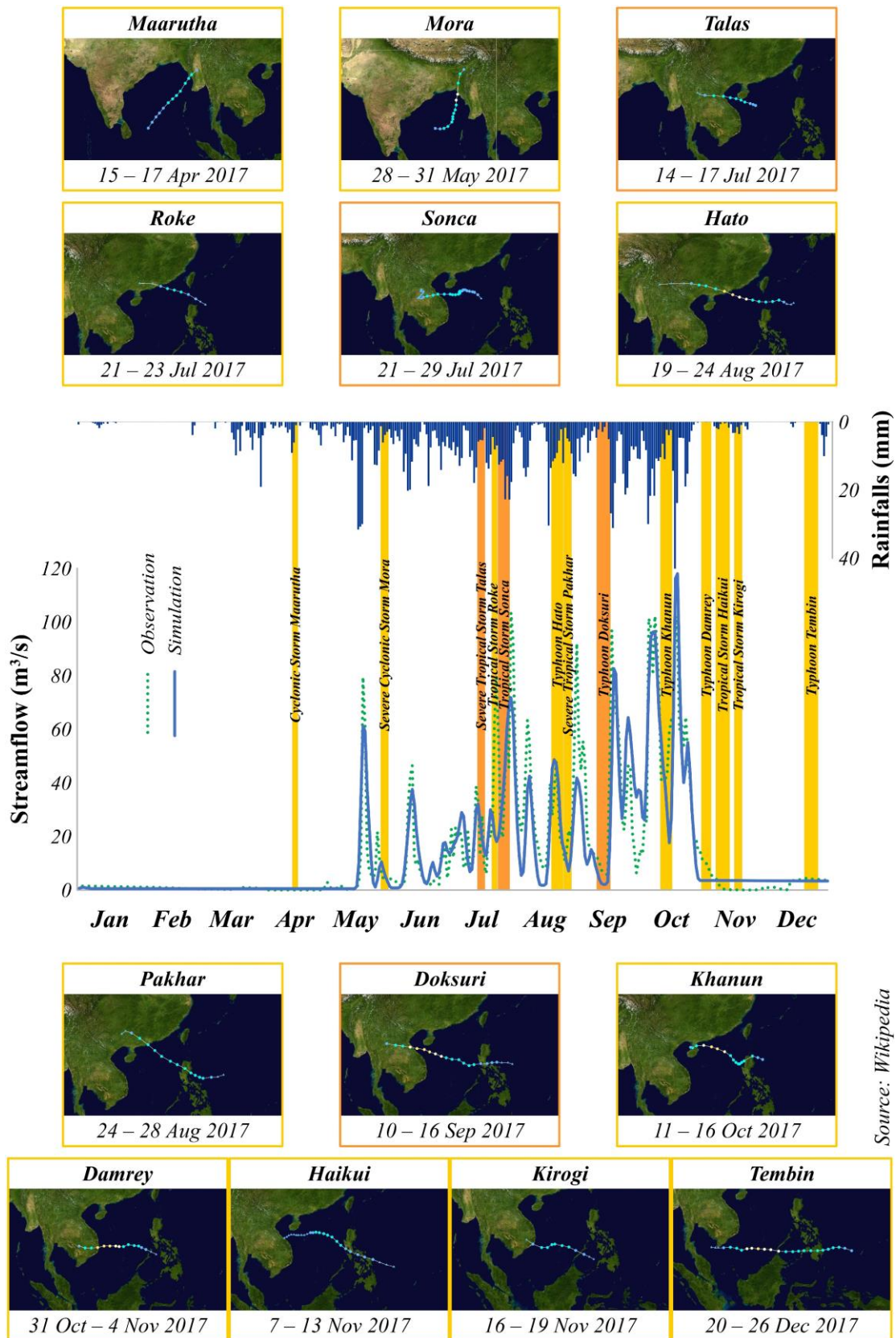
In 2016, there was a storm that affected rainfall and runoff in the Huai Nam Phung subbasin, namely, the tropical storm Rai (**Figure 5.4**). This tropical storm originated in the South China Sea and moved through Vietnam and Laos eventually to Thailand. Importantly, it moved directly into the study area. The period of heavy rain occurred when the storm reached Thailand on 13 September 2016. After the 1 – 2 days of heavy rainfall, the amount of streamflow increased dramatically. The heavy rains increase the accumulated runoff from the upstream and finally is drained to the downstream (Dunne and Black, 1970; Verdi et al., 2017). In conclusions, the simulated streamflow was close to the observed streamflow data. Based on rainfall amounts, the weather in 2016 can be defined as a drought year as compared to that in 2017. Furthermore, it can be observed by the number of storms approaching Thailand in 2016, which were obviously less than those in 2017.

In 2017, there were 3 storms which obviously affected rainfall and streamflow in the Huai Nam Phung subbasin (**Figure 5.5**). Firstly, the severe tropical storm Talas originated in the South China Sea and moved through Hainan Island, Gulf of Tonkin, Vietnam and Laos eventually to Thailand during 14 – 17 July 2017. Secondly, the tropical storm Sonca originated in the South China Sea and moved through Vietnam and Laos to Thailand during 21 – 29 July 2017. The last one, the typhoon Doksuri originated in the Philippine Sea and moved through Philippines, South China Sea, Vietnam and Laos to Thailand during 10 – 16 September 2017. In addition, there are many heavy rainfalls in October 2017, which coincides with a warning of TMD and previous study of Yoshifuji et al. (2006) that the rain generally is heavy at the end of the rainy season.



Source: Wikipedia

**Figure 5.4** Streamflow and rainfall in the Huai Nam Phung subbasin and storm events in 2016



Source: Wikipedia

**Figure 5.5** Streamflow and rainfall in the Huai Nam Phung subbasin and storm events in 2017

As mentioned, it could state that in 2017, there was a greater amount of rainfall and streamflow than in 2016. Thus, it is possible that landslides occur during the heavy rains in 2017.

### 5.3.2 Height between soil surface and groundwater level

According to the results in Chapter 4, the heights between soil surface and groundwater level continuously decreased (**Figures 4.20 and 4.21**). It is coincided with the accumulation of groundwater after rainfall events (Freeze and Cherry, 1979). If the value of the height between soil surface and groundwater level approach zero, the groundwater rises to the ground surface. If the values of height between soil surface and groundwater level is less than 0, overland flow occurs on the ground surface as shown in **Figure 3.17**.

The record of the National Water Resources Database of Thailand organized by Hydro - Informatics Institute (Public Organization) shows that many flooding events were recorded in 2017. In addition, there was a lot of flooding news in the study area in 2017 as compared to those in 2016 (**Table 5.1**). From the news and meteorological data, it can be concluded that year 2017 was a wet year. Particularly, there was a report of landslide and flash flood near the Phu Thap Boek, which is in the southwestern part of the Huai Nam Phung subbasin on 23 October 2017. The heavy rainfalls probably result in landslides in many areas. In addition, the graph shows that the height between soil surface and groundwater level was lower than 0 starting in August, 2017 (**Figure 4.20**). It means an occurrence of overland flow. When investigating the simulated height between soil surface and groundwater level with the news on flooding in 2017, it can be concluded that the simulation results are close to the real-world conditions.

**Table 5.1** News on floodings in Phetchabun Province, the location of the Huai Nam Phung subbasin

| Year | Date              | Reporter          | News picture  |
|------|-------------------|-------------------|---|
| 2016 | 15 September 2016 | Post Today (2016) |  <p>Reference (in Thai):<br/> <a href="https://www.posttoday.com/social/local/454545">https://www.posttoday.com/social/local/454545</a></p> |

| Year | Date                   | Reporter                        | News picture  |
|------|------------------------|---------------------------------|---|
| 2017 | 18<br>May<br>2017      | Channel 3<br>Thailand<br>(2017) |  <p data-bbox="715 752 1246 824">Reference (in Thai):<br/><a href="http://news.ch3thailand.com/local/43715">http://news.ch3thailand.com/local/43715</a></p>                             |
| 2017 | 29<br>July<br>2017     | Daily<br>News<br>(2017)         |  <p data-bbox="715 1252 1310 1323">Reference (in Thai):<br/><a href="https://www.dailynews.co.th/regional/588419">https://www.dailynews.co.th/regional/588419</a></p>                  |
| 2017 | 1<br>September<br>2017 | Thairath<br>(2017)              |  <p data-bbox="715 1751 1374 1823">Reference (in Thai):<br/><a href="https://www.thairath.co.th/news/local/north/1056960">https://www.thairath.co.th/news/local/north/1056960</a></p> |

| Year | Date            | Reporter          | News picture   |
|------|-----------------|-------------------|--|
| 2017 | 11 October 2017 | Post Today (2017) |  <p>Reference (in Thai):<br/> <a href="https://www.posttoday.com/social/local/519679">https://www.posttoday.com/social/local/519679</a></p>                                    |
| 2017 | 23 October 2017 | Workpoint (2017)  |  <p>Reference (in Thai):<br/> <a href="https://workpointnews.com/2017/10/23/เกิดดินสไลด์ปิดทับเส้นทาง">https://workpointnews.com/2017/10/23/เกิดดินสไลด์ปิดทับเส้นทาง</a></p> |

#### 5.4 Model parameters

From the sensitivity analysis, there are 3 most sensitive parameters, consisting of logarithm of the areal average of saturated soil transmissivity ( $\ln T_e$ ), surface hydraulic conductivity ( $k_0$ ), and capillary drive (CD). The parameters that are moderately sensitive are initial subsurface flow per unit area ( $qs_0$ ), channel flow inside catchment ( $vr$ ), and model parameter controlling the rate of decline of transmissivity in the soil profile ( $m$ ). The last 3 parameters that are very low sensitive are maximum root zone storage deficit ( $Sr_{max}$ ), unsaturated zone time delay per unit storage deficit ( $td$ ), and initial root zone storage deficit ( $Sr_0$ ).

This study simulated streamflow in 2016 and 2017. The streamflow 2016 and 2017 cannot be simulated by the same parameter set because some parameters are very sensitive. In other word, small changes of parameter values may strongly affect the results. Moreover, as mentioned before, the weather of these two consecutive years (a drought and wet years, respectively) are relatively different, which caused the

sensitive parameters of these two years are different. However, the parameters would be carefully checked with other previous studies and guidelines as follows. For the most sensitive parameter, the  $\ln T_e$ , it should be a negative value. From previous study of Silva et al. (2008), the value of saturated soil transmissivity is  $0.11 \text{ m}^2/\text{h}$  ( $\ln T_e = -2.21 \text{ m}^2/\text{h}$ ). For our study area, the calibrated values of the  $\ln T_e$ 's in 2016 and 2017 are  $-6.45 (0.0016 \text{ m}^2/\text{h})$  and  $-7.87 (0.00038 \text{ m}^2/\text{h})$ , respectively, which are reliable. The second most sensitive parameter is the surface hydraulic conductivity ( $k_0$ ). The **Table 5.2** shows the values of the hydraulic conductivities of soil medias classified by their sizes which are in the range of  $0 - 0.1 \text{ m/s}$  (Domenico and Schwartz, 1998). The calibrated values of the  $k_0$ 's in 2016 and 2017 are  $0.002 \text{ m/h}$  and  $0.004 \text{ m/h}$  (or  $5.6 \times 10^{-6}$  and  $1.1 \times 10^{-6} \text{ m/s}$ ), respectively. These values are in the range of  $10^{-7} - 10^{-2} \text{ m/s}$  which indicates that that soil materials in the study area are sand (Phewnil et al., 2010; Samrit et al., 2008). It is associated with the observation in the field study which reveals that most of the soils in the study area are sand. The last most sensitive parameter is the capillary drive (CD). From the previous study of Morel-Seytoux and Nimmo (1999), the values of the CD are between  $0.1 - 1 \text{ m}$ . The values of CD in our study are similar,  $0.024 \text{ m}$  for 2016 and  $0.045 \text{ m}$  for in 2017. Therefore, they are reliable.

For the other parameters, which are moderately and low sensitive, we set them as the values used in the TOPMODEL tutorial following the study of Buytaert (2009) which simulates a streamflow in Huagrahuma basin. These fitted parameters are acceptable because these parameters have little effect on the simulated streamflow.

**Table 5.2** Hydraulic conductivities of unconsolidated sedimentary materials, sedimentary rocks and crystalline rock materials (Domenico and Schwartz, 1998)

| <b>Material</b>                                    | <b>hydraulic conductivity (m/s)</b>      |
|--|--|
| <b><i>Unconsolidated sedimentary materials</i></b> |  |
| Coarse sand  | $9 \times 10^{-7} - 6 \times 10^{-3}$    |
| Medium sand  | $9 \times 10^{-7} - 5 \times 10^{-4}$    |
| Fine sand  | $2 \times 10^{-7} - 2 \times 10^{-4}$    |
| Silt, loess  | $1 \times 10^{-9} - 2 \times 10^{-5}$    |
| Till   | $1 \times 10^{-12} - 2 \times 10^{-6}$   |
| Clay   | $1 \times 10^{-11} - 4.7 \times 10^{-9}$ |
| Unweathered marine clay                            | $8 \times 10^{-13} - 2 \times 10^{-9}$   |
| <b><i>Sedimentary rocks</i></b>                    |  |
| Karst and reef limestone                           | $1 \times 10^{-6} - 2 \times 10^{-2}$    |
| Limestone, dolomite                                | $1 \times 10^{-9} - 6 \times 10^{-6}$    |
| Sandstone  | $3 \times 10^{-10} - 6 \times 10^{-6}$   |
| Siltstone  | $1 \times 10^{-11} - 1.4 \times 10^{-8}$ |
| Salt   | $1 \times 10^{-12} - 1 \times 10^{-10}$  |
| Anhydrite  | $4 \times 10^{-13} - 2 \times 10^{-8}$   |
| Shale  | $1 \times 10^{-13} - 2 \times 10^{-9}$   |

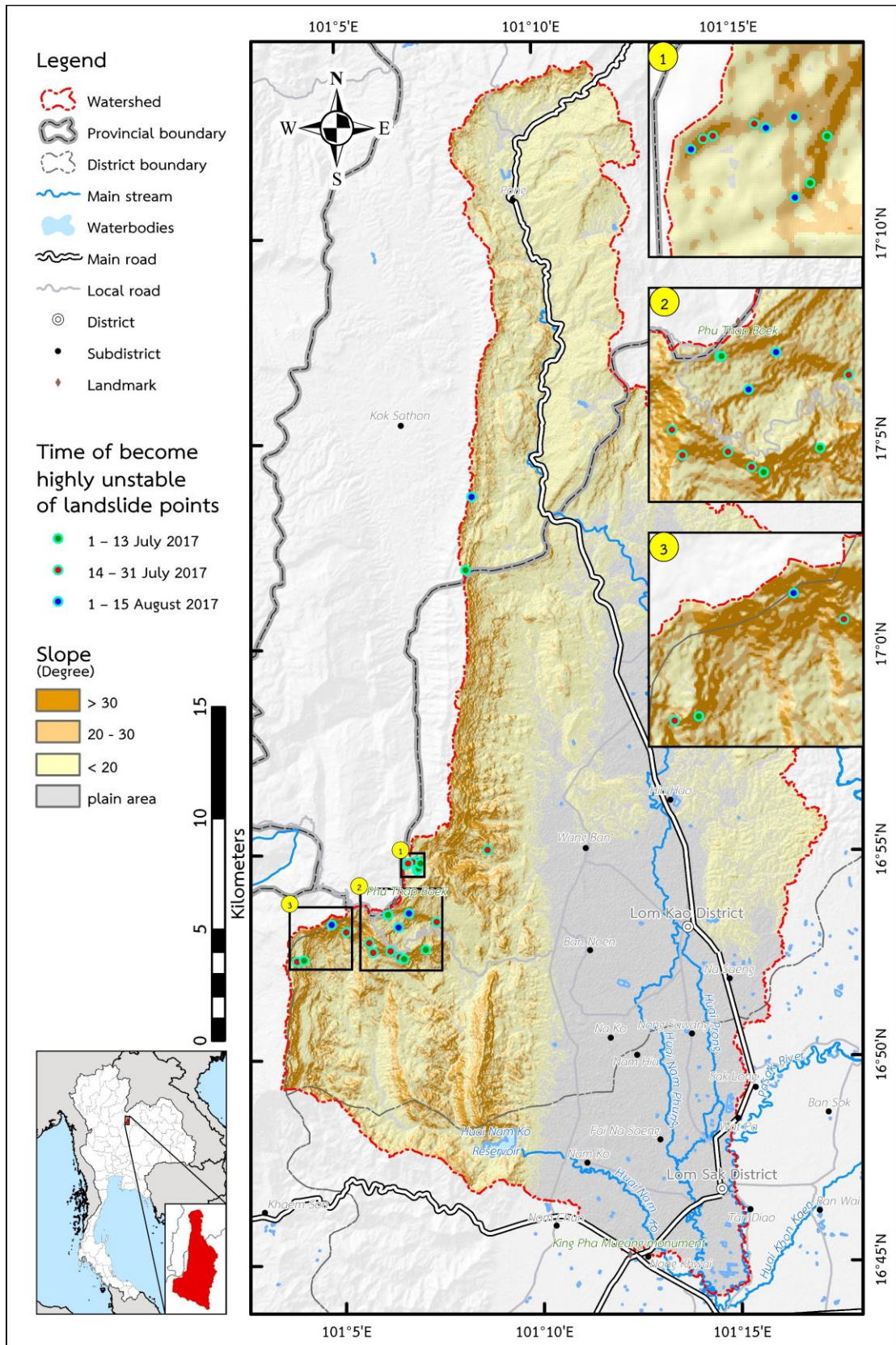


| <b>Material</b>                          | <b>hydraulic conductivity (m/s)</b>       |
|--|---|
| <i>Crystalline rocks</i>                 |   |
| Permeable basalt                         | $4 \times 10^{-7} - 2 \times 10^{-2}$     |
| Fractured igneous and metamorphic rock   | $8 \times 10^{-9} - 3 \times 10^{-4}$     |
| Weathered granite                        | $3.3 \times 10^{-6} - 5.2 \times 10^{-5}$ |
| Weathered gabbro                         | $5.5 \times 10^{-7} - 3.8 \times 10^{-6}$ |
| Basalt                                   | $2 \times 10^{-11} - 4.2 \times 10^{-7}$  |
| Unfractured igneous and metamorphic rock | $3 \times 10^{-14} - 2 \times 10^{-10}$   |

### 5.5 Slope stability

This study has found that the study area was stable in 2016, while it was consecutively unstable in 2017. The maps showing the factor of safety in slope stability are different for each day as shown in **Figure 4.26**. The areas had been consecutively unstable starting from April 2017 until the peak on 30 October 2017. The unstable slope results in landslides. This study can identify when the areas became unstable but still cannot determine when the landslide occurred because there has been no clear record of landslides. In addition, the satellite imageries used in the study is available only on 2 days (5 April 2016 and 17 December 2017). According to the landslide handbook (Highland and Bobrowsky, 2008), landslides usually occur after the slope become unstable. Therefore, it can be inferred that landslides in each area may occur after the value of the factor of safety in slope stability reduced to less than 1.2. However, the instability of the slope does not mean the landslide certainly occurs. It is possible that there is no landslide at all even though the slope is unstable. Slope instability is only an indication that the landslide likely occurs with high probability.

In July 2017, there are 2 storms entering the Huai Nam Phung subbasin. They caused the slope to become highly unstable (factor of safety lower than 1) for 13 points (**Figures 5.6 and 5.7**). The severe tropical storm Talas originated in the South China sea and moved to the study area between 14 to 17 July 2017. The tropical storm Sonca originated in the South China sea and moved to the study area between 21 to 29 July 2017. The model results revealed that the landslide points are the most unstable (19 points) in accordance with previous study of Casagli et al. (2006), Guthrie and Evans (2004), and Keefer et al. (1987) that stated that landslides often occur when heavy rainfall. The previous study of Lee et al. (2009) has showed event of Typhoon Xangxane (29 October, 2000 to 2 November, 2000) caused landslides in Taiwan with the highest rainfall of 80 mm/h around 1 November, 2000. However, landslides may not occur as soon as the slopes are unstable, but landslides can occur at any time after the slopes become unstable or landslides may not occur.



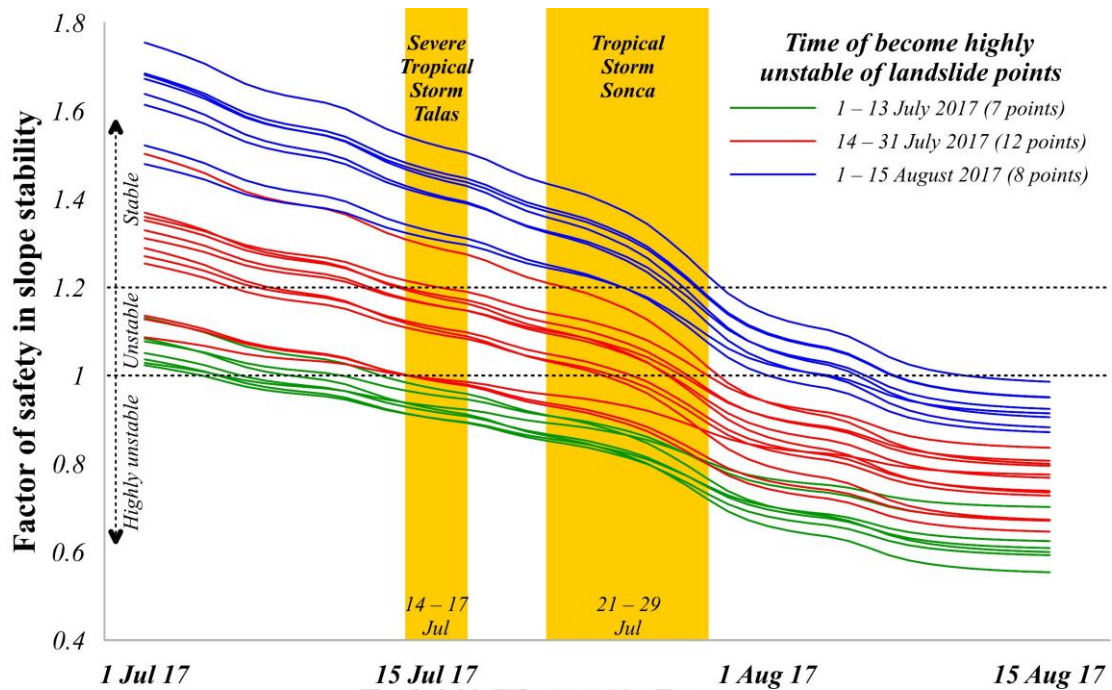


**Figure 5.7** Factor of safety in slope stability of 27 unstable locations in the Huai Nam Phung subbasin from 1 July to 15 August, 2017 due to two tropical storms (Talas and Sonca)

Based on the peak of the instability on 30 October, 2017, it is found that almost all of the unstable areas were located in the area with the slope of more than 6% (**Figure 5.8**), while the plain areas were still stable. When focusing on the areas with slopes of more than 30 degrees, it appears that those areas were totally unstable. The result is consistent with the study of Sassa et al. (2005) which suggested that landslides often occur on the areas with the slope of more than 30 degree. In combination with the news of landslide at the entrance of Phu Thap Boek on 23 October 2017 (Workpoint, 2017), it can be concluded that the factor of safety in slope stability obtained from this study is reliable. However, landslides may occur in certain areas and does not occur in all areas that are unstable. Thus, slope stability is able to indicate risk areas of landslide occurrence.

According to the factor of safety in slope stability on 30 October 2017 in 9 sub-catchments of the Huai Nam Phung subbasin by using 6% slope as the border of plain area (), the revealed that most of the slope stability become unstable occurred on the western mountain ranges of the study area. , there are 7 sub-catchments were found unstable areas as shown in the descending order, including, Huai Nam Ko (92.49%), the upper part of Huai Nam Phung (90.14%), Huai Nam Hia (89.97%), Huai Nam Krang (87.38%), Khlong Wang Hang (82.69%), Khlong Wang Hin (82.11%), and Huai Khrai (80.27%), and there are 2 sub-catchments that the unstable areas are slightly more than half of the sub-catchment areas, which are Huai Ilert (60.70%) and Huai Phai Yai (56.15%) (**Figure 5.9**).

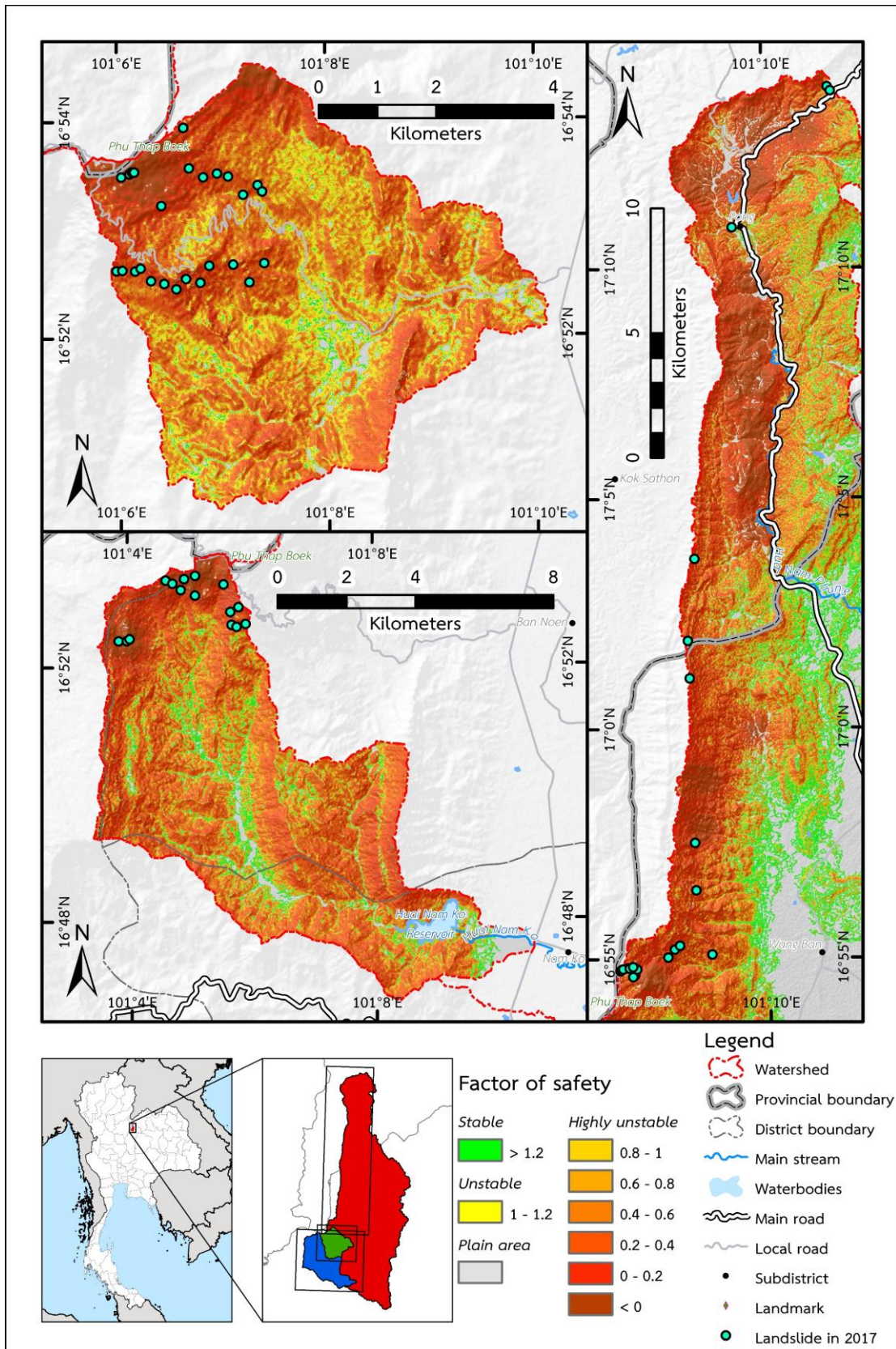


**Figure 5.8** Factor of safety in slope stability in the Huai Nam Phung subbasin on 30 October, 2017 in each sub-catchment

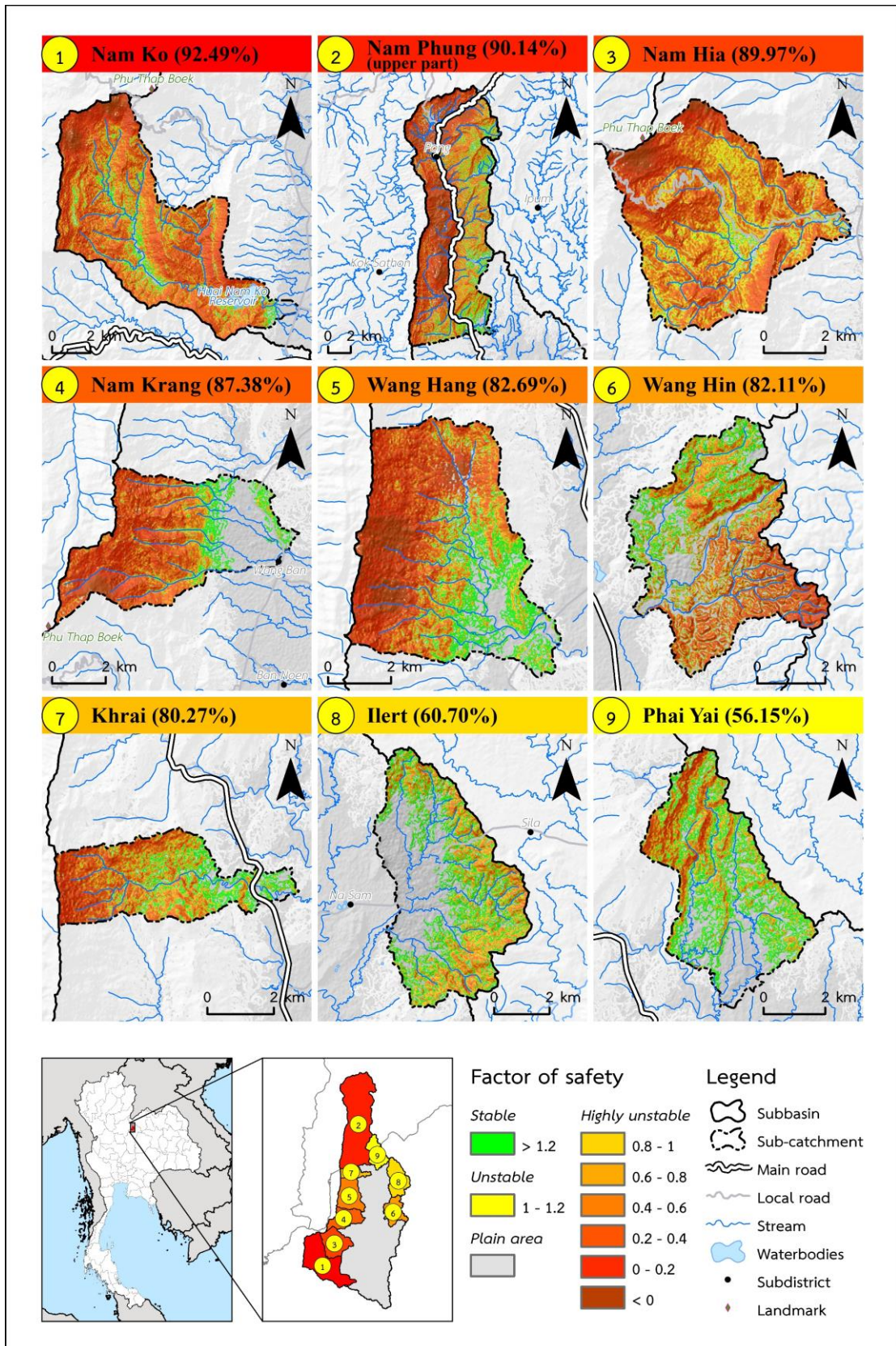


**Figure 5.9** Factor of safety in slope stability in the areas with slope higher than 6% in 9 sub-catchments of the Huai Nam Phung subbasin on 30 October, 2017

The finding that the Huai Nam Ko sub-catchment has the most unstable areas in accordance with the previous event in August, 2001 that severe debris flow and debris flood occurred (Ono et al., 2014; Yumuang, 2005). According to the study of Yumuang (2005), there are many scar-scourings occurred on the western hillside of the Huai Nam Ko sub-catchment due to debris flow and debris flood in 2001, which corresponds to the highest unstable areas in the Huai Nam Phung subbasin obtained from the current study (**Figure 5.10**). Landslide scars on the high slope areas of Yumuang (2005) matched with the unstable areas from slope stability map. Landslide scars on the high slope areas caused by the failure of slope stability while scar-scouring in the stream bank caused by scouring of water and materials. However, although the scar-scouring in the stream bank are not caused by the slope stability directly, but the sediments that collapsed from the high slope areas would continuously accumulate in the valley and further transport to the lowland as debris flow scouring stream bank along flow ways (May and Gresswell, 2003).

The author validated the factor of safety in slope stability on 30 October 2017, the time with most unstable areas, with the results of the previous studies of Yumuang (2005) and the Department of Mineral Resources Thailand (2016). Yumuang (2005) had evaluated the occurrence of debris flow and debris flood in the Huai Nam Ko sub-catchment that is a branch of the Huai Nam Phung subbasin in August 2001 and generated the debris flow and debris flood susceptibility map in the Huai Nam Ko sub-catchment. That map shows that high susceptible areas are in the valley while the low susceptible areas are near the ridge. However, that study focused on debris flow and debris flood, which gave an importance on the flow of sediment and minerals (e.g., timbers, boughs, leaves, roots, or garbage) from the upstream to downstream. Therefore, that susceptibility map shows the high susceptible areas just in the valley. The debris flow and debris flood susceptibility map of Yumuang (2005) was in accordance with the landslide and flash flood susceptibility map of the Department of Mineral Resources Thailand (2016) which shows high susceptible areas in the valley. It is because the susceptibility map of the Department of Mineral Resources Thailand (2016) focused on flash flood. Debris flow, debris flood, and flash flood are the transport of water and sediments from upstream to downstream. If sediments mixed with water more than 50%, it would be debris flow. If sediments mixed with water less than 50%, it would be debris flood. While only water or very few of sediments in severe flooding, it would be flash flood (Wieczorek et al., 1983).

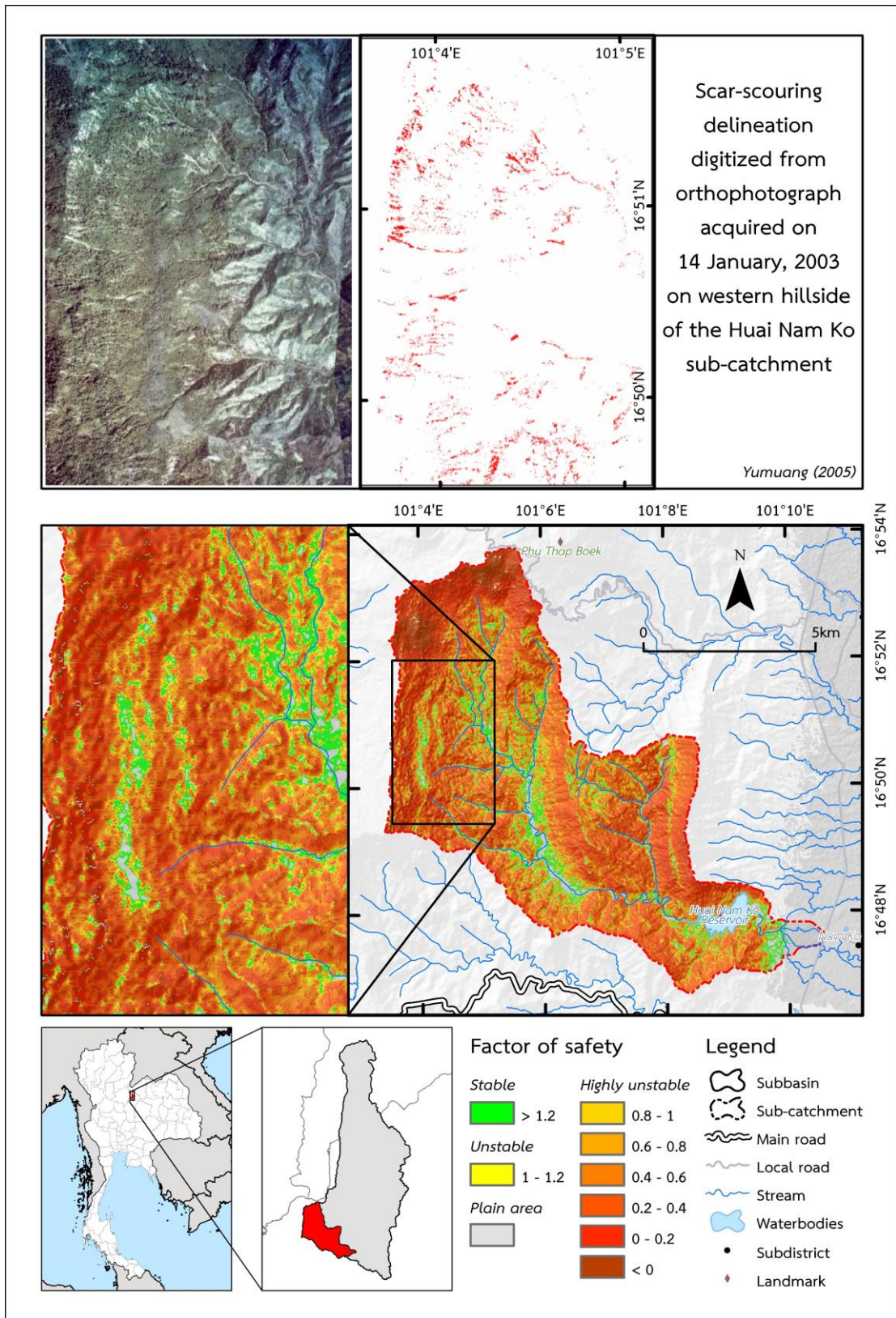


**Figure 5.10** Slope stability map on 30 October, 2017 and scar-scouring on 14 January, 2003 of Yumuang (2005) in the western hillside of the Huai Nam Ko sub-catchment

The factor of safety in slope stability map on 30 October 2017 derived in this study is different from the susceptibility maps of Yumuang (2005) and the Department of Mineral Resources Thailand (2016). It shows the transition from the highly unstable areas in the ridge to the stable areas near the valley, while those from Yumuang (2005) and the Department of Mineral Resources Thailand (2016) showed the high susceptible areas in the valley and the low susceptible areas near the ridge (**Figure 5.11**). It is because this study focused on the shallow landslides which occurred on the cliffs or the high slope areas while the studies of Yumuang (2005) and the Department of Mineral Resources Thailand (2016) focused on the debris flow and flash flood, respectively, in the catchment. From the factor of safety in slope stability on 30 October 2017, the high susceptible areas for shallow landslide are near the ridge and low susceptible areas are near the valley and plain areas (**Figure 5.12**).

However, soil mantles that collapse from the cliffs or high slope areas can accumulate in the valley and may cause a severe debris flow to heap in the alluvial fan areas near the foothill (Blair and McPherson, 1994; Santangelo et al., 2011; Sohn et al., 1999; Yu et al., 2018). In addition, the natural dams caused by materials that obstructs the streams (e.g., timbers, boughs, leaves, roots, or garbage) and manmade structures (dams, weirs, or dikes) can cause the severe debris flow and flood in the downstream areas when these dams fails (Shangfu, 1993; Takahashi and Nakagawa, 1993; Yumuang, 2005). Because the landslide process are linked from the high slope areas down to the valley, the evaluation of landslides occurrence just analyzes in the terms of soil mantles collapsing and debris flow and flood in the valley and alluvial fan areas (Kritikos and Davies, 2015).





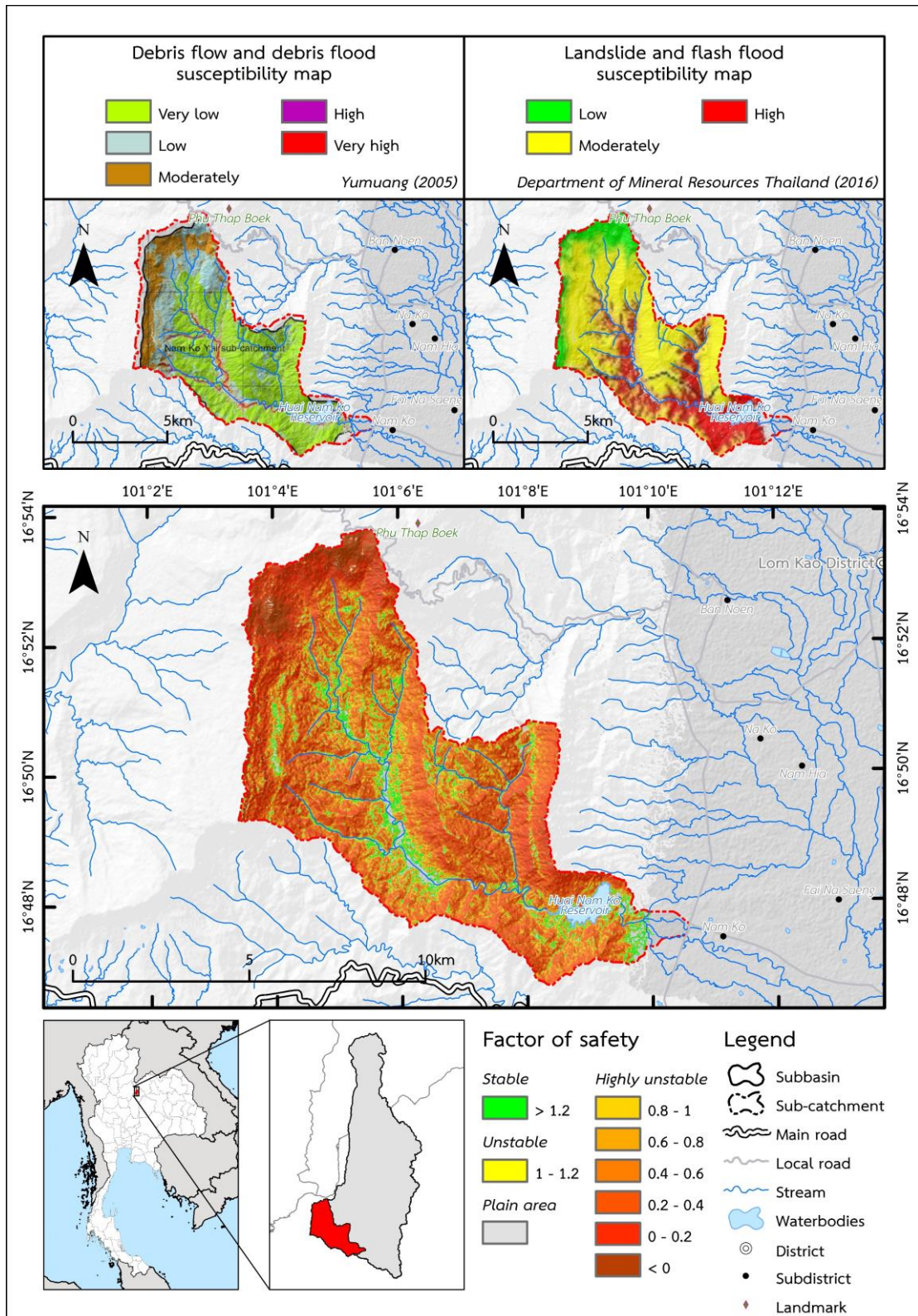


**Figure 5.11** Slope stability map on 30 October 2017, debris flow and debris flood susceptibility map by Yumuang (2005), and landslide and flash flood susceptibility map by the Department of Mineral Resources Thailand (2016) in the Huai Nam Ko sub-catchment

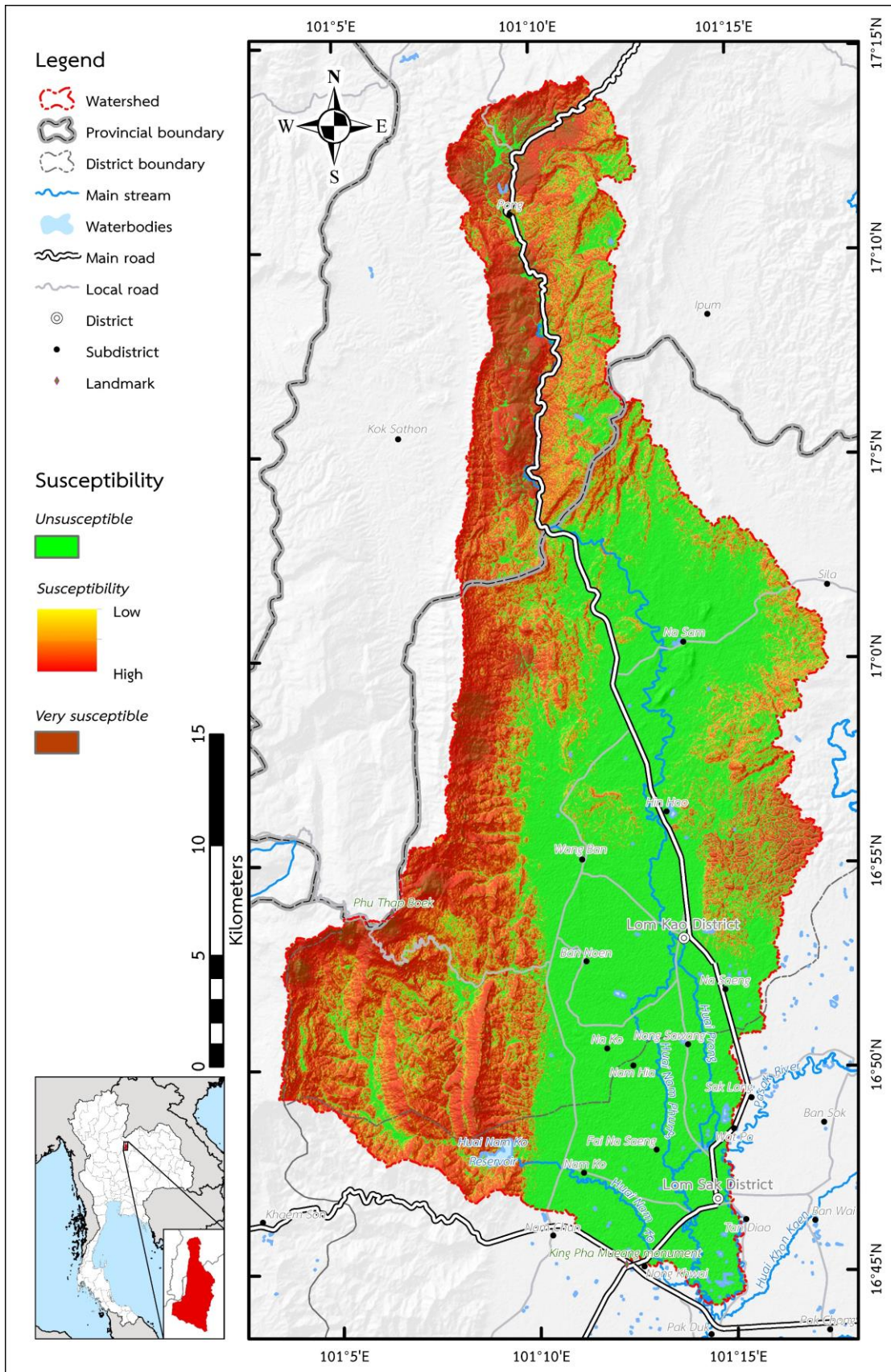


**Figure 5.12** Shallow landslide susceptibility map of the Huai Nam Phung subbasin

## **CHAPTER VI**

### **CONCLUSIONS AND RECOMMENDATIONS**

The evaluation of landslide occurrence in Huai Nam Phung subbasin has conclusions and recommendations as follows:

#### **6.1 Conclusions**

This study has analyzed the landslide occurrence mechanism in the terms of meteorological and hydrological factors which are the main reasons of landslide occurrence in the Huai Nam Phung subbasin by evaluating soil slope stability using theory of factor of safety. It reveals that the slope stability is an important component to predict the landslides. The conclusions of this study were described as follows.

This study used the remote sensing and field study combined with the Geographic Information System (GIS) technique to surveyed landslide occurrence. The topography based hydrological model (TOPMODEL) has used to simulated the groundwater level that is an important variable to analyze the factor of safety in slope stability, which is a theory to evaluate the shallow landslide occurrence.

Based on surveying of landslide occurrence in the Huai Nam Phung subbasin, 63 points of shallow landslide occurrence was found in 2017. All of landslide points situates in the areas with slope higher than 20 degree. From the calibration of parameters in the TOPMODEL, there are 3 most sensitive parameters, consisting of log of the areal average of saturated soil transmissivity ( $\ln T_e$ ), surface hydraulic conductivity ( $k_0$ ), and capillary drive (CD). From the analysis of factor of safety in slope stability, most of unstable areas are in the areas with slopes higher than 20 degree while the areas with slopes lower than 20 degree have very little unstable area (less than 10%). This study has found a method to determine landslide areas which are the areas with the slope higher than 20 degree, especially in the areas near the Phu Thap Boek where the slope become unstable before the other areas. This area has a lot of steep cliffs that are sensitive to landslide occurrence. Therefore, a good monitoring and warning systems are required in the area near the Phu Thap Boek.

From the evaluation of landslide occurrence in the Huai Nam Phung subbasin, it is found that landslides occurred in this area are shallow landslides. The main cause of the landslides in this area is a heavy rain that causes soil to be saturated with water and collapses. The evaluation of slope with the theory of factor of safety in slope stability makes it possible to see the stability of the slope at each time. Landslides may occur after the slope becomes unstable. Focusing of slope stability in July, 2017, where 2 tropical storms entered the study area (Talas and Sonca), it found that a lot of landslide points (19 points) became unstable. Therefore, the storm event is a factor affecting the slope stability and it may cause landslides occurrence.

However, the lack of stability in the soil does not mean that the landslide will always occur because there are other factors that affect the occurrence of landslides such as soil compactness, volume and density and man-made structure. These factors

may affect the strength of soils. In addition, even when the slope is stable, the landslides may occur for many reasons such as earthquake or human activities.

## 6.2 Recommendations

There are still many limitations in this study which limit an ability to conduct the study in some details. These limitations include a resolution of satellite imageries, a difficulty to access the study area, a resolution of the Digital Elevation Model (DEM), a number of observing and sampling points, and an incompleteness of meteorological and hydrological data.

In the landslide surveys, the high resolution of satellite imageries and the data from the field survey throughout the study areas are required. Satellite imageries with higher spatial and temporal resolutions can provide the result with more details. For this study, there were still too few satellite imageries. The first imagery was taken in April 2016 while the next one was taken in December 2017. Therefore, it is not possible to determine the exactly time of landslide occurrences from these imageries. The access to the study area and surveying tools are important for field check. Because of the limitations of tools and the high slope in some locations of the area, some landslide occurrences could not be checked.

The digital elevation model (DEM) used in this study is with a resolution of  $12.5 \times 12.5$  meters. An elevation data from the model is important for calculations of several variables. Some shallow landslide areas are smaller than  $12.5 \times 12.5$  meters. Therefore, if the DEM had higher resolution, the study could be done with more detailed.

The soil thickness is a variable used to analyze the factor of safety in slope stability. The complete soil thickness map can lead to more detailed result. However, because the complete map is unavailable, this study created a map by calculating the linear relationship between the Topographic Wetness Index (TWI) and the soil thickness which is randomly measured in the study area. The randomization was limited by the tools and accessibility to the study area. The soil in some areas is very thick. A drilling core and geophysical investigation will obtain deep soil data.

Rainfall, evaporation, and observed streamflow data are variables used in this study. During the study period there have been some inaccurate and missing data. If more data is available, the results would be more reliable. In addition, for the observed streamflow, there is no a hydrological gauging station at the outlet of the study area. The streamflow was estimated from the data at the nearby area. Therefore, the results may have some discrepancies. If there was a station at the outlet of the basin, the result would be more accurate. In short, the future study with more detailed data is recommended to get the results with more reliability.

## REFERENCES

- Akkrawintawong, K., Chotikasathien, W., Daorerk, V., and Charusiri, P. 2008. GIS application for landslide hazard mapping in Phang Nga Region, Southern Thailand. Paper presented at the Proceedings of the International Symposia on Geoscience Resources and Environments of Asian Terranes (GREAT 2008).
- Arai, K. and Tagyo, K. 1985. Determination of noncircular slip surface giving the minimum factor of safety in slope stability analysis. Soils and Foundations 25(1): 43-51.
- Arunyanart, N., Limsiri, C., and Uchaipichat, A. 2017. Flood hazards in the Chi River Basin, Thailand: impact management of climate change. Applied Ecology and Environmental Research 15(4): 841-861.
- Aversa, S., Cascini, L., Picarelli, L., and Scavia, C. 2018. Landslides and Engineered Slopes. Experience, Theory and Practice: Proceedings of the 12th International Symposium on Landslides (Napoli, Italy, 12-19 June 2016): CRC Press.
- Bai, S., Lu, P., and Thiebes, B. 2020. Comparing characteristics of rainfall-and earthquake-triggered landslides in the Upper Minjiang catchment, China. Engineering Geology 268: 105518.
- Bera, S., Guru, B., and Ramesh, V. 2019. Evaluation of landslide susceptibility models: A comparative study on the part of Western Ghat Region, India. Remote Sensing Applications: Society and Environment 13: 39-52.
- Beven, K., Kirkby, M., Schofield, N., and Tagg, A. 1984. Testing a physically-based flood forecasting model (TOPMODEL) for three UK catchments. Journal of hydrology 69(1-4): 119-143.
- Beven, K. and Kirkby, M. 1979. A physically based, variable contributing area model of basin hydrology/Un modèle à base physique de zone d'appel variable de l'hydrologie du bassin versant. Hydrological Sciences Journal 24(1): 43-69.
- Blair, T.C. and McPherson, J.G. 1994. Alluvial fan processes and forms. Geomorphology of desert environments: 354-402.
- Bobrowsky, P. and Highland, L. 2013. The landslide handbook-a guide to understanding landslides: A landmark publication for landslide education and preparedness. Landslides: Global Risk Preparedness: 75-84.
- Bordoni, M., Galanti, Y., Bartelletti, C., Persichillo, M.G., Barsanti, M., Giannecchini, R., Avanzi, G., Cevasco, A., Brandolini, P., and Galve, J.P. 2020. The influence of the inventory on the determination of the rainfall-induced shallow landslides susceptibility using generalized additive models. CATENA 193: 104630.
- Bui, D.T., Tsangaratos, P., Nguyen, V.-T., Van Liem, N., and Trinh, P.T. 2020. Comparing the prediction performance of a Deep Learning Neural Network model with conventional machine learning models in landslide susceptibility assessment. CATENA 188: 104426.
- Buytaert, W. 2009. Implementation of the hydrological model TOPMODEL in R.
- Casagli, N., Dapporto, S., Ibsen, M., Tofani, V., and Vannocci, P. 2006. Analysis of the landslide triggering mechanism during the storm of 20th–21st November

- 2000, in Northern Tuscany. *Landslides* 3(1): 13-21.
- Channel 3 Thailand. 2017. Phetchabun flood expanded widely [online]. Available from: <http://news.ch3thailand.com/local/43715> (in Thai).
- Chen, J. and Wu, Y. 2012. Advancing representation of hydrologic processes in the Soil and Water Assessment Tool (SWAT) through integration of the TOPographic MODEL (TOPMODEL) features. *Journal of hydrology* 420: 319-328.
- Chen, W., Li, W., Chai, H., Hou, E., Li, X., and Ding, X. 2016. GIS-based landslide susceptibility mapping using analytical hierarchy process (AHP) and certainty factor (CF) models for the Baozhong region of Baoji City, China. *Environmental Earth Sciences* 75(1): 63.
- Chen, W., Zhang, S., Li, R., and Shahabi, H. 2018. Performance evaluation of the GIS-based data mining techniques of best-first decision tree, random forest, and naïve Bayes tree for landslide susceptibility modeling. *Science of the total environment* 644: 1006-1018.
- Chen, Z.-Y. and Shao, C.-M. 1988. Evaluation of minimum factor of safety in slope stability analysis. *Canadian Geotechnical Journal* 25(4): 735-748.
- Cheng, Y., Lansivaara, T., and Wei, W. 2007. Two-dimensional slope stability analysis by limit equilibrium and strength reduction methods. *Computers and Geotechnics* 34(3): 137-150.
- Daily News. 2017. Order to handle large masses of water, Phetchabun is the heaviest around 40 years [online]. Available from: <https://www.dailynews.co.th/regional/588419> (in Thai).
- Depina, I., Oguz, E.A., and Thakur, V. 2020. Novel Bayesian framework for calibration of spatially distributed physical-based landslide prediction models. *Computers and Geotechnics* 125: 103660.
- DeYoung, J. 2018. Forest measurements: an applied approach.
- Domenico, P.A. and Schwartz, F.W. 1998. *Physical and chemical hydrogeology* 506: Wiley New York.
- Dou, J., Paudel, U., Oguchi, T., Uchiyama, S., and Hayakavva, Y.S. 2015. Shallow and Deep-Seated Landslide Differentiation Using Support Vector Machines: A Case Study of the Chuetsu Area, Japan. *Terrestrial, Atmospheric & Oceanic Sciences* 26(2).
- Du, H., Song, D., Chen, Z., Shu, H., and Guo, Z. 2020. Prediction model oriented for landslide displacement with step-like curve by applying ensemble empirical mode decomposition and the PSO-ELM method. *Journal of Cleaner Production*: 122248.
- Dunne, T. and Black, R.D. 1970. Partial area contributions to storm runoff in a small New England watershed. *Water resources research* 6(5): 1296-1311.
- Farshad, A., Shrestha, D.P., and Moonjun, R. 2013. Do the Emerging Methods of Digital Soil Mapping Have Anything to Learn from the Geopedologic Approach to Soil Mapping and Vice Versa?. *Developments in Soil Classification, Land Use Planning and Policy Implications*: 109-131.
- Fowze, J., Bergado, D., Soralump, S., Voottipreux, P., and Dechasakulsom, M. 2012.

- Rain-triggered landslide hazards and mitigation measures in Thailand: From research to practice. Geotextiles and geomembranes 30: 50-64.
- Freeze, R.A. and Cherry, J.A. 1979. Groundwater.
- Gökçeoglu, C. and Aksoy, H. 1996. Landslide susceptibility mapping of the slopes in the residual soils of the Mengen region (Turkey) by deterministic stability analyses and image processing techniques. Engineering Geology 44(1-4): 147-161.
- Google. 2017. Google street view [online]. Available from: <https://www.google.co.th/maps/@16.8034072,101.1555775,3a,75y,222.33h,99.3t/data=!3m8!1e1!3m6!1sAF1QipMk9UZE0Ve3wJDWBi368ThLUFNVceJDG8UPM2Pd!2e10!3e11!6shhttps:%2F%2Fh5.googleusercontent.com%2Fp%2FAF1QipMk9UZE0Ve3wJDWBi368ThLUFNVceJDG8UPM2Pd%3Dw203-h100-k-no-pi-0-ya121.42426-ro-0-fo100!7i4608!8i2304>.
- Gumindoga, W., Rientjes, T., Haile, A., and Dube, T. 2014. Predicting streamflow for land cover changes in the Upper Gilgel Abay River Basin, Ethiopia: A TOPMODEL based approach. Physics and Chemistry of the Earth, Parts A/B/C 76: 3-15.
- Gumindoga, W., Rwasoka, D., and Murwira, A. 2011. Simulation of streamflow using TOPMODEL in the Upper Save River catchment of Zimbabwe. Physics and Chemistry of the Earth, Parts A/B/C 36(14-15): 806-813.
- Guthrie, R. and Evans, S. 2004. Magnitude and frequency of landslides triggered by a storm event, Loughborough Inlet, British Columbia.
- Highland, L. and Bobrowsky, P.T. 2008. The landslide handbook: a guide to understanding landslides: US Geological Survey Reston.
- Ho, J.-Y. and Lee, K.T. 2017. Performance evaluation of a physically based model for shallow landslide prediction. Landslides 14(3): 961-980.
- Ho, J.-Y., Lee, K.T., Chang, T.-C., Wang, Z.-Y., and Liao, Y.-H. 2012. Influences of spatial distribution of soil thickness on shallow landslide prediction. Engineering Geology 124: 38-46.
- Ikechukwu, M.N., Ebinne, E., Idorenyin, U., and Raphael, N.I. 2017. Accuracy assessment and comparative analysis of IDW, spline and kriging in spatial interpolation of landform (Topography): An experimental study. Journal of Geographic Information System 9(3): 354-371.
- Institute of Water Resources and Agriculture Information Thailand. 2012. Data collection and data analysis operations of the 25 basin water resources system development project and drought flooding models: Pasak river basin. (in Thai).
- Jiao, Y., Zhao, D., Ding, Y., Liu, Y., Xu, Q., Qiu, Y., Liu, C., Liu, Z., Zha, Z., and Li, R. 2019. Performance evaluation for four GIS-based models purposed to predict and map landslide susceptibility: A case study at a World Heritage site in Southwest China. CATENA 183: 104221.
- Keefer, D.K., Wilson, R.C., Mark, R.K., Brabb, E.E., Brown, W.M., Ellen, S.D., Harp, E.L., Wieczorek, G.F., Alger, C.S., and Zatzkin, R.S. 1987. Real-time landslide warning during heavy rainfall. Science 238(4829): 921-925.
- Kim, S., Kim, M., An, H., Chun, K., Oh, H.-J., and Onda, Y. 2019. Influence of

- subsurface flow by Lidar DEMs and physical soil strength considering a simple hydrologic concept for shallow landslide instability mapping. CATENA 182: 104137.
- Komori, D., Rangsiwanichpong, P., Inoue, N., Ono, K., Watanabe, S., and Kazama, S. 2018. Distributed probability of slope failure in Thailand under climate change. Climate Risk Management 20: 126-137.
- Kritikos, T. and Davies, T. 2015. Assessment of rainfall-generated shallow landslide/debris-flow susceptibility and runout using a GIS-based approach: application to western Southern Alps of New Zealand. Landslides 12(6): 1051-1075.
- Leblond, J.-P. 2019. Revisiting forest transition explanations: The role of “push” factors and adaptation strategies in forest expansion in northern Phetchabun, Thailand. Land Use Policy 83: 195-214.
- Lee, K.T. and Ho, J.-Y. 2009. Prediction of landslide occurrence based on slope-instability analysis and hydrological model simulation. Journal of hydrology 375(3-4): 489-497.
- Lenhart, T., Eckhardt, K., Fohrer, N., and Frede, H.-G. 2002. Comparison of two different approaches of sensitivity analysis. Physics and Chemistry of the Earth, Parts A/B/C 27(9-10): 645-654.
- Li, C., Fu, Z., Wang, Y., Tang, H., Yan, J., Gong, W., Yao, W., and Criss, R.E. 2019. Susceptibility of reservoir-induced landslides and strategies for increasing the slope stability in the Three Gorges Reservoir Area: Zigui Basin as an example. Engineering Geology 261: 105279.
- Li, Y. and Mo, P. 2019. A unified landslide classification system for loess slopes: A critical review. Geomorphology 340: 67-83.
- Limsakul, A., Limjirakan, S., and Suttamanuswong, B. 2010. Asian summer monsoon and its associated rainfall variability in Thailand. Environment Asia 3(2): 79-89.
- Liu, Z., Gilbert, G., Cepeda, J.M., Lysdahl, A.O.K., Piciullo, L., Hefre, H., and Lacasse, S. 2020. Modelling of shallow landslides with Machine Learning algorithms. Geoscience Frontiers.
- Long, K., Zhang, S., Wei, F., Hu, K., Zhang, Q., and Luo, Y. 2020. A hydrology-process based method to correlate debris flow density to rainfall parameters and its application on debris flow prediction. Journal of hydrology: 125124.
- Maharaj, R.J. 1993. Landslide processes and landslide susceptibility analysis from an upland watershed: a case study from St. Andrew, Jamaica, West Indies. Engineering Geology 34(1-2): 53-79.
- Marin, R.J. and Velásquez, M.F. 2020. Influence of hydraulic properties on physically modelling slope stability and the definition of rainfall thresholds for shallow landslides. Geomorphology 351: 106976.
- May, C.L. and Gresswell, R.E. 2003. Processes and rates of sediment and wood accumulation in headwater streams of the Oregon Coast Range, USA. Earth Surface Processes and Landforms: The Journal of the British Geomorphological Research Group 28(4): 409-424.
- McCombie, P. and Wilkinson, P. 2002. The use of the simple genetic algorithm in



- finding the critical factor of safety in slope stability analysis. Computers and Geotechnics 29(8): 699-714.
- McNamara, J.P., Ziegler, A.D., Wood, S.H., and Vogler, J.B. 2006. Channel head locations with respect to geomorphologic thresholds derived from a digital elevation model: A case study in northern Thailand. Forest Ecology and Management 224(1-2): 147-156.
- Meisina, C. and Scarabelli, S. 2007. A comparative analysis of terrain stability models for predicting shallow landslides in colluvial soils. Geomorphology 87(3): 207-223.
- Metropolis, N. 1987. The beginning. Los Alamos Science 15: 125-130.
- Montgomery, D.R. and Dietrich, W.E. 1994. A physically based model for the topographic control on shallow landsliding. Water resources research 30(4): 1153-1171.
- Moreiras, S.M. 2005. Landslide susceptibility zonation in the Rio Mendoza valley, Argentina. Geomorphology 66(1-4): 345-357.
- Morel-Seytoux, H. and Khanji, J. 1974. Derivation of an equation of infiltration. Water resources research 10(4): 795-800.
- Morel-Seytoux, H. and Nimmo, J. 1999. Soil water retention and maximum capillary drive from saturation to oven dryness. Water resources research 35(7): 2031-2041.
- Mouri, G., Shiiba, M., Hori, T., and Oki, T. 2011. Modeling shallow landslides and river bed variation associated with extreme rainfall-runoff events in a granitoid mountainous forested catchment in Japan. Geomorphology 125(2): 282-292.
- Naidu, S., Sajinkumar, K., Oommen, T., Anuja, V., Samuel, R.A., and Muraleedharan, C. 2018. Early warning system for shallow landslides using rainfall threshold and slope stability analysis. Geoscience Frontiers 9(6): 1871-1882.
- Nash, J.E. and Sutcliffe, J.V. 1970. River flow forecasting through conceptual models part I—A discussion of principles. Journal of hydrology 10(3): 282-290.
- Nicu, I.C. and Asăndulesei, A. 2018. GIS-based evaluation of diagnostic areas in landslide susceptibility analysis of Bahluiet River Basin (Moldavian Plateau, NE Romania). Are Neolithic sites in danger?. Geomorphology 314: 27-41.
- Oktorie, O. 2017. A Study of Landslide Areas Mitigation and Adaptation in Palupuah Subdistrict, Agam Regency, West Sumatra Province, Indonesia. Sumatra Journal of Disaster, Geography and Geography Education 1(1): 43-49.
- Ono, K., Kazama, S., and Ekkawatpanit, C. 2014. Assessment of rainfall-induced shallow landslides in Phetchabun and Krabi provinces, Thailand. Natural hazards 74(3): 2089-2107.
- Pal, I., Tularug, P., Jana, S.K., and Pal, D.K. 2018. Risk assessment and reduction measures in landslide and flash flood-prone areas: A case of Southern Thailand (Nakhon Si Thammarat Province). Integrating Disaster Science and Management: 295-308).
- Peng, D., Zhijia, L., and Fan, X. 2008. Application of TOPMODEL in Buliu River Basin and comparison with Xin'anjiang model. Water Science and Engineering 1(2): 25-32.

- Peng, J., Fan, Z., Wu, D., Zhuang, J., Dai, F., Chen, W., and Zhao, C. 2015. Heavy rainfall triggered loess–mudstone landslide and subsequent debris flow in Tianshui, China. Engineering Geology 186: 79-90.
- Pham, B.T., Van Phong, T., Nguyen-Thoi, T., Trinh, P.T., Tran, Q.C., Ho, L.S., Singh, S.K., Duyen, T.T.T., Nguyen, L.T., and Le, H.Q. 2020. GIS-Based Ensemble Soft Computing Models for Landslide Susceptibility Mapping. Advances in Space Research.
- Phewnil, O., Panichsakpatana, S., Tungkananuruk, N., and Pitiyont, B. 2010. Atrazine Transport from The Maize (*Zea mays* L.) Cultivated Upland Soil in Huay Kapo Watershed, Nam Nao District, Phetchabun Province, Thailand. Thai Journal of Agricultural Science 43(3): 119-127.
- Phien-Wej, N., Nutalaya, P., Aung, Z., and Zhibin, T. 1993. Catastrophic landslides and debris flows in Thailand. Bulletin of the International Association of Engineering Geology-Bulletin de l'Association Internationale de Géologie de l'Ingénieur 48(1): 93-100.
- Pirone, M., Papa, R., Nicotera, M.V., and Urciuoli, G. 2015. In situ monitoring of the groundwater field in an unsaturated pyroclastic slope for slope stability evaluation. Landslides 12(2): 259-276.
- Post Today. 2016. Lom Sak district be worse, mass flooding economic zones [online]. Available from: <https://www.posttoday.com/social/local/454545> (in Thai).
- Post Today. 2017. Phetchabun still be worse, Pasak has flooded many communities [online]. Available from: <https://www.posttoday.com/social/local/519679> (in Thai).
- Pourghasemi, H.R., Moradi, H., Aghda, S.F., Gokceoglu, C., and Pradhan, B. 2014. GIS-based landslide susceptibility mapping with probabilistic likelihood ratio and spatial multi-criteria evaluation models (North of Tehran, Iran). Arabian Journal of Geosciences 7(5): 1857-1878.
- Pourghasemi, H.R., Jirandeh, A.G., Pradhan, B., Xu, C., and Gokceoglu, C. 2013. Landslide susceptibility mapping using support vector machine and GIS at the Golestan Province, Iran. Journal of Earth System Science 122(2): 349-369.
- Pourghasemi, H.R., Mohammady, M., and Pradhan, B. 2012. Landslide susceptibility mapping using index of entropy and conditional probability models in GIS: Safarood Basin, Iran. CATENA 97: 71-84.
- Pradhan, A. and Kim, Y. 2016. Evaluation of a combined spatial multi-criteria evaluation model and deterministic model for landslide susceptibility mapping. CATENA 140: 125-139.
- Rahardjo, H., Nio, A.S., Leong, E.C., and Song, N.Y. 2010. Effects of groundwater table position and soil properties on stability of slope during rainfall. Journal of geotechnical and geoenvironmental engineering 136(11): 1555-1564.
- Rencher, A.C. and Christensen, W.F. 2012. Chapter 10, Multivariate regression–Section 10.1, Introduction. Methods of multivariate analysis, Wiley Series in Probability and Statistics 709: 19.
- Ritter, A. and Muñoz-Carpena, R. 2013. Performance evaluation of hydrological models: Statistical significance for reducing subjectivity in goodness-of-fit

- assessments. Journal of hydrology 480: 33-45.
- Romeo, R., Vita, A., Manuelli, S., Zanini, E., Freppaz, M., and Stanchi, S. 2015. Understanding Mountain Soils: A contribution from mountain areas to the International Year of Soils 2015. FAO, Rome.
- Royal Irrigation Department Thailand. 2009. Pasak river basin development project due to the royal initiative.
- Royal Irrigation Department Thailand. 2011. Huai Nam Hia reservoir project, Lom Kao district, Phetchabun province.
- Ruangpanit, N. and Songprai, A. 1984. Impact of land use on water quality at Doi Pui and Tung Jaw Chiang Mai [Thailand]. Warasan Wanarasat.
- Samrit, B., Kheoruenromne, I., Suddhiprakarn, A., and Swasdiphanich, S. 2008. Properties and Fertility Capability of Highland Soils in Khao Kho Area, Phetchabun Province, Thailand. Thai Journal of Agricultural Science 41(3-4): 153-167.
- Santangelo, N., Santo, A., Di Crescenzo, G., Foscari, G., Liuzza, V., Sciarrotta, S., and Scorpio, V. 2011. Flood susceptibility assessment in a highly urbanized alluvial fan: the case study of Sala Consilina (southern Italy). Natural Hazards and Earth System Sciences 11(10): 2765.
- Sassa, K., Fukuoka, H., Wang, F., and Wang, G. 2006. Landslides: risk analysis and sustainable disaster management: Springer Science & Business Media.
- Shangfu, K. 1993. Formation mechanisms and prediction models of debris flow due to natural dam failures. Journal of Sediment Research 4: 42-57.
- Sharpe, C. 1938. Landslides and related phenomena.
- Shirzadi, A., Bui, D.T., Pham, B.T., Solaimani, K., Chapi, K., Kavian, A., Shahabi, H., and Revhaug, I. 2017. Shallow landslide susceptibility assessment using a novel hybrid intelligence approach. Environmental Earth Sciences 76(2): 60.
- Silva, R., Grison, F., and Kobiyama, M. 2008. Conceptual investigation of time of concentration: Case study of the Pequeno River watershed, Sao Jose dos Pinhais, PR, Brazil. TANIGUCHI, M.; BURNETT, WC; FUKUSHIMA, Y. HAIGH, M: 271-275.
- Singhrattna, N., Rajagopalan, B., Clark, M., and Krishna Kumar, K. 2005. Seasonal forecasting of Thailand summer monsoon rainfall. International Journal of Climatology: A Journal of the Royal Meteorological Society 25(5): 649-664.
- Singhroy, V., Mattar, K., and Gray, A. 1998. Landslide characterisation in Canada using interferometric SAR and combined SAR and TM images. Advances in Space Research 21(3): 465-476.
- Skempton, A.W. and DeLory, F. 1984. Stability of natural slopes in London clay. Selected Papers on Soil Mechanics: 70-73.
- Sohn, Y.K., Rhee, C.W., and Kim, B.C. 1999. Debris flow and hyperconcentrated flood-flow deposits in an alluvial fan, northwestern part of the Cretaceous Yongdong Basin, Central Korea. The Journal of Geology 107(1): 111-132.
- Soralump, S. 2010. Rainfall-triggered landslide: from research to mitigation practice in Thailand. Geotechnical Engineering 41(1): 39.
- Sørensen, R., Zinko, U., and Seibert, J. 2005. On the calculation of the topographic

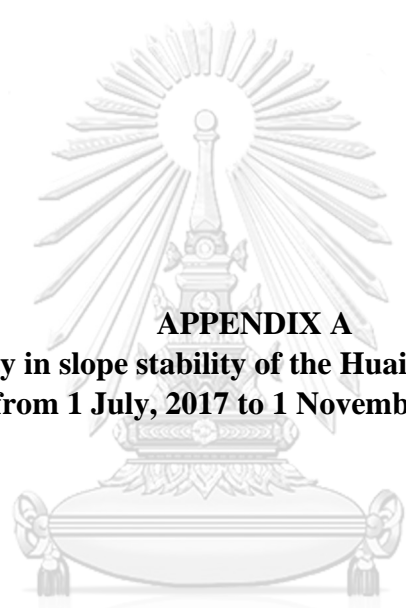
- wetness index: evaluation of different methods based on field observations.
- Takahashi, T. and Nakagawa, H. 1993. Flood and debris flow hydrograph due to collapse of a natural dam by overtopping. Proceedings of Hydraulic Engineering 37: 699-704.
- Tangtham, N. and Yuwananont, S. 1996. Impact of land use changes on streamflow and flow characteristics of Pasak basin. Warasan Wanasat.
- Thairath. 2017. Heavy rains in Phetchabun cause floods in urban areas, dozens of houses drowned [online]. Available from: <https://www.thairath.co.th/news/local/north/1056960> (in Thai).
- Thammapala, P. and Weng, J. 2015. Using geo-informatics for landslide risk map in northern Thailand. Paper presented at the International Conference on Intelligent Earth Observing and Applications 2015.
- Tsutsumi, D. and Fujita, M. 2008. Relative importance of slope material properties and timing of rainfall for the occurrence of landslides. International Journal of Erosion Control Engineering 1(2): 79-89.
- Turkelboom, F., Poesen, J., and Trébuil, G. 2008. The multiple land degradation effects caused by land-use intensification in tropical steeplands: A catchment study from northern Thailand. CATENA 75(1): 102-116.
- Verdi, R.J., Lotspeich, R.R., Robbins, J.C., Busciolano, R.J., Mullaney, J.R., Massey, A.J., Banks, W.S., Roland, M.A., Jenter, H.L., and Pepler, M.C. 2017. The surge, wave, and tide hydrodynamics (SWaTH) network of the US Geological Survey—Past and future implementation of storm-response monitoring, data collection, and data delivery: US Geological Survey.
- Wang, Y., Feng, L., Li, S., Ren, F., and Du, Q. 2020. A hybrid model considering spatial heterogeneity for landslide susceptibility mapping in Zhejiang Province, China. CATENA 188: 104425.
- Wangwongchai, A., Sixiong, Z., and Qingcun, Z. 2005. A case study on a strong tropical disturbance and record heavy rainfall in Hat Yai, Thailand during the winter monsoon. Advances in Atmospheric Sciences 22(3): 436-450.
- Weigel, A.P. and Rotach, M.W. 2004. Flow structure and turbulence characteristics of the daytime atmosphere in a steep and narrow Alpine valley. Quarterly Journal of the Royal Meteorological Society: A journal of the atmospheric sciences, applied meteorology and physical oceanography 130(602): 2605-2627.
- Wieczorek, G.F., Ellen, S., Lips, E.W., Cannon, S.H., and Short, D.N. 1983. Potential for debris flow and debris flood along the Wasatch Front between Salt Lake City and Willard, Utah, and measures for their mitigation: US Department of the Interior, Geological Survey.
- Workpoint. 2017. There was a landslide covering the path and wild water flowed along the road to the Phu Thap Boek [online]. Available from: <https://workpointnews.com/2017/10/23/เกิดดินสไลค์ปิดทับเส้นทาง> (in Thai).
- Wu, Y. and Hung, M.-C. 2016. Comparison of spatial interpolation techniques using visualization and quantitative assessment. Applications of Spatial Statistics: 17-34.
- Xing, Y., Yue, J., Chen, C., Qin, Y., and Hu, J. 2020. A hybrid prediction model of

- landslide displacement with risk-averse adaptation. Computers & Geosciences: 104527.
- Yoshifuji, N., Kumagai, T.o., Tanaka, K., Tanaka, N., Komatsu, H., Suzuki, M., and Tantasirin, C. 2006. Inter-annual variation in growing season length of a tropical seasonal forest in northern Thailand. Forest Ecology and Management 229(1-3): 333-339.
- Yu, X., Li, S., and Li, S. 2018. Alluvial Fan Depositional System. Clastic Hydrocarbon Reservoir Sedimentology: 325-351.
- Yumuang, S. 2005. Evaluation of Potential for 2001 Debris Flow and Debris Flood in the Vicinity of Nam Ko Area, Amphoe Lom Sak Changwat Phetchabun, Central Thailand. Thesis (dissertation): Chulalongkorn University.
- Zhang, G., Xu, J., and Bi, B. 2009. Relations of landslide and debris flow hazards to environmental factors. Ying yong sheng tai xue bao= The journal of applied ecology 20(3): 653-658.
- Zhang, K., Xue, X., Hong, Y., Gourley, J.J., Lu, N., Wan, Z., Hong, Z., and Wooten, R. 2016. iCRESTRIGRS: a coupled modeling system for cascading flood-landslide disaster forecasting. Hydrology & Earth System Sciences 20(12).
- Zheng, H., Tham, L., and Liu, D. 2006. On two definitions of the factor of safety commonly used in the finite element slope stability analysis. Computers and Geotechnics 33(3): 188-195.
- Ziegler, A.D., Benner, S.G., Tantasirin, C., Wood, S.H., Sutherland, R.A., Sidle, R.C., Jachowski, N., Nullet, M.A., Xi, L.X., and Snidvongs, A. 2014. Turbidity-based sediment monitoring in northern Thailand: Hysteresis, variability, and uncertainty. Journal of hydrology 519: 2020-2039.



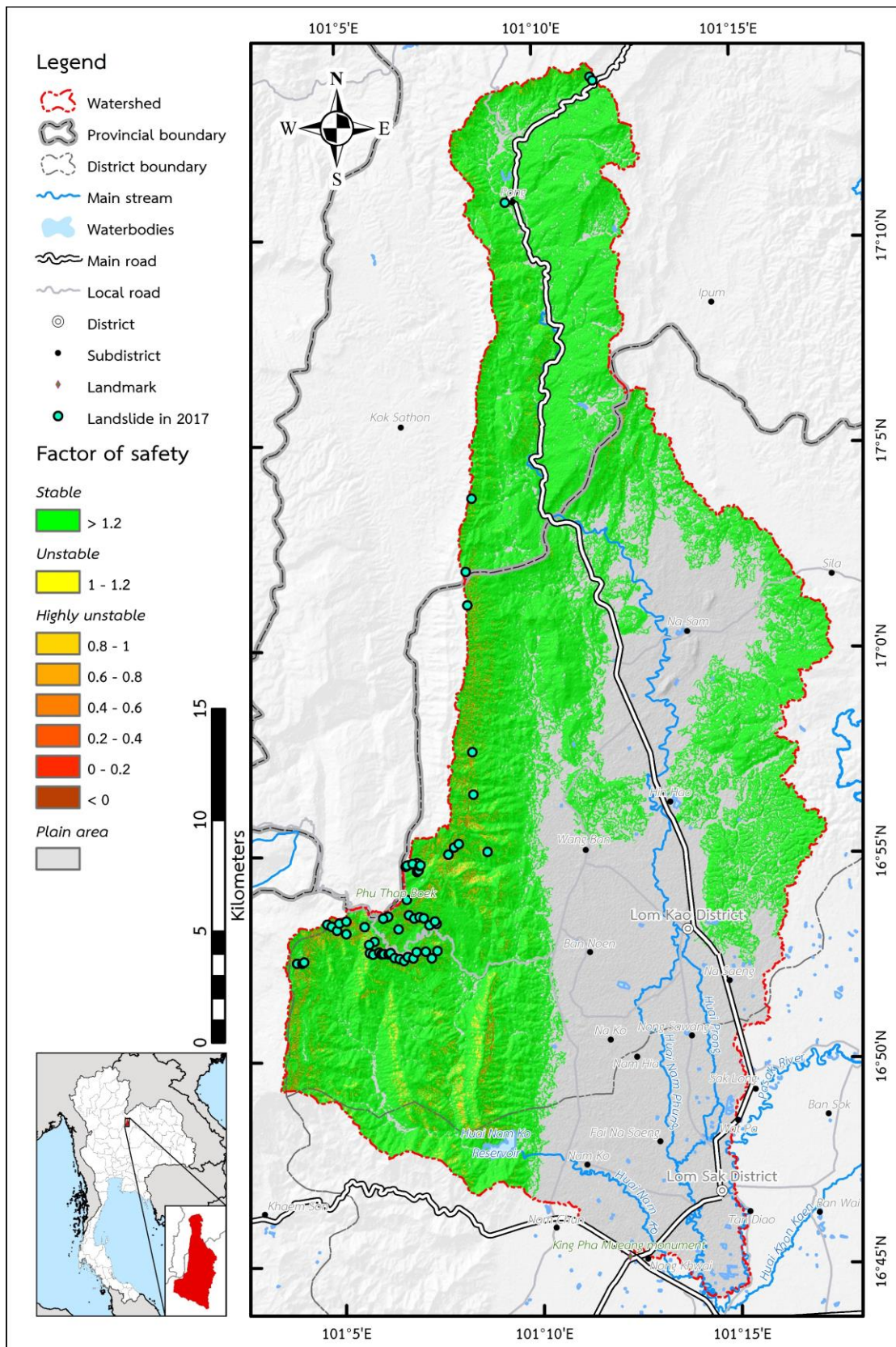
**APPENDICES**

จุฬาลงกรณ์มหาวิทยาลัย  
**CHULALONGKORN UNIVERSITY**



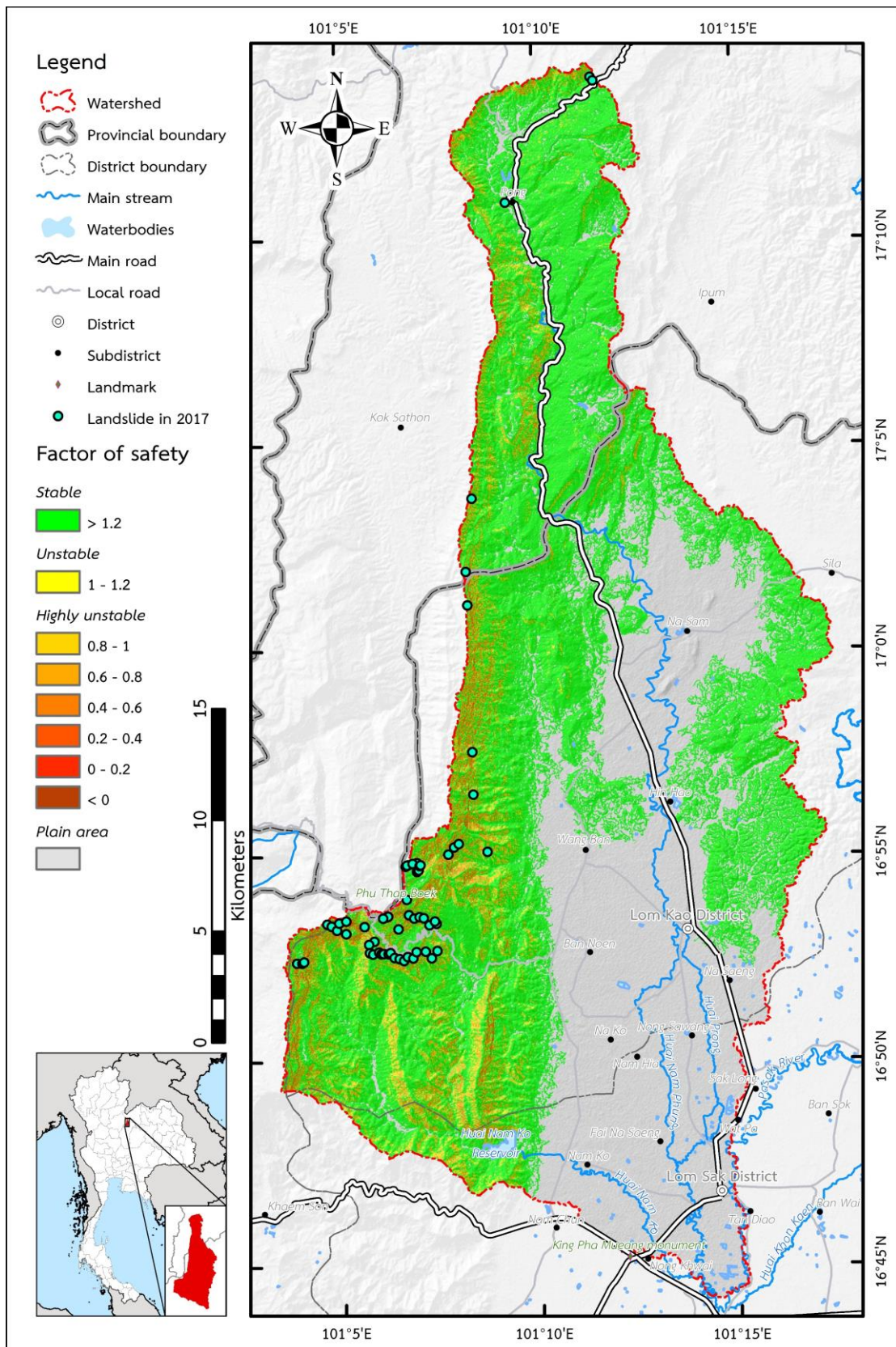
**APPENDIX A**  
**Factor of safety in slope stability of the Huai Nam Phung subbasin**  
**from 1 July, 2017 to 1 November, 2017**

จุฬาลงกรณ์มหาวิทยาลัย  
**CHULALONGKORN UNIVERSITY**

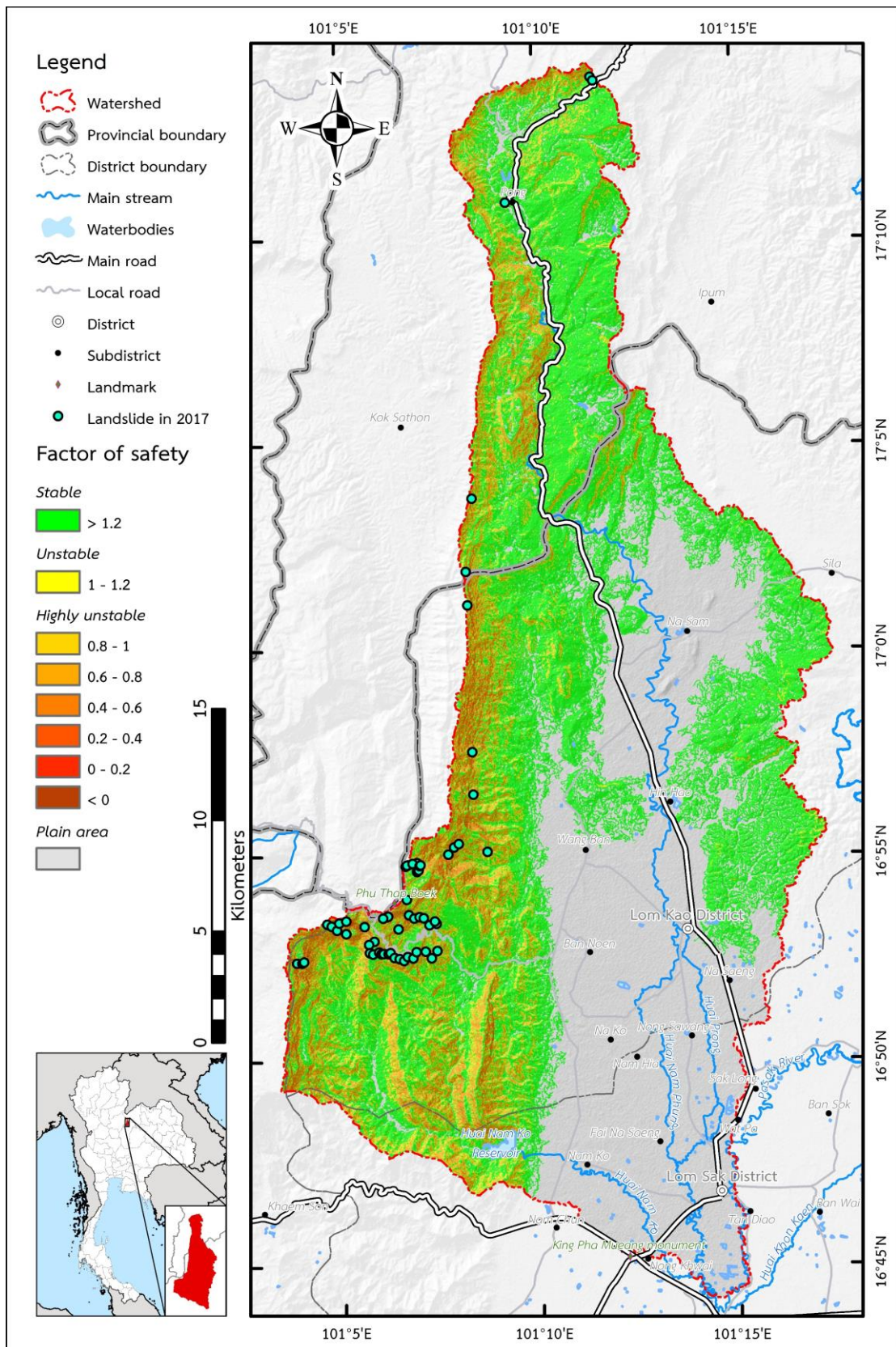


Factor of safety in slope stability of the Huai Nam Phung subbasin on 1 July, 2017

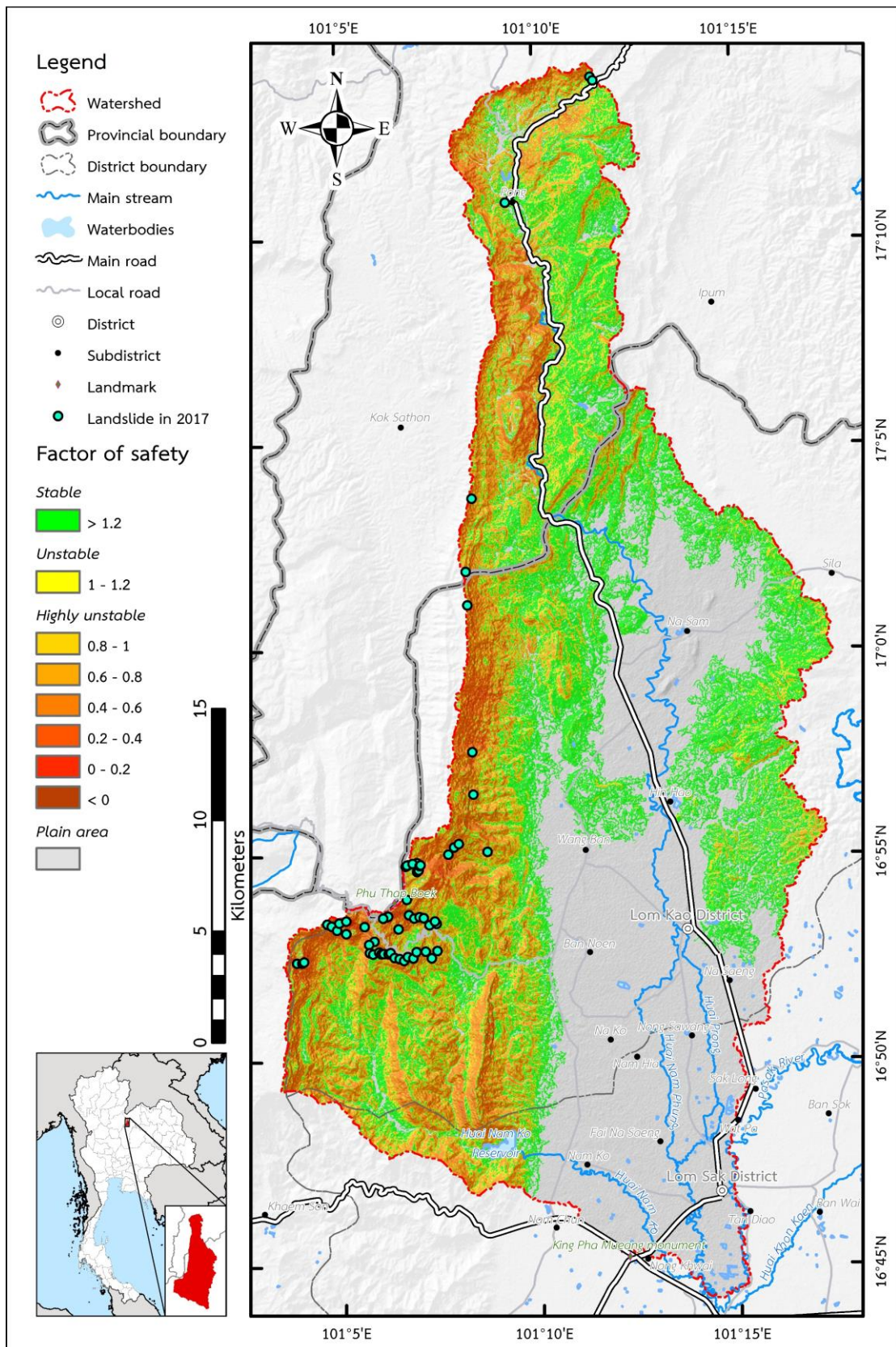




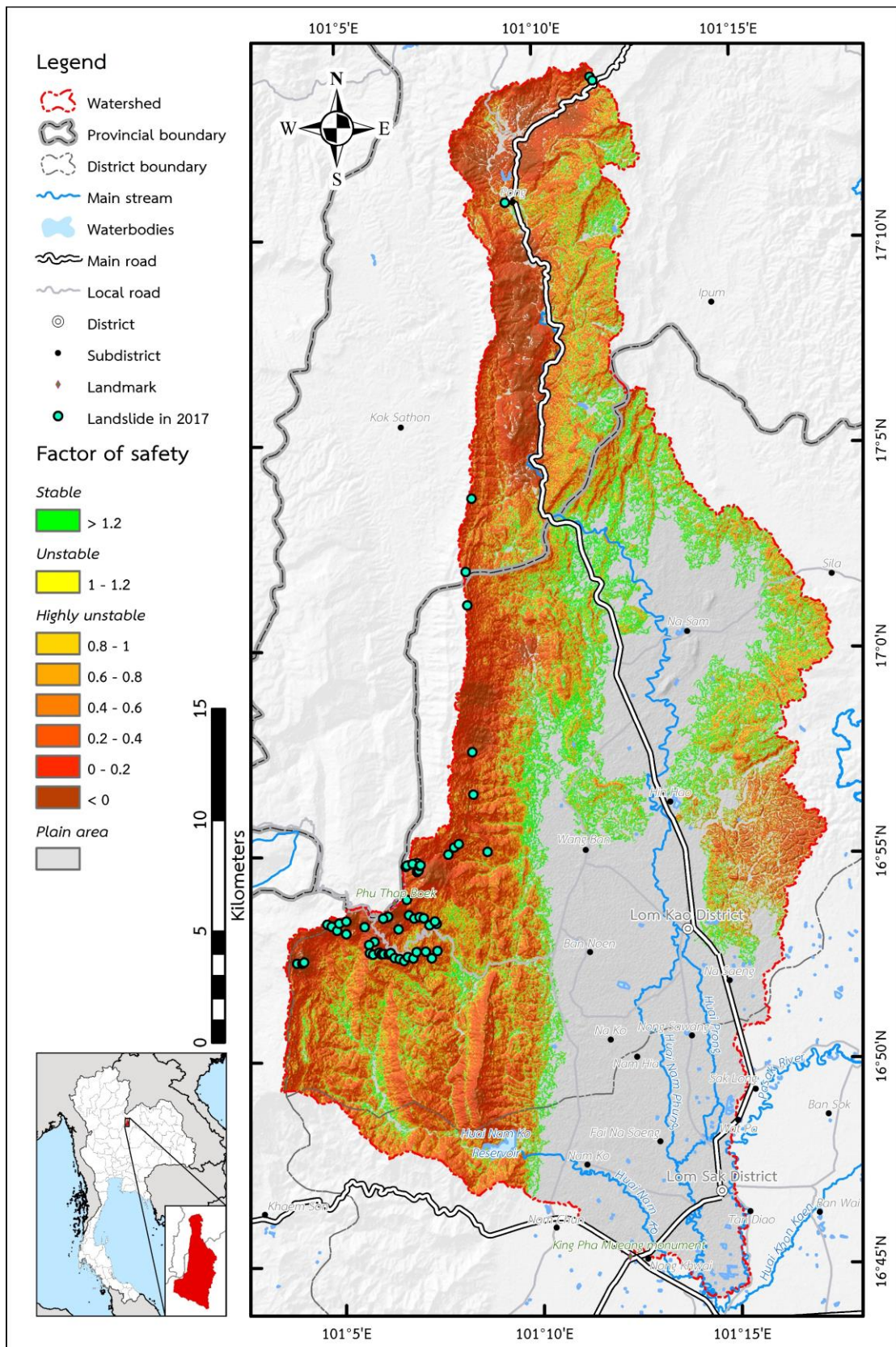
Factor of safety in slope stability of the Huai Nam Phung subbasin on 1 August, 2017



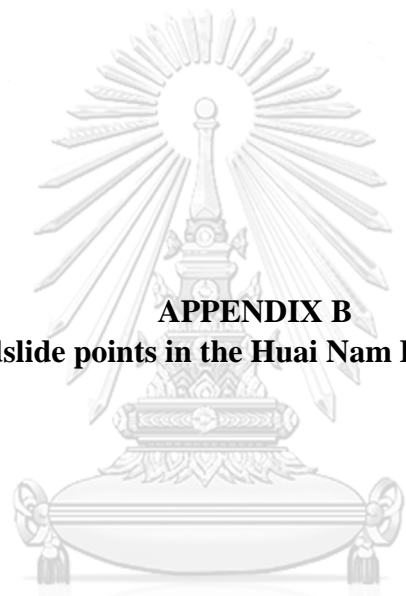
Factor of safety in slope stability of the Huai Nam Phung subbasin on 1 September, 2017



Factor of safety in slope stability of the Huai Nam Phung subbasin on 1 October, 2017

















Factor of safety in slope stability of the Huai Nam Phung subbasin on 1 November, 2017































**APPENDIX B**

**Scars of 63 landslide points in the Huai Nam Phung subbasin in 2017**













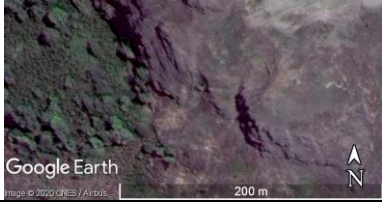

จุฬาลงกรณ์มหาวิทยาลัย  
**CHULALONGKORN UNIVERSITY**













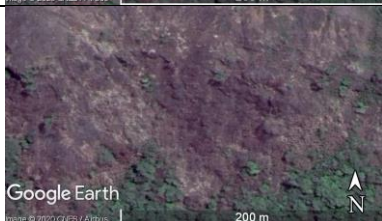

| No. | Longitude,<br>Latitude         | Shallow landslide scars   |   |
|-----|--------------------------------|---|---|
|     |                                | 5 April 2016  | 17 December 2017  |
| 1   | 101°06'01.8"E,<br>16°53'29.1"N |    |    |
| 2   | 101°06'24.8"E,<br>16°53'13.1"N |    |    |
| 3   | 101°06'40.9"E,<br>16°53'33.8"N |   |   |
| 4   | 101°06'48.9"E,<br>16°53'28.8"N |  |  |
| 5   | 101°06'57.0"E,<br>16°53'30.7"N |  |  |
| 6   | 101°07'03.3"E,<br>16°53'29.1"N |  |  |
| 7   | 101°07'20.2"E,<br>16°53'24.2"N |  |  |















| No. | Longitude,<br>Latitude         | Shallow landslide scars   |   |
|-----|--------------------------------|---|---|
|     |                                | 5 April 2016  | 17 December 2017  |
| 8   | 101°06'36.6"E,<br>16°54'44.6"N |    |    |
| 9   | 101°06'38.7"E,<br>16°54'46.2"N |    |    |
| 10  | 101°06'47.2"E,<br>16°54'48.6"N |   |   |
| 11  | 101°06'56.3"E,<br>16°54'39.0"N |  |  |
| 12  | 101°06'57.8"E,<br>16°54'45.2"N |  |  |
| 13  | 101°06'59.2"E,<br>16°54'46.5"N |  |  |
| 14  | 101°11'29.0"E,<br>17°13'56.0"N |  |  |















| No. | Longitude,<br>Latitude         | Shallow landslide scars   |   |
|-----|--------------------------------|---|---|
|     |                                | 5 April 2016  | 17 December 2017  |
| 15  | 101°11'33.2"E,<br>17°13'50.8"N |    |    |
| 16  | 101°09'18.1"E,<br>17°10'53.4"N |    |    |
| 17  | 101°08'14.6"E,<br>17°01'05.6"N |   |   |
| 18  | 101°03'50.5"E,<br>16°52'24.4"N |  |  |
| 19  | 101°03'58.3"E,<br>16°52'24.4"N |  |  |
| 20  | 101°04'01.1"E,<br>16°52'26.1"N |  |  |
| 21  | 101°04'36.9"E,<br>16°53'21.2"N |  |  |









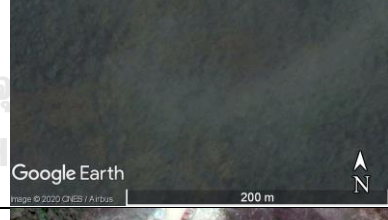


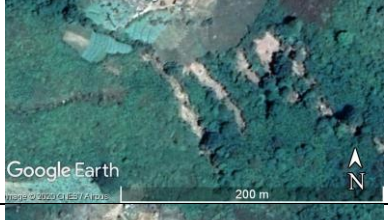


















| No. | Longitude,<br>Latitude         | Shallow landslide scars   |   |
|-----|--------------------------------|---|---|
|     |                                | 5 April 2016  | 17 December 2017  |
| 22  | 101°04'43.5"E,<br>16°53'18.2"N |    |    |
| 23  | 101°04'51.7"E,<br>16°53'12.1"N |    |    |
| 24  | 101°04'55.1"E,<br>16°53'22.4"N |   |   |
| 25  | 101°05'05.8"E,<br>16°53'25.4"N |  |  |
| 26  | 101°05'33.2"E,<br>16°53'17.0"N |  |  |
| 27  | 101°05'05.6"E,<br>16°53'06.8"N |  |  |
| 28  | 101°05'48.0"E,<br>16°52'55.4"N |  |  |

| No. | Longitude,<br>Latitude         | Shallow landslide scars   |   |
|-----|--------------------------------|---|---|
|     |                                | 5 April 2016  | 17 December 2017  |
| 29  | 101°05'40.1"E,<br>16°52'51.0"N |    |    |
| 30  | 101°05'41.1"E,<br>16°52'38.7"N |    |    |
| 31  | 101°05'46.0"E,<br>16°52'36.8"N |   |   |
| 32  | 101°05'54.9"E,<br>16°52'39.5"N |  |  |
| 33  | 101°05'58.6"E,<br>16°52'37.1"N |  |  |
| 34  | 101°06'02.0"E,<br>16°52'37.4"N |  |  |
| 35  | 101°06'09.3"E,<br>16°52'37.0"N |  |  |

| No. | Longitude,<br>Latitude         | Shallow landslide scars  |   |
|-----|--------------------------------|--|---|
|     |                                | 5 April 2016   | 17 December 2017  |
| 36  | 101°06'12.5"E,<br>16°52'38.4"N |  A satellite image showing a landslide scar on a hillside. The scar is a light-colored, linear feature cutting through the vegetation. The image includes a 'Google Earth' watermark, a '200 m' scale bar, and a north arrow.   |  A satellite image of the same area as in 2016, showing the same landslide scar. The vegetation appears denser and greener. The image includes a 'Google Earth' watermark, a '200 m' scale bar, and a north arrow.   |
| 37  | 101°06'18.4"E,<br>16°52'31.5"N |  A satellite image showing a landslide scar on a hillside. The scar is a light-colored, linear feature cutting through the vegetation. The image includes a 'Google Earth' watermark, a '200 m' scale bar, and a north arrow.   |  A satellite image of the same area as in 2016, showing the same landslide scar. The vegetation appears denser and greener. The image includes a 'Google Earth' watermark, a '200 m' scale bar, and a north arrow.   |
| 38  | 101°06'25.9"E,<br>16°52'29.8"N |  A satellite image showing a landslide scar on a hillside. The scar is a light-colored, linear feature cutting through the vegetation. The image includes a 'Google Earth' watermark, a '200 m' scale bar, and a north arrow.  |  A satellite image of the same area as in 2016, showing the same landslide scar. The vegetation appears denser and greener. The image includes a 'Google Earth' watermark, a '200 m' scale bar, and a north arrow.  |
| 39  | 101°06'32.9"E,<br>16°52'26.9"N |  A satellite image showing a landslide scar on a hillside. The scar is a light-colored, linear feature cutting through the vegetation. The image includes a 'Google Earth' watermark, a '200 m' scale bar, and a north arrow. |  A satellite image of the same area as in 2016, showing the same landslide scar. The vegetation appears denser and greener. The image includes a 'Google Earth' watermark, a '200 m' scale bar, and a north arrow. |
| 40  | 101°06'38.6"E,<br>16°52'32.5"N |  A satellite image showing a landslide scar on a hillside. The scar is a light-colored, linear feature cutting through the vegetation. The image includes a 'Google Earth' watermark, a '200 m' scale bar, and a north arrow. |  A satellite image of the same area as in 2016, showing the same landslide scar. The vegetation appears denser and greener. The image includes a 'Google Earth' watermark, a '200 m' scale bar, and a north arrow. |
| 41  | 101°06'46.8"E,<br>16°52'30.3"N |  A satellite image showing a landslide scar on a hillside. The scar is a light-colored, linear feature cutting through the vegetation. The image includes a 'Google Earth' watermark, a '200 m' scale bar, and a north arrow. |  A satellite image of the same area as in 2016, showing the same landslide scar. The vegetation appears denser and greener. The image includes a 'Google Earth' watermark, a '200 m' scale bar, and a north arrow. |
| 42  | 101°06'52.0"E,<br>16°52'39.7"N |  A satellite image showing a landslide scar on a hillside. The scar is a light-colored, linear feature cutting through the vegetation. The image includes a 'Google Earth' watermark, a '200 m' scale bar, and a north arrow. |  A satellite image of the same area as in 2016, showing the same landslide scar. The vegetation appears denser and greener. The image includes a 'Google Earth' watermark, a '200 m' scale bar, and a north arrow. |

| No. | Longitude,<br>Latitude         | Shallow landslide scars  |  |
|-----|--------------------------------|--|--|
|     |                                | 5 April 2016   | 17 December 2017   |
| 43  | 101°07'05.8"E,<br>16°52'40.2"N |  A satellite image showing a shallow landslide scar on a hillside. The scar is a light-colored, irregularly shaped area. The surrounding terrain is covered in dense vegetation. A scale bar indicates 200 m, and a north arrow is present.   |  A satellite image showing the same landslide scar as in the 2016 image. The scar is now more defined and appears to have expanded or changed shape. The surrounding vegetation is denser and greener. A scale bar indicates 200 m, and a north arrow is present.   |
| 44  | 101°07'23.6"E,<br>16°52'40.9"N |  A satellite image showing a shallow landslide scar on a hillside. The scar is a light-colored, irregularly shaped area. The surrounding terrain is covered in dense vegetation. A scale bar indicates 200 m, and a north arrow is present.   |  A satellite image showing the same landslide scar as in the 2016 image. The scar is now more defined and appears to have expanded or changed shape. The surrounding vegetation is denser and greener. A scale bar indicates 200 m, and a north arrow is present.   |
| 45  | 101°07'15.0"E,<br>16°52'30.4"N |  A satellite image showing a shallow landslide scar on a hillside. The scar is a light-colored, irregularly shaped area. The surrounding terrain is covered in dense vegetation. A scale bar indicates 200 m, and a north arrow is present.  |  A satellite image showing the same landslide scar as in the 2016 image. The scar is now more defined and appears to have expanded or changed shape. The surrounding vegetation is denser and greener. A scale bar indicates 200 m, and a north arrow is present.  |
| 46  | 101°06'37.7"E,<br>16°53'56.3"N |  A satellite image showing a shallow landslide scar on a hillside. The scar is a light-colored, irregularly shaped area. The surrounding terrain is covered in dense vegetation. A scale bar indicates 200 m, and a north arrow is present. |  A satellite image showing the same landslide scar as in the 2016 image. The scar is now more defined and appears to have expanded or changed shape. The surrounding vegetation is denser and greener. A scale bar indicates 200 m, and a north arrow is present. |
| 47  | 101°07'41.5"E,<br>16°55'01.7"N |  A satellite image showing a shallow landslide scar on a hillside. The scar is a light-colored, irregularly shaped area. The surrounding terrain is covered in dense vegetation. A scale bar indicates 200 m, and a north arrow is present. |  A satellite image showing the same landslide scar as in the 2016 image. The scar is now more defined and appears to have expanded or changed shape. The surrounding vegetation is denser and greener. A scale bar indicates 200 m, and a north arrow is present. |
| 48  | 101°07'50.5"E,<br>16°55'12.1"N |  A satellite image showing a shallow landslide scar on a hillside. The scar is a light-colored, irregularly shaped area. The surrounding terrain is covered in dense vegetation. A scale bar indicates 200 m, and a north arrow is present. |  A satellite image showing the same landslide scar as in the 2016 image. The scar is now more defined and appears to have expanded or changed shape. The surrounding vegetation is denser and greener. A scale bar indicates 200 m, and a north arrow is present. |
| 49  | 101°07'57.7"E,<br>16°55'17.0"N |  A satellite image showing a shallow landslide scar on a hillside. The scar is a light-colored, irregularly shaped area. The surrounding terrain is covered in dense vegetation. A scale bar indicates 200 m, and a north arrow is present. |  A satellite image showing the same landslide scar as in the 2016 image. The scar is now more defined and appears to have expanded or changed shape. The surrounding vegetation is denser and greener. A scale bar indicates 200 m, and a north arrow is present. |

| No. | Longitude,<br>Latitude         | Shallow landslide scars   |   |
|-----|--------------------------------|---|---|
|     |                                | 5 April 2016  | 17 December 2017  |
| 50  | 101°08'41.2"E,<br>16°55'05.2"N |    |    |
| 51  | 101°08'20.5"E,<br>16°56'29.0"N |    |    |
| 52  | 101°08'19.6"E,<br>16°57'31.0"N |   |   |
| 53  | 101°08'12.6"E,<br>17°01'54.5"N |  |  |
| 54  | 101°08'22.6"E,<br>17°03'41.4"N |  |  |
| 55  | 101°06'06.6"E,<br>16°53'30.7"N |  |  |
| 56  | 101°06'08.0"E,<br>16°53'31.8"N |  |  |

| No. | Longitude,<br>Latitude         | Shallow landslide scars   |   |
|-----|--------------------------------|---|---|
|     |                                | 5 April 2016  | 17 December 2017  |
| 57  | 101°06'09.2"E,<br>16°53'31.8"N |    |    |
| 58  | 101°07'11.9"E,<br>16°53'18.9"N |    |    |
| 59  | 101°07'22.8"E,<br>16°53'20.6"N |   |   |
| 60  | 101°06'40.3"E,<br>16°54'46.7"N |  |  |
| 61  | 101°06'49.1"E,<br>16°54'47.9"N |  |  |
| 62  | 101°06'53.8"E,<br>16°54'49.6"N |  |  |
| 63  | 101°06'53.8"E,<br>16°54'36.7"N |  |  |

## VITA

**NAME** Rugkiet Chansorn

**DATE OF BIRTH** 10 February 1993

**PLACE OF BIRTH** Krabi, Thailand

**INSTITUTIONS ATTENDED** Bachelor of Science (Geography and Geoinformatics)  
Department of Geography, Faculty of Social Sciences,  
Srinakharinwirot University, (2012-2016)

**HOME ADDRESS** 82/9 Moo.2, Prudinna-Chongsiad Rd., Prudinna, Khlong  
Thom, Krabi, Thailand, 81120



จุฬาลงกรณ์มหาวิทยาลัย  
CHULALONGKORN UNIVERSITY